2014-12-18

Genetic analysis of the Caenorhabditis elegans M1 neuron axon guidance and embryonic elongation

Refai, Osama

UNIVERSITY OF CALGARY

Genetic analysis of the *Caenorhabditis elegans* M1 neuron axon guidance and embryonic elongation

by

Osama Moustafa Refai

A THESIS

SUBMITTED TO THE FACULTY OF GRADUATE STUDIES

IN PARTIAL FULFILMENT OF THE REQUIREMENTS FOR THE

DEGREE OF DOCTOR OF PHILOSOPHY

DEPARTMENT OF BIOCHEMISTRY AND MOLECULAR BIOLOGY

CALGARY, ALBERTA

December, 2014

Abstract

Embryonic morphogenesis is a complicated process that involves several critical processes such as cell migration and body shape changes. The cell cytoskeleton is the basic machinery that drives many morphogenic events. Defects in regulators of the cytoskeleton components, especially actin and myosin, can result in birth defects. In this thesis, I carried out genetic analyses to study both morphogenesis of a single cell and the embryo as a whole in the nematode *Caenorhabditis elegans*. Axon guidance of the M1 neuron depends on multiple signaling cues and mechanisms. M1 uses the growth cone controlling genes such as *unc-119, unc-51, unc-34* and *unc-115* to build part of its trajectory. After its birth, M1 appears to use the mechanical tension to extend its initial projection, in a manner similar to another pharyngeal neuron M2. The g1P gland cell also participates in M1 guidance, analogous to glia cells or pioneer neurons. A forward genetic screen identified more genes that control M1 pathfinding including three novel genes. The variety of molecules and mechanisms used by the M1 neuron indicates that morphogenic processes at a single cell level are complicated and robust. Morphogenic processes are much more complicated in embryonic elongation, which involves the whole animal. Although major regulators of embryonic elongation have been identified, little is known about their function and genetic interactions. Here, I investigated the genetic interactions of the formin homology protein *fhod-1* with other members of its family, showing that *fhod-1* might be the sole formin acting in embryonic elongation. Additionally, I characterized the expression pattern of *fhod-1*, indicating it is expressed homogenously during elongation. Structural analysis of the *fhod-1* gene identified a novel

short isoform, which results from an alternative splicing event. Finally, I investigated the expression and function of the sex determination gene *fem-2* in embryonic elongation. Although *fem-2* is likely expressed ubiquitously in the epidermis, it appears to function specifically in dorsal/ventral epidermal cells to regulate elongation.

Acknowledgements

I would foremost like to express my special appreciation and thanks to Dr. Paul E. Mains for his great and excellent mentorship. I would especially like to thank Dr. Mains for allowing me to pursue and complete my graduate work in his lab, after the departure of my previous supervisor Dr. Jeb Gaudet, whom I thank for supervising me earlier in my graduate program. I would like to thank my Supervisory Committee Members, Dr. Jim McGhee, Dr. Sarah McFarlane and Dr. Sarah Childs for all suggestions and ideas. My appreciations and thanks for all past and present members of the Mains Lab, in particular Dr. Ryan Smit, Ben Chan, Dr. Christopher Vanneste and Sarah Beard. Also, I would like to thank previous members of the Gaudet Lab, in paticular Dr. Indra Raharjo, E. Rollins, Michelle Vogelaar, Dr. Jay Kormish, Dr. Vikas Ghai and Aiden Dineen. I extend my appreciations to members of the University of Calgary *C. elegans* group and the Genes and Development Research Group. I would like to thank Dr. David Pruyne for sending formin mutant stains and Dr. David Pilgrim for sending the *fem-2* cDNA construct. I would like to thank Dr. David Pilgrim and Dr. Jillian Parboosingh for being part of the examination committee.

Words cannot express how grateful I am to my father, mother, older brother Walid, brothers and sisters for all the support. Special thanks to my wife Rania, my kids, my mother-in law and father-in law.

To Moustafa A. Refai and Hamda I. Hegazy

"I dedicate this PhD thesis to my parents, for all their sacrifices that made the completion of my education possible."

Table of Contents

List of Tables

List of Figures and Illustrations

List of Symbols, Abbreviations and Nomenclature

Symbol	Definition
ADP	Adenosine diphosphate
ARP	Actin related protein
ATP	Adenosine Triphosphate
ATPase	Adenosine Triphosphatase
BSA	Bovine serum albumin
CAMs	Cell-adhesion molecules
Ce	*Caenorhabditis elegans*
Cbr	*Caenorhabditis briggsae*
Cre	*Caenorhabditis remanei*
CC	Coiled-coil domain
CCC	Catenin cadherin complex
CFB	Circumferential actin filament bundles
CNS	Central nervous system
cyk	Cytokinesis defect
DAAM	Dishevelled associated activator of morphogenesis
DAC	Discs-large (DLG-1), an apical junction molecule (AJM-1) complex
DAD	diaphanous autoregulatorydomain
DAPI	4',6-diamidino-2-phenylindole
DCC	Deleted in Colorectal Cancer
DD	dimerization domain
DIA	Diaphanous
DIC	Differential interference contrast
DID	Diaphanous Inhibitory domain
DNA	Deoxyribonucleic Acid
DPY	Dumpy
eMLC	essential myosin light chains
EMS	Ethyl methane sulfonate
F-actin	Actin filament
FH2	Formin homology domain

Symbol	Definition
FHOD	Formin homology domain containing protein
fhod-1 let-502	Space (or comma) separates linked genes in a double mutant
FMN	Formin
FMNL(FRL)	Formin related protein
FOZI	Formin encodes an unusual zinc-finger protein
FRL	Formin-Related proteins identified in Leucocytes
g1P	Posterior pharyngeal g1 gland
G-actin	Globular actin monomer
GAP	GTPase activating protein
GBD	GTPase binding domain
GDP	guanosine diphosphate
GEF	Guanine exchange factors
GEX	Gut external
GFP	Green fluorescent protein
glr	Glutamate receptor
hlh	Helix Loop Helix
HMP	Hump back
HMR	Hammer head
IF	Intermediate filaments
INF	Inverted formin
IPTG	isopropyl β-D-1-thiogalactopyranoside
let	Lethal
let-502; mel-11	semicolon separates unlinked genes in a double mutant
LG	Linkage Group
M1	M1 Pharyngeal neuron
mel	Maternal-effect lethal
mel-11	genotype, understood to be homozygous
MF	Microfilaments
MHC	Myosin heavy chain
MLC	Myosin light chain
MLCK	Myosin light chain kinase
MLCP	Myosin light chain phosphatase
mnm	M Neuron Morphology abnormal
MT	Microtubules

Symbol	Definition
MYPT	Myosin phosphatase targeting subunit
NGM	Nematode growth medium
NMY	non-muscle myosin heavy chains
PAT	Paralyzed at 2 fold
PB(S)T	Phosphate buffered saline with Tween 20
PB(S)X	Phosphate buffered saline with triton
PBS	Phosphate Buffered Saline
PCR	Polymerase Chain Reaction
PP1C	Myosin phosphatase catalytic subunit
rMLC	regulatory myosin light chain
RNA	Ribonucleic Acid
RNAi	RNA interference
ROCK/ROK	Rho kinase/Rho-binding kinase/Rho associated kinase
RT-PCR	Reverse transcription PCR
SNP	Single nucleotide polymorphism
TGFβ	Transforming growth factor β
ts	Temperature sensitive
UNC	Uncoordinated
VNC	Ventral nerve cord
WASP	Wiskott-Aldrich Syndrome Protein
WAVE	WASP and verprolin homologs

Chapter One: **GENERAL INTRODUCTION**

Preface: Embryonic morphogenesis

The final form or shape of an organism is a result of a highly complicated biological processes, known as morphogenesis, much of which occurs during embryonic life. Thus, morphogenesis is an important topic in developmental biology. Morphogenic changes involve changes in cell shape, size, migration, proliferation and tissue re-organization. In general, these changes are controlled by morphogenic signals that target downstream regulators such as transcription factors and remodel the cytoskeleton and cell adhesion. Such changes give a tissue its ultimate shape. Local changes in cells and tissues can result in global changes that shape the body plan, and thus transform the embryo into an adult form. Disruption of embryonic morphogenesis in many organisms due to environmental teratogens or genetic mutations can result in disfigurement or death (VAN GELDER *et al.* 2010).

The formation of the neural tube in *Xenopus* is a classic example for morphogenic changes that transform embryonic shape. This process is known as primary neurulation, which establishes the basic foundations of the nervous system in vertebrate embryos (Figure 1). The notochord initiates neurulation by secreting growth factors such as Bone Morphogenetic Protein 4, Noggin and Chordin, which cause the overlying cuboidal ectodermal cells to elongate and become columnar, forming the neural plate (KELLER *et al.* 1992). The ectodermal cells undergo a process called convergent extension, where the cells intercalate towards the midline (conversion) and migrate along the anteroposterior axis (extension), causing the body to elongate. Finally, the flat neural plate folds to form

the cylindrical neural tube, as the growing epidermal cells push the plate to fold at the medial hinge points (where cells have become wedge shaped), leading to neural tube invagination (POZNANSKI *et al.* 1997). Analogous to this process, the invertebrate nematode *Caenorhabditis elegans* embryo undergoes dorsal intercalation, which leads to changes in cell shape that result in the initial phase of embryonic elongation. Notably, all these processes involve actin and myosin contractions.

In the current study, I take advantages of the simple model organism *C. elegans*, which is amenable to genetic analysis, to study embryonic morphogenesis at two levels. First, I looked at single cell resolution, how a neuron (M1) elongates its long axonal process and establishes its final shape. Axon guidance molecules induce cytoskeletal changes that help the neuron to navigate towards its targets (this will be described in the form of a published manuscript in Chapters Three). The worm pharynx is an ideal and simple model to understand how a neuron can build its trajectory in the context of a developing organ. M1 neuron has a unique morphology that spans the whole pharynx, which makes it a compelling example for axon guidance of the pharyngeal nervous system.

Second, I looked at a larger scale, to learn how cell and tissue changes lead to transformation of the ball-shaped embryo into the adult worm-like shape (this will be described in details in Chapters Four). A single cell layer (the epidermis) is responsible for the embryonic elongation. A smooth muscle-like contraction of the lateral epidermal cells causes epidermal cell elongation, which is the driving force for elongation of the rest of the embryo. Although, the central elongation pathway (*let-502/mel-11*) was identified some time ago, little is known about its downstream targets and the parallel

pathways. For instance, it is not clear whether muscle has a role in early elongation, redundant with epidermis. Additionally, the involvement of actin nucleators other than FHOD-1 is not clear. Finally, it is not known whether parallel pathways such as *fem-2/pak-1* function in the seam cells, similar to the central pathway, or in the dorsal/ventral epidermis. Answer to these questions will broaden our understanding of embryonic morphogenesis in *C. elegans,* as well as other organisms.

Figure 1. Embryonic neural tube morphogenesis

A schematic diagram explaining *Xenopus* neural tube formation, as a typical example of embryonic morphogenesis. (A) The movement of the ectodermal cells involves two steps; first, they move from the lateral sides (right and left) to the dorsal midline and converge in between each other, in a process known as “intercalation”. Second, this intercalation results in a process termed “extension”, which elongates along the anterior posterior axis and in a perpendicular to the axis of intercalation. (B) Formation of the cylindrical neural tube. The flat neural plate becomes a wedge shape as result of the actin (blue) localized in a specific sites (wedging). Next, wedged ectoderm forms hinge points and eventually invaginates to form the neural tube.

Figure 1 Embryonic neural tube morphogenesis

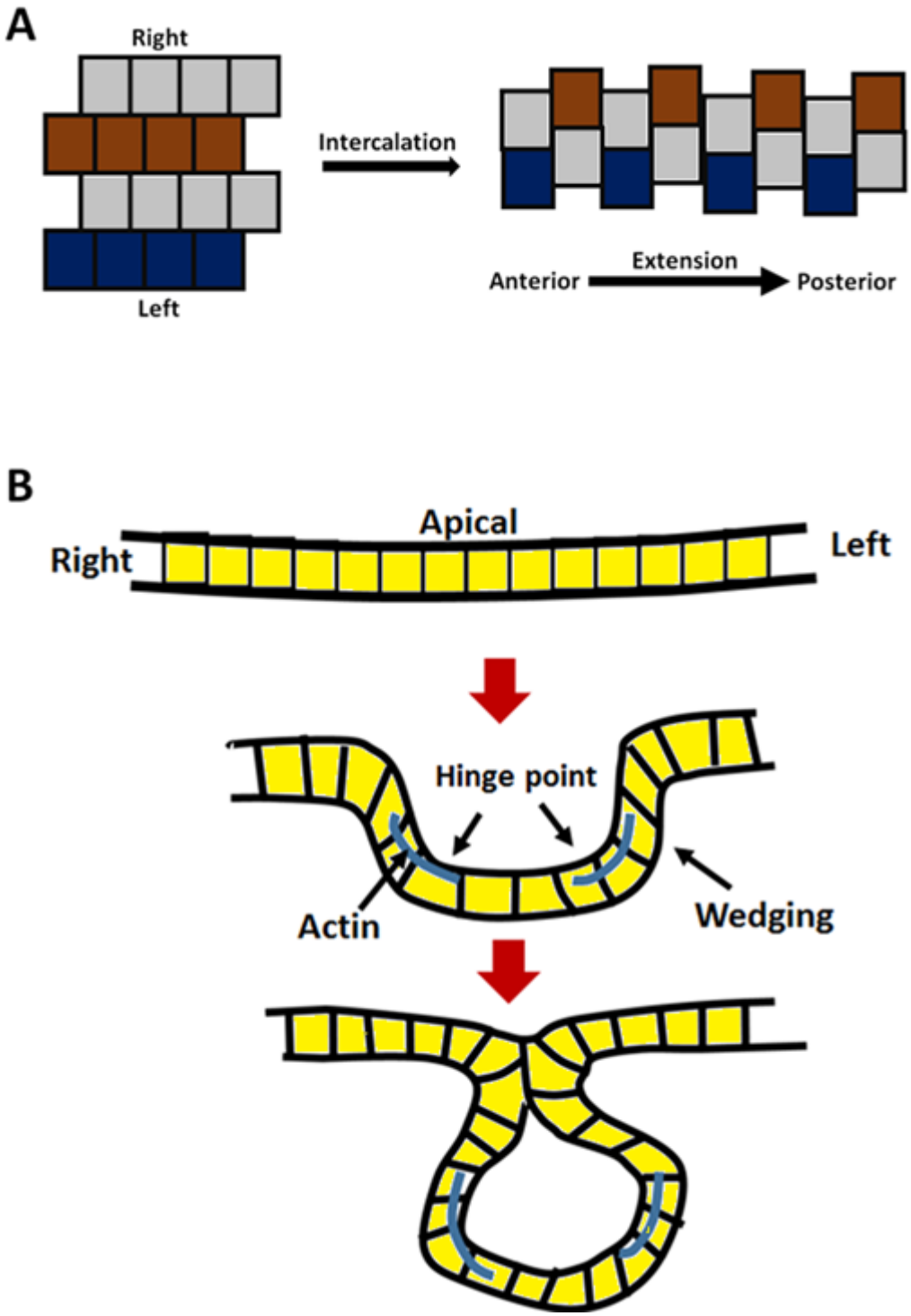

C. elegans embryonic morphogenesis

Embryonic morphogenesis in *C. elegans* is mainly mediated by a single epithelial layer, the epidermis, which surrounds the embryo. Earlier morphogenic events that do not involve epidermis include gastrulation, in which primordial intestine and muscle cells migrate inward from the ventral side to form the ventral cleft (GEORGE *et al.* 1998). Next, the ventral neuroblast cells fill the ventral cleft and provides a substrate for the subsequent epidermal migration (LIU *et al.* 2007). The final shape of the animal is determined by the epidermis. Epidermal morphogenesis involves cell rearrangements, cell fusion, cell shape changes and interactions. Three major events involved in epidermal morphogenesis will be discussed in this thesis: dorsal intercalation, epidermal enclosure, and elongation (elongation is discussed in detail in Chapter Four).

Epidermal intercalation

After their specification, epidermal cells are found as two rows of cells at the posterior dorsal side of the embryo (Figure 2). Dorsal epidermal cells undergo a process known as dorsal intercalation, where the two rows of cells intercalate to form a single cell layer along the dorsal midline of the embryo (WILLIAMS-MASSON *et al.* 1998). To change their position, dorsal cells form protrusions and move toward the midline, where they intercalate between their contralateral cells and elongate to the opposite side of the embryo (WILLIAMS-MASSON *et al.* 1998). This process is analogous to cellular rearrangements that occur in the neural plate of *Xenopus* (ELUL and KELLER 2000). Mechanisms and genetic interactions that underline epidermal intercalation in *C. elegans* are not fully understood (CHISHOLM and HARDIN 2005). The epidermal cytoskeleton elements such as microtubules and actin microfilaments are thought to play an essential

role in intercalation (WILLIAMS-MASSON *et al.* 1998). The C2H2 Zinc finger transcription factor DIE-1 and the T box proteins, TBX-8 and TBX-9 are necessary for normal dorsal intercalation (HEID *et al.* 2001; ANDACHI 2004; POCOCK *et al.* 2004).

Epidermal enclosure

Shortly after the dorsal intercalation begins, ventral epidermal cells migrate toward the ventral midline, thereby enclosing the embryo in an epidermal sheath. At the beginning of ventral enclosure, two pair of anterior cells migrate to the ventral midline while extending long protrusions; these cells are known as "leading cells". Laser killing of these cells can block ventral enclosure completely (WILLIAMS-MASSON *et al.* 1998). Following the leading cells migration, posterior ventral cells elongate to the ventral midline, covering the ventral pocket and the underlying neuroblasts (Figure 2). After elongating to the ventral midline, ventral epidermal cell on the left and right sides establish new junctional connections along the ventral midline, with the extreme anterior cells completing epidermal enclosure of the embryo.

Mutations in molecules that control epidermal enclosure result in abnormalities known as the Gex phenotype (or external gut). These molecules include the RAC ligands GEX-2 and -3, actin-related proteins Arp-2/3, ephrins EFN1-4 and their receptor VAB-1 (GEORGE *et al.* 1998; SOTO *et al.* 2002; SAWA *et al.* 2003; GHENEA *et al.* 2005; PATEL *et al.* 2008; ROH-JOHNSON and GOLDSTEIN 2009). Furthermore, mutations in the adhesion complex molecules that interconnect the epidermal sheath cause enclosure defects and weaken the epidermal sheath integrity (COSTA *et al.* 1998). Adhesion complexes include the cadherin catenin complex (CCC), the apical junction molecule (AJM-1), and the discs-large (DLG-1) (COSTA *et al.* 1998; PETTITT *et al.* 2003; SIMSKE *et al.* 2003).

Figure 2. *C. elegans* epidermal morphogenesis

Two major events in epidermal morphogenesis: (A) Dorsal intercalation, which involves migration of the two dorsal epidermal cell rows (left and right) to the dorsal midline to form a single cell row along the anterior-posterior axis. (B) Ventral enclosure, where the ventral epidermal cells migrate towards the ventral midline over the ventral pocket (neuroblasts) (left panel). This process encloses the whole embryo by a sheath of epidermal cells (right panel).

Figure 2. *C. elegans* epidermal morphogenesis

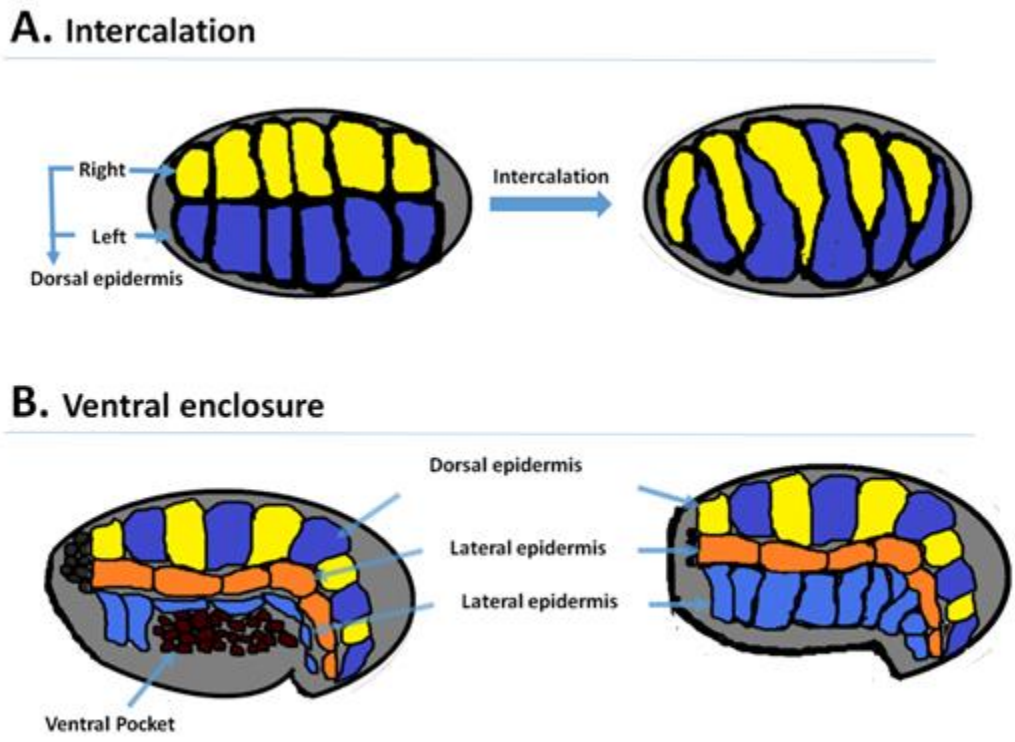

Actin cytoskeleton

Axon extension and embryonic elongation are driven by the actin cytoskeleton. Actin is one of the most abundant proteins in the eukaryotic cell, and compromises 10% of a muscle cell's total protein and up to 5% of the non-muscle cellular proteins (LODISH *et al.* 1999). Vertebrates express three main actin isoforms that differ by only a few amino acids, including the *alpha* isoform, which is expressed in muscle and contractile cell actin filaments (KHAITLINA 2001). The other two isoforms, *beta* and *gamma* are expressed in non-muscle and all other cells (KHAITLINA 2001).

Most of the morphogenetic processes such as cell motility, migration, division, contraction and cell shape changes depend on the actin cytoskeleton (DOMINGUEZ and HOLMES 2011). Cellular actin presents in two forms, either globular (G-actin**)** or filamentous (F-actin). G-actin is a conserved globular protein that can bind and hydrolyze the adenosine triphosphate (ATP) and so acts as an ATPase enzyme. G-actin can be present in cell as free actin monomers that can polymerize spontaneously into F-actin. Thus, the actin filament forms a helical structure (BREMER and AEBI 1992; LEE and DOMINGUEZ 2010). The F-actin has a distinct polarity, with a fast growing (+) "barbed" end and a slow growing (–) "pointed" end (Figure 3). The balance between disassembly and polymerization rate of the actin filament helps determine and maintain a specific cell shape.

Figure 3. Actin nucleation

The formation of the thin F-actin filament depends on actin's ability to hydrolyze ATP. G-actin binds to ATP and uses the energy resulting from ATP/ADP exchange for polymerization of the F-actin, releasing a phosphate group.

Figure 3. Actin nucleation

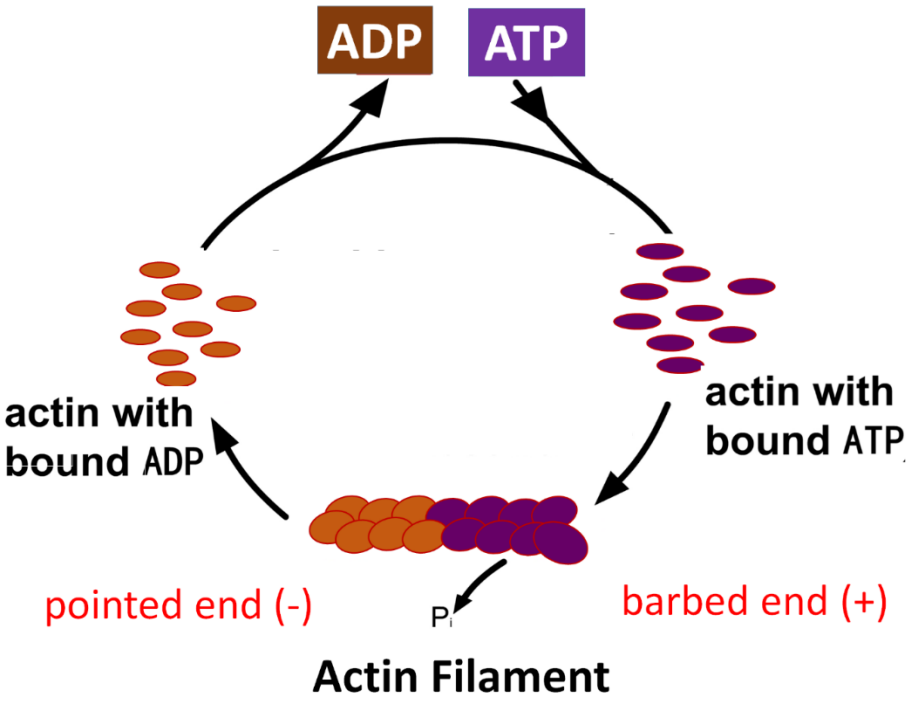

Mechanisms of actin nucleation and assembly

Nucleation is the first step in polymerization of the actin filaments, which starts by the aggregation of actin monomers to form a core of a stable multimer. Following the first dimerization, assembly of actin monomers continues at the fast growing barbed (+) end of the growing actin filament by recruiting new ATP-loaded monomers. ATP hydrolysis switches the monomer into a stable ADP-bound actin that is trapped in the filament, with the release of a phosphate (Figure 4). An actin-ATP cap can be formed on the barbed end due to slow ATP hydrolyzation due to high rates of polymerization (VAVYLONIS *et al.* 2005). The instability of the actin dimer and the activity of depolymerization factors that inhibit spontaneous assembly make actin nucleation the rate limiting step in actin filament assembly (CHESARONE and GOODE 2009). Cells use a wide range of actin nucleator/binding proteins to regulate actin dynamics by maintaining the pool of monomers and/or disassembly, severing, and cross linking of the actin filament (Lee and Dominguez 2010; URIBE and JAY 2009). Actin nucleator proteins include three groups: tandem-monomer-binding nucleators, the actin-related protein 2/3 (Arp2/3) complex and formins (Arp2/3 and Formins will be discussed in Chapter Four).

The tandem-monomer-binding nucleators are characterized by tandem repeats of G-actin binding motifs. Members of this group include the Cordon-bleu, Leiomodin, Junction Mediating Regulatory, Adenomatous Polyposis Coli and Spire proteins. These proteins are also known for having the actin binding motif Wiskott-Aldrich syndrome protein (WASP) homology 2 domain in addition to other protein binding elements

(WELCH *et al.* 1997). The last two sets of actin nucleator, the actin-related protein 2/3 (Arp2/3) are discussed below.

Figure 4. Mechanisms of actin assembly

A schematic diagram describes three means of actin assembly. (A) The spontaneous initiation of actin-filament assembly that starts by actin nucleation (formation of dimers or trimers). (B) The Arp2/3 complex actin assembly and its nucleation promoting factors activators, which produces branches of an existing actin filament. (C) Formin assembly of actin filaments, which depend on their formin homology domain (FH2) for polymerization and remains bound to the progressive barbed end during elongation.

Figure 4. Mechanisms of actin assembly

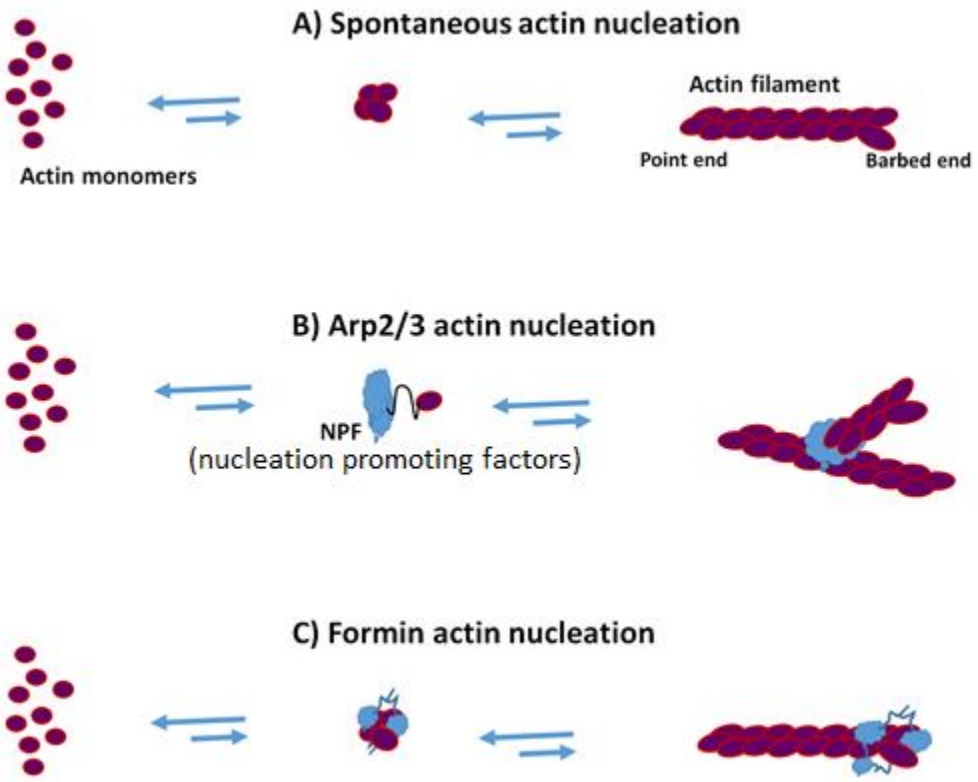

Actin-myosin interactions

Myosins are a superfamily of ATP-dependent motor proteins that are highly conserved in function and structure. Myosin is an actin-binding protein that uses actin filament as a track to move along and produce force for muscle contraction, cell division and other forms of cell motility (IKONEN *et al.* 1997; SWEENEY and HOUDUSSE 2010a; SWEENEY and HOUDUSSE 2010b). The typical structure of myosin proteins includes several light chains (MLC) and two heavy chains (MHC) composed of three domains (Figure 5). In the N-terminal half of the heavy chain lies the "head" domain, which is the most conserved region among myosins. The head is responsible for generating force and has the enzymatic Mg^{2+}-ATPase motor domains and the actin-binding regions. Adjacent to the head domain, the "neck" domain, which regulates the activity of the head domain and is associated with light chains. Finally, at the C-terminal half of the heavy chain lies the "tail" domain, which determines the specificity of myosin. The interaction between the myosin head and actin, which is ATP mediated, leads to the head sliding or "walking" along the actin filament. Myosin movement is mainly towards the (+) end of the actin filament, with the exception of myosin IV (IKONEN *et al.* 1997; SWEENEY and HOUDUSSE 2010a; SWEENEY and HOUDUSSE 2010b).

The actin-myosin interaction is responsible for contraction of both striated muscles and smooth muscles, albeit in different manners. The building units of striated muscles, sarcomeres, are composed of parallel arrays of myosin bundles (thick filaments) and actin bundles (thin filaments), and their interaction produces the muscle contraction. Smooth muscle myosin is usually composed of two essential light chains (eMLC), two regulatory light chains (rMLC) and two heavy chains (MHC) (CRAIG *et al.* 1983; SMITH

et al. 1983). Myosin interaction with actin and its Mg^{2+}-ATPase activity results in conformational changes of myosin head, which lead to its movement along the actin filament (UYEDA *et al.* 1996). Smooth muscle contraction is enhanced by Ca^{2+}release, which induces calmodulin that in turn activates the myosin light chain kinase (MLCK) (SMITH *et al.* 1987). Phosphorylation of rMLC by MLCK allows the assembly of non-muscle myosin motor protein complex, and thereby the contraction of the smooth muscle actin network (GRIFFITH *et al.* 1987). Dephosphorylation of the rMLC protein by the myosin light chain phosphatase (MLCP) causes the muscle relaxation, which makes the muscle ready for another cycle of contraction and relaxation (GRIFFITH *et al.* 1987; HARTSHORNE 1998). In *C. elegans,* embryonic elongation depends on a smooth muscle-like contraction, which occurs in lateral epidermal cells of the embryo. *C. elegans* myosin homologs include non-muscle myosin 1 and 2 (NMY-1/2), myosin light chain-4 (MLC-4), and the essential myosin light chain (MLC-5) (SHELTON *et al.* 1999a; PIEKNY *et al.* 2003).

Figure 5. Myosin and muscle structures

Domain structure of the myosin is organized from the N-terminus to the C-terminus as follows. The globular "head" domain contains the enzymatic Mg^{2+}-ATPase motor domains and the actin-binding regions. The "neck" domain is associated with light chains and is necessary for regulation of the head domain activity. At the C-terminal half of the heavy chain lies the "tail" domain, which determines the specificity of myosin binding. The interaction between the myosin head and actin, which is ATP mediated, allows the head to slide, or "walk", along the actin filament. (B) The sarcomere is the basic unit of a muscle structure. Sarcomeres are composed mainly of two alternatively overlapping layers of filaments: the thick filaments (myosin) and thin filaments (actin). The two proteins slide past each other when the muscles contract (lower panel) and relax (upper panel). Z line is a region that defines the end of a sarcomere.

Figure 5. Myosin and muscle structures

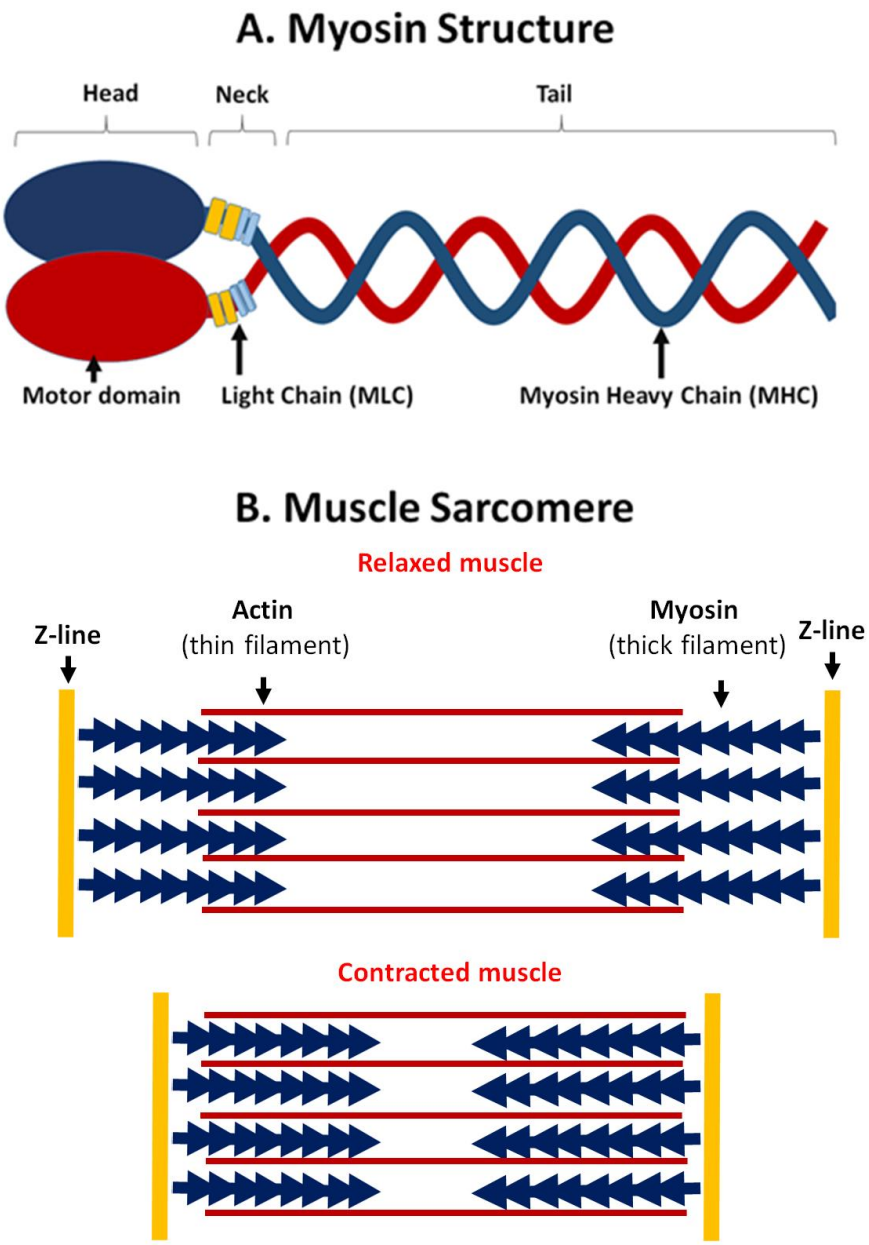

Small GTPase and actin organization

Small GTPases are a type of guanine nucleotide-binding protein (G-proteins) that binds to and hydrolyzes the guanosine triphosphate (GTP) and convert it to guanosine diphosphate (GDP). GTP bound G-protein is active, while GDP bound G-protein is inactive. Thus, GTPases can switch between on and off by hydrolyzing GTP to GDP. GTPase activating proteins (GAPs) can accelerate GTP hydrolysis, while activation of G-protein can be catalyzed by guanine nucleotide exchange factors (GEFs) (Figure 6) (FUKUHARA *et al.* 2000).

Members of the superfamily of Ras GTPases are involved in many cellular and developmental processes, including cell differentiation, cell division, and control of the cytoskeleton (ETIENNE-MANNEVILLE and HALL 2002). The *C. elegans* genome encodes five Rho family members, including Rho (*rho-1*), Cdc42 (*cdc-42*), Rac (*ced-10 and rac-2*) and MtlRac (*mig-2*) (LUNDQUIST 2006). Members of the Rho GTPase family and their effectors were found to be involved in the *C. elegans* axon pathfinding and embryonic elongation (PIEKNY *et al.* 2000; HALL and LALLI 2010). For instance, Rho GTPases such as Rac/CDC42 and the Rac GEF UNC-73 (Trio) have the ability to control axon extension in many systems including *C. elegans* (HALL and LALLI 2010). In *C. elegans* embryonic elongation, the Rho GAP RGA-2 and the Rho-binding kinase (ROCK) LET-502 achieve a balance of actomyosin-dependent forces required to control epidermal elongation (WISSMANN *et al.* 1997a; PIEKNY and MAINS 2002; PIEKNY *et al.* 2003; DIOGON *et al.* 2007).

Figure 6. Regulation of small GTPases

Small GTPases can regulate intracellular signalling by acting as molecular switches. Small GTPases bind to and hydrolyze GTP and convert it to GDP. Activation of small G-proteins is mediated by GDP/GTP GEFs and deactivation by GAPs. G-protein is active when bound to GTP, which enable it to bind to its effector molecules and transduce the signal. A G-protein is inactive when bound to GDP.

Figure 6. Regulation of small GTPases

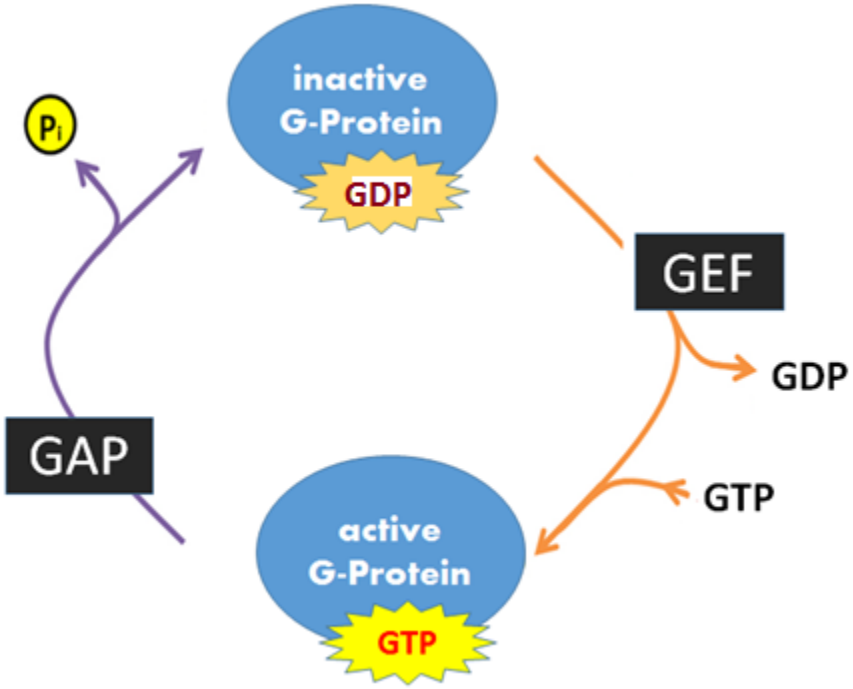

Introduction to axon guidance

Axon guidance is an important developmental step that is critical for successful embryonic development. Formation of a functional nervous system requires that neurons have to extend their axons, often over long distances, to reach their final targets. To achieve this, neurons respond to biochemical and mechanical forces. These processes are controlled by highly-conserved families of guidance molecules. Guidance molecules can either repel or attract a highly specific structure found at the growing end of the axon, the growth cone (Figure 7). Upon receiving guidance cues, receptors in the growth cone trigger a series of changes that affect the final decision of the axon, causing it to either extend further or retract.

Guidance cues ultimately influence cytoskeletal components that determine the structure and motility of growth cones, thereby controlling axon guidance (SCHMITZ *et al.* 2007; O'DONNELL *et al.* 2009). The neuronal growth cone sends out finger-like projections called filopodia and sheet-like projections called lamellipodia, which contain dense and highly polymerized actin microfilaments (Figure 7). Growth cones, in response to guidance cues, extend toward attractive cues and retract from repulsive cues, which result in axon's attachment or detachment from the substrate. Accordingly, the dynamics of filopodial and lamellipodial projections reflect the patterns of actin polymerization and depolymerization (MERZ and CULOTTI 2000). It is worth noting that it is not the guidance cues that have the ultimate decision to direct the growing axon, but rather the type of receptors on the surface of the growth cone and how they interpret the incoming signal (HUBER *et al.* 2003; SCHMITZ *et al.* 2007; O'DONNELL *et al.* 2009).

Figure 7: Neuron and growth cone structures

(A) A simplified structure of a neuron, which is characterized by having a long process (axon) extending out from its cell body (soma). Branching from the cell body are tree-like structure, dendrites, which receive signals form adjacent neurons and deliver them to the cell body. (B) The structure of the growing tip of the exon, the "growth cone", which is essential for neuronal axon pathfinding. Actin cytoskeleton dynamics determine the shape of the growth cone, where it forms projections beyond the leading edge, containing actin bundles (filopodia) or an actin mesh (lamellipodia).

Figure 7. Neuron and growth cone structures

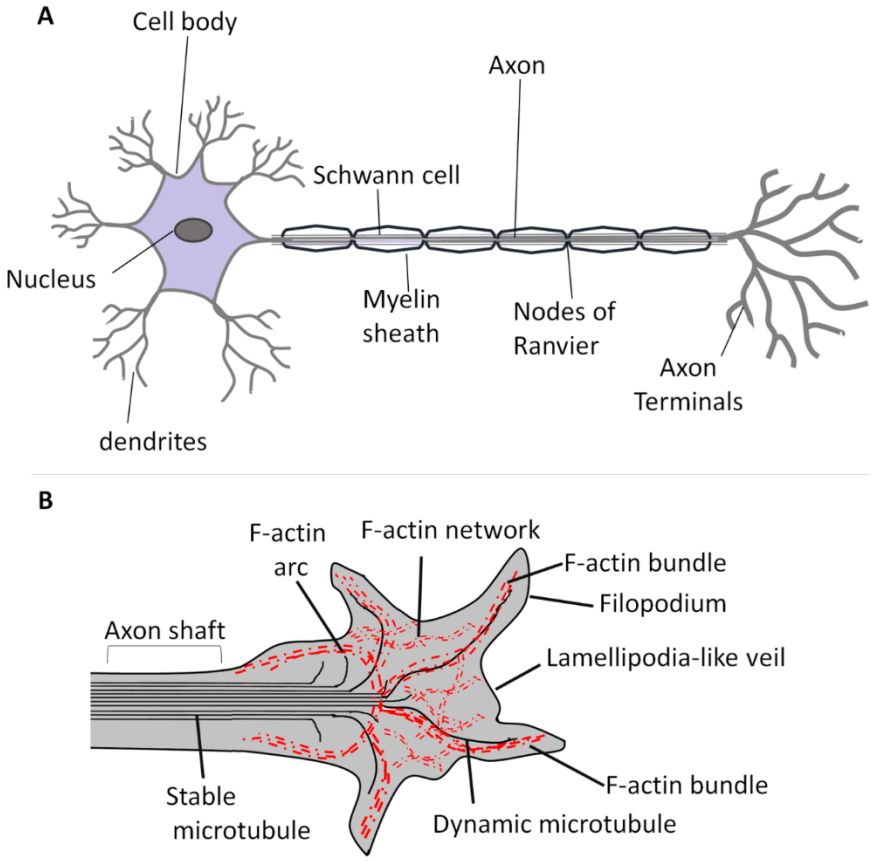

Genetic analysis identified four essential families of guidance cues and their receptors that are highly conserved in both vertebrates and invertebrates, including (i) semaphorins and their plexin and neuropilin receptors; (ii) Netrins and their Deleted in Colorectal Carcinoma (DCC) and UNC5 receptors; (iii) Slits and their roundabout (Robo) receptors, and (iv) Ephrins and their Eph receptors. In *C. elegans*, there are three semaphorins: two trans-membrane molecules, SMP-1 and SMP-2, which signal through the PLX-1 plexin receptor (TESSIER-LAVIGNE and GOODMAN 1996; CASTELLANI and ROUGON 2002; FUJII *et al.* 2002), and one secreted molecule, MAB-20, which signals through the PLX-2 receptor. UNC-6 is the *C. elegans* homolog of the vertebrate Netrin and it has two receptors, UNC-40/DCC and UNC-5. EVA-1 acts cell-autonomously with SAX-3 as Robo receptors for SLT-1, the only slit protein in *C. elegans* (HAO *et al.* 2001; FUJISAWA *et al.* 2007). VAB-1 is the sole Ephrin receptor in *C. elegans* that receives signals from four potential GPI-modified ephrins (EFN-1, EFN-2, EFN-3 and EFN-4) (GEORGE *et al.* 1998; ARVANITIS and DAVY 2008). Moreover, many other molecules were identified to play a role in axon guidance, along with their original functions in other developmental contexts. For instance, members of the immunoglobulin (Ig) and cadherin super families and cell-adhesion molecules (CAMs) were found to regulate some aspects of axon pathfinding. Additionally, morphogens and growth factors such as members of the Hedgehog (Hh), transforming growth factor beta (TGFβ), and the Wnt signaling pathway have been described for function in neuronal wiring in diverse organisms (CHILTON 2006).

Intermediate targets in axon guidance

To reach their final targets, axons use intermediate targets to break the distance down into a series of shorter trajectories. In the grasshopper limb bud, the Ti1 neuron uses the neuronal somata, known as "guidepost cells", as land marks to navigate its way to the central nervous system (CNS) (BATE 1976; BENTLEY and CAUDY 1983; COLAMARINO and TESSIER-LAVIGNE 1995; HIDALGO and BOOTH 2000; ARAUJO and TEAR 2003; HIDALGO 2003; HUTTER 2003; COLON-RAMOS and SHEN 2008; RAPER and MASON 2010). Ablation of guidepost cells results in the failure of the Ti1 axon to complete its trip to the CNS (BATE 1976; BENTLEY and CAUDY 1983; COLAMARINO and TESSIER-LAVIGNE 1995; HIDALGO and BOOTH 2000; ARAUJO and TEAR 2003; HIDALGO 2003; HUTTER 2003; COLON-RAMOS and SHEN 2008; RAPER and MASON 2010). A more compelling example for intermediate targets is the midline of the ventral nerve cord (VNC) or the floor plate that are described in both vertebrates and invertebrates (BATE 1976; BENTLEY and CAUDY 1983; COLAMARINO and TESSIER-LAVIGNE 1995; HIDALGO and BOOTH 2000; ARAUJO and TEAR 2003; HIDALGO 2003; HUTTER 2003; COLON-RAMOS and SHEN 2008; RAPER and MASON 2010). Upon reaching the midline, the commissural neuron axons decide whether to cross from one side of the nervous system to the other.

In *C. elegans*, axons join the VNC and choose either to fasciculate on the left or right side, extend over the midline to the contralateral side or extend ipsilaterally on their side (HUTTER 2003; HUTTER *et al.* 2005). Changes in directions require changes in cues impinging on the growth cone as it migrates to new locations. Thus, growth cones of

developing axons are often subjected to opposing gradients of attractive and repellant cues. Molecular guidance cues include both secreted molecules and trans-membrane molecules (e.g., adhesive cues). These cues are produced by neurons and non-neuronal support cells that can provide a substrate to direct the growth of the axons of new neurons.

Pleiotropic nature of guidance molecules

Some of the guidance molecules are characterized as either attractive or repulsive cues. Many guidance cues are known for their pleiotropic nature, where a cue can induce antagonistic effects on the growing axon, i.e., repulsive or attractive, according to the environmental context. A compelling example of a dual-function signaling molecule is the class 3 semaphorins that initially were characterized according to their role in repulsive axon guidance. Sema3E repels through its receptor Plexin-D1, whereas in the presence of the co-receptor neuropilin 1 (Npn-1) this repulsive effect converts to attraction (CHAUVET *et al.* 2007). Similarly, the UNC-6/Netrin guidance cue can trigger attraction or repulsion of a growing axon, depending on the composition of its receptors on the surface of the growth cone. The Netrin receptor UNC-40/DCC mediates Netrin-induced axon attraction in *C. elegans, Drosophila* and vertebrates. However, the other receptor, UNC-5, in *C. elegans* and its vertebrate homologs mediate Netrin-induced axon repulsion (ROUND and STEIN 2007).

The nervous system of *C. elegans* consists of 302 neurons that can be easily followed through development and visualized *in vivo* with GFP reporters, since the worm is transparent. As a result, *C. elegans* has had a prominent role in the identification of the essential genes and mechanisms (described above) that are necessary for normal axon

guidance. Interestingly, the basic mechanisms and molecules involved in axon guidance are conserved amongst the invertebrates and vertebrates (CHISHOLM and TESSIER-LAVIGNE 1999; YU and BARGMANN 2001; DICKSON 2002). Thus, the study of the simple model systems such as *C. elegans*, which allows the use of classical genetic analyses and mutagenesis, will improve our understanding of the neuronal development in human.

The pharynx of C. elegans as a model for axon guidance

The pharynx (or foregut) of *C. elegans* presents an excellent model to study cell-cell interactions during development. The pharynx is a neuromuscular organ that is mainly responsible for food intake (typically the *E. coli* strain OP50 in the laboratory) and initiation of digestion. The pharynx is divided into distinct anatomical regions which are, from anterior to posterior, the procorpus, the metacorpus, the isthmus, and the terminal bulb (Figure 8).

The *C. elegans* pharynx begins as a ball of cells originating from various cellular lineages; these pharyngeal cells cluster into a primordium surrounded by a basal lamina (SULSTON *et al.* 1983). The pharyngeal cell identity is conferred early in development by the forkhead transcription factor gene *pha-4* (GAUDET and MANGO 2002). At a later stage in development the pharyngeal primordium undergoes morphogenesis and gives rise to a mature pharynx. Morphogenesis of the pharynx occurs during embryonic elongation and during this time the primordium elongates and acquires the unique bi-lobed shape of the mature pharynx (SULSTON *et al.* 1983; PORTEREIKO and MANGO 2001). Prior to elongation of the pharynx, the primordial cells attach anteriorly to the buccal cavity. Pharynx elongation is coupled to the elongation of the embryo as a whole, which occurs between 400 and 640 minutes post-fertilization and is due to circumferential smooth

muscle like contraction within the epidermis. The length of the embryo increases about four-fold during elongation, while it becomes three-fold thinner (SULSTON *et al.* 1983).

The mature pharynx is composed of 80 cells, and several of these cells are multinucleate as a result of cell fusions. Pharyngeal cells are categorized into five types: neurons (20), muscles (37 nuclei), marginal cells (9 nuclei), epithelial cells (9), and gland cells (5) (ALBERTSON and THOMSON 1976; SULSTON *et al.* 1983). Sometimes two additional types of cells, arcade cells (9) and pharyngeal intestinal valve cells (6), are considered pharyngeal cells, although they are not encompassed by the pharyngeal basement membrane, for a total of 95 nuclei (Mango, 2007). The variety of cell types in the pharynx makes it a suitable model for the study of cell-cell interactions during organogenesis. The current study focuses on the mechanisms and molecules required for axon guidance of the pharyngeal neuron M1.

Figure 8. The *C. elegans* pharynx

Nomarski DIC image of the *C. elegans* pharynx (A). The mature pharynx is composed of 80 cells, which are categorized into five types (shown in diagrams): gland cells (B), neurons (C), muscles (D), epithelial cells (E), and marginal cells (F) (ALBERTSON and THOMSON 1976; SULSTON *et al.* 1983).

Figure 8. The *C. elegans* pharynx

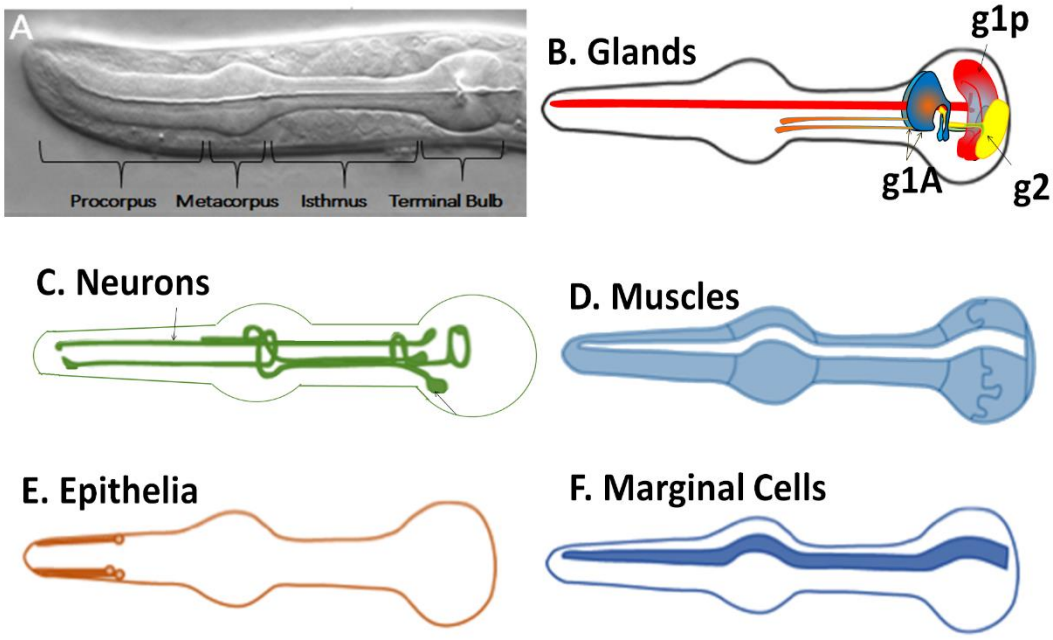

Pharyngeal nervous system

The pharynx has its own nervous system that is largely separated from the main nervous system. The pharyngeal nervous system is organized into four general structures: two subventral nerve cords, one dorsal nerve cord and one circular nerve ring located within the posterior half of the metacorpus. The pharyngeal neurons are thought to regulate the rhythmic contractions of the pharynx, though ablation of most of these neurons in the adult worm has no visible effects on pharyngeal function (AVERY and HORVITZ 1989; AVERY 1993; AVERY and THOMAS 1997; PILON and MORCK 2005). Therefore, severe defects in some pharyngeal neurons should still produce viable worms, which constitute a potential advantage for mutant screens. For example, mutants with severe M2 motorneuron defects are viable (MORCK *et al.* 2003). Despite the ambiguity of their function, pharyngeal neurons are thought to play an instructive developmental role in the pharynx. For example, the pharyngeal interneuron I5 expresses the guidance cue UNC-6, while the interneuron I4 secretes another guidance molecule, UNC-129 (WADSWORTH *et al.* 1996). These data imply that these two pharyngeal neurons play a role in axon guidance of other neurons in the pharynx (e.g., *unc-6* mutants have abnormal M2 motorneuron trajectories) (ALBERTSON and THOMSON 1976; WADSWORTH *et al.* 1996; AVERY and THOMAS 1997; GRAHAM *et al.* 1997; PILON and MORCK 2005).

Each of the 20 individual neurons in the *C. elegans* pharynx has a unique axonal trajectory. My research is focused on how one of these neurons, the motorneuron M1, establishes its trajectory. The M1 motorneuron has its cell body located in the posterior bulb and sends an axon along the length of the pharynx. The M1 axon has four distinct

components to its trajectory. In Chapter Three, I will demonstrate that each of these components are regulated differently.

Pharyngeal glands

There are five pharyngeal glands, which are further divided into two sub-groups, g1 (the left and right g1A cells and g1P) and g2 glands (left and right), based on their appearance in electron micrographs. The pharyngeal gland cell bodies lie in the posterior bulb of the pharynx. All five glands have cellular projections that connect to the pharyngeal lumen at discrete points along the length of the pharynx. Each g1 cell sends a projection anteriorly, and each projection is within the pharyngeal nerve cord. Two of these projections extend from g1A cells and pass through the isthmus before emptying into the pharyngeal lumen near the anterior bulb. The posterior g1P gland projection travels much farther and empties near the anterior limit of the pharynx. The g2 cells have shorter projections, which empty into the lumen of the posterior bulb (ALBERTSON and THOMSON 1976) (Figure 8B). The transcription factor HLH-6 is necessary for pharyngeal gland development and function (SMIT *et al.* 2008).

My work showed that ablation of glands resulted in defects of the M1 axon at the region where it contacts the g1P gland, suggesting a role for glands in axon guidance in the pharynx. Since axon guidance mechanisms and molecules are mainly conserved between vertebrates and invertebrates, our understanding of axon guidance in the *C. elegans* pharynx may add to our knowledge of axon guidance in human and other organisms.

The model organism C. elegans

The nematode *C. elegans* is a powerful tool for genetic analysis that has many advantages. In addition to being very easy to propagate and maintain, it has a short life cycle (two generations a week), is self-fertilizing (hermaphroditic) and has a large broad size (BRENNER 1974). The animal is small in size, with adult being 1.2 mm long and containing only 959 somatic nuclei. Moreover, *C. elegans* has a simple body structures with all cell lineages known (SULSTON and HORVITZ 1977; SULSTON *et al.* 1983) and a sequenced genome (CONSORTIUM 1999). The worm community has many shared resources, including the Wormbase.org database, the *Caenorhabditis* Genetics Center (a strain center that distributes mutant and transgenic strains), an RNAi (RNA interference) library (containing bacterial RNAi clones for knocking down of almost 85% of *C. elegans* genes), two knockout consortia (generating knockout alleles for nearly every gene). The transparency of the worm body as well as the availability of cell-specific promoter constructs, antibodies and GFP (green fluorescent protein) make cellular identification and live imaging in *C. elegans* relatively easy. Nomarski differential interference microscopy (DIC) allows live embryos and animals to be viewed at high resolution.

C. elegans embryogenesis is well characterized, with the timing of events and cell numbers as well as animal shape known for every embryonic stage. Embryonic development is rapid and takes only about 12 hours from the first cleavage to the hatching of the freely moving larva. Mutations that cause embryonic arrest at many of the embryonic stages are available and provide a great opportunity to study embryonic morphogenesis. Genetic interactions that underline embryonic elongation can be tracked

using available mutants and RNAi. These advantages make the *C. elegans* a valuable tool for understanding the molecular basis of embryonic development in larger organisms, such as humans, where the process is much more complicated and much less amenable to genetic manipulation.

Chapter Two: **MATERIALS AND METHODS**

A. Materials and methods for the axon guidance analyses

"*Work presented in this section was published in (REFAI et al. 2013). It was written by me (Osama Refai) and edited by my supervisor (Paul E. Mains). Experiments were mainly designed by me, with my previous supervisor (Jeb Gaudet) and my current supervisor (Paul E. Mains). Patricia Rohs, a previous undergraduate student in the Gaudet Lab, participated in the cell ablation experiments*."

Nematode strains and culture

C. elegans var. Bristol was used as the reference wild type (BRENNER 1974). Standard methods for the culture, manipulation and genetics of *C. elegans* were employed (SULSTON and HODGKIN 1988). All strains were cultured at 20° unless otherwise stated. The following mutations were used. Alleles with an "*iv*" designation were derived in this study. Descriptions of all others are found at www.wormbase.org. Linkage group (LG) I:*lin-17(n3091), mab-20(bx24), smp-1(ev715), smp-2(ev709), unc-40(e271), unc-73(e936), rig-5(hd48), pry-1(mu38), mnm-8(iv82).* LG II: *vab-1(dx31*and*e2), rig-6(gk376), plx-2(ev773).* LG III: *unc-69(e587), unc-119(e2498), mnm-7(iv77* and *iv90), cdh-4(ok1323).* LG IV: *unc-5(e53), unc-129(ev554), rig-4(hd47), mnm-6(iv88), egl-20(hu105), plx-1(ev724), ced-3(n717).* LG V:*vab-8(ct33) dpy-11(e224), unc-34(e315), unc-51(e369) dpy-21(e428), unc-51(iv84), him-5(e1490), unc-76(e911), rpm-1(js317, ur299, iv78, iv79, iv80* and *iv81), fmi-1(rh308),ced-10(n1993).* LG X: *sax-3(ky123), slt-1(eh15), unc-6(ev400* and *e78), unc-115(e2225), rig-1(hd15), wrk-1(hd45), rig-3(hd51), rig-2(hd18), ncam-1(hd49), mig-2(mu28), egl-15(n484).* The *mab-20(bx24), smp-1(ev715), smp-2(ev709), plx-1(ev724), plx-2(ev773)* and *smp-1(ev715); smp-*

2(ev709) strains included *him-5(e1490).* The *smp-1(ev715); smp-2(ev709)* strain was generously provided by J. Culotti (GINZBURG *et al.* 2002). The octuple mutant *rig-5; rig-6; rig-4; rig-1 wrk-1 rig-3 syg-1 ncam-1*was a kind gift from H. Hutter (SCHWARZ *et al.* 2009). *rpm-1(ur299)* was kindly provided by W.G. Wadsworth (LI *et al.* 2008).

In all of our experiments, the five pharyngeal gland cells, including g1P, were visualized using the gland markers *hlh-6::yfp, hlh-6::mTomato* (SMIT *et al.* 2008) or *phat-1::wCherry*, which is a worm-optimized form of mCherry. The integrated worm transgene *ivIs26[phat-1::wCherryglr-2::gfp pRF4(rol-6(su1006))] I* and the following transgenic lines were developed for this work:*ivEx136[glr-2::gfp hlh-6::mTomato rol-6(su1006)]*,*ivEx138[hlh-6::egl-1 glr-2::gfprol-6(su1006)], ivEx139[ceh-2::egl-1 glr-2::gfpelt-2::mTomato rol-6(su1006)], ivEx140[ceh-2::egl-1 ceh-2::gfpelt-2::mTomato rol-6(su1006)], ivEx143[hlh-6::egl-1 ceh-2::egl-1 elt-2::mTomato], Ex144[ceh-2::gfp elt-2::mTomato], ivEx272[glr-2::gfprol-6(su1006)], ivEx273[glr-2::wCherryrol-6(su1006)], ivEx366[hlh-6::egl-1 hlh-6::yfp elt-2::mCherry rol-6(su1006)], ivEx387[phat-1::wCherry glr-2::gfp pRF4(rol-6(su1006))]*.

Chi square was used to calculate the p-values to test for statistical significance between strains.

Construction of transgenic lines

All reporters were made by PCR amplification of promoter fragments from genomic DNA, followed by cloning into either pPD95.77, pPD95.77-YFP (gifts from A. Fire) or pJH1774 (a gift from M. Zhen), which contain the coding sequence for *gfp*, *yfp* or *wCherry*, respectively. The M1 reporters were constructed by PCR amplification of the *glr-2* promoter (1.7 kb upstream of the ATG), followed by cloning into pPD95.77 or

pJH1774. Similarly, I3 reporter was constructed by PCR amplification of the *ceh-2* promoter (1.6 kb upstream of the ATG), followed by cloning into pPD95.77.

Transformation was carried out as described by (MELLO and FIRE 1995). DNA was injected at 20–30 ng/mL together with 50 ng/mL pRF4 *(rol-6(su1006))*, which confers a dominant Roller phenotype (MELLO *et al.* 1991) and sufficient pBS II (SK+) to bring the total DNA concentration to 100 ng/mL. For some analyses, we included 20 ng/mL of an intestine specific reporter, *elt-2::tdTomato::HIS2B* (FUKUSHIGE *et al.* 1998) that served as an independent marker for transgenic arrays. Extrachromosomal arrays were integrated using 3,000 R of gamma-irradiation following the standard methods and were outcrossed five times to N2 background.

Cell ablation

To induce gland cell death, the *hlh-6::egl-1* construct was injected at 20 ng/mL with 20 ng/mL *elt-2::mTomato::HIS2B*, 30 ng/mL pBS II (SK+) and 20 ng/mL *hlh-6::yfp* as described (SMIT *et al.* 2008). Transgenic (*i.e., elt-2::tdTomato::HIS2B*expressing) embryos were collected at different times to analyze the efficiency and timing of the gland cell death as assessed by YFP expression. Embryos were mounted on 2% agarose pads and scored with a Zeiss Axioplan compound microscope. I3 ablation was induced using the ce*h-2::egl-1* construct, which was injected at 20 ng/mL with 20 ng/mL *elt-2::mTomato::HIS2B*, 30 ng/mL pBS II (SK+) and 20 ng/mL *ceh-2::gfp*. GFP negative, *elt-2::mTomato* positive L4 and young adult transgenics were scored under the fluorescent microscope to determine I3 ablation efficiency.

Screen for M1 neuron defects mutants

EMS Mutagenesis was carried out according to the standard protocol (SULSTON and HODGKIN 1988). Mutagenized *ivIs26[phat-1::wCherry glr-2::gfp pRF4(rol-6(su1006)]* hermaphrodites, which carry reporters for the M1 neuron and gland cells, were cultured on 9 cm plates in groups of five at 20°. Four days later, L3 and L4 F1 progeny were placed individually on 35 mm plates and cultured at 15° or 20°. Between 6 and 9 days later, F2 or F3 L1 progeny were screened under a fluorescence dissecting microscope for individuals with abnormal M1 neurons. Mutations were outcrossed at least five times to wild type. Mutants were mounted on 2% agarose pads, paralyzed with 100 mM levamisole and scored with a Zeiss Axioplan compound microscope for detailed analysis. Unless stated otherwise, we scored defects in newly hatched L1 larva.

Mapping of mutations

Single Nucleotide Polymorphism (SNP) mapping was carried out as described by Wicks et al (WICKS *et al.* 2001) and Davis et al (DAVIS *et al.* 2005). The *ivIs26[phat-1::wCherry glr-2::gfp pRF4(rol-6(su1006)]* bearing mutants were crossed with Hawaiian strain (CB4856) males. For each mutation, fifty M1 defective F2 segregants and fifty M1 normal F2 animals were separately pooled and lysed following standard protocols (DAVIS *et al.* 2005). The mutant and non-mutant lysates were then separately used as DNA templates for PCR amplification as described (DAVIS *et al.* 2005). We used primer pairs for SNP markers described at genome.wustl.edu or from (DAVIS *et al.* 2005). Mutations that mapped to the same chromosome and had similar phenotypes were tested for complementation.

B. Materials and methods for the embryonic elongation analyses

Strains used for embryonic elongation analysis

The following alleles were used: *let-502(sb118) I, fhod-1(tm2363)I, wve-1(ok3308) I, mel-11(it26) II, fem-2(b245)III, frl-1(ok460) III, inft-1(gk386)III, pat-4(st551) III* (rescued by *zpEx184[myo-3::pat-4(+)]*), *inft-2(ok1296)V, fozi-1(ok1182)III, cyk-1(or36)III, wsp-1(gm324) IV,daam-1(tm2133)V*. These mutations are described in Wormbase.org and were obtained from David Pruyne (State University of New York Upstate Medical University), the *Caenorhabditis* Genetics Center or were isolated in our lab. Alleles were often linked to visible morphological markers and the following balancers were also used: *hT2[bli-4(e937) let-?(q782) qIs48](I;III), mnC1[dpy-10(e128) unc-52(e444)]II, qC1[dpy-19(e1259) glp-1(q339)] III, mls10[myo-2:gfp] V*, FHOD-1::GFP analysis were carried out using the following strain: *unc-119(ed4) III; qaIs8004[unc-119(+) fhod-1::gfp]* (a gift from D. Pruyne). *lin-26p::ABD$_{vab-10}$::GFP* was used to visualize actin (Gally et al., 2009).

Screening for elongation defects

The elongation phenotype of the seven formin mutants was examined. Elongation defects were categorized into four groups according to the time of arrest (see Results). Judgments were made using a dissecting stereomicroscope. Screening for redundancy between formins was carried out by RNA interference (RNAi) by feeding according to the standard protocol (FIRE *et al.* 1998; FRASER *et al.* 2000; KAMATH *et al.* 2001). RNAi clones were chosen from the Ahringer RNAi library (www.lifesciences.sourcebioscience.com/) and confirmed by sequencing (all sequencing was done at University of Calgary DNA Services). Bacteria carrying an RNAi clone that

targeted the gene of interest were grown and seeded onto NGM agar plates, which included isopropyl l β-D-1-thiogalactopyranoside (IPTG), tetracycline and ampicillin. Plates were kept in dark at 4°C for subsequent use. Three L3 or L4 larvae were transferred to the RNAi plate and kept at the desired temperature and subsequently transferred to a fresh RNAi plate twice every 24 hours. After removing the hermaphrodites, the brood on the third plate was scored, as RNAi should have taken effect. The plate was scored 24 and 48 hours after hermaphrodite removal to assess the hatching and adulthood percentages, respectively (MAINS *et al.* 1990). All analyses were carried out at 25ºC, except if otherwise mentioned.

DIC microscopy

To examine the elongation phenotype of unhatched embryos, hermaphrodites were moved to fresh plate and allowed to lay eggs for few hours. Embryos were mounted with a drop of M9 buffer (6 g Na_2HPO_4, 3 g KH_2PO_4, 5 g NaCl, 0.25 g of $MgSO_47H_2O$ per litre H_2O) on a 2% agar pad. Cover slips were sealed with Vaseline, and examined with a Carl Zeiss Axio Imager 2 microscope and images where taken by AxioCam camera collected with Axiovision software (Carl Zeiss). Photos were taken every hour.

Immunostaining and microscopy

Immunostaining was carried out using the methanol-acetone method as described in (VANNESTE *et al.* 2013). Embryos were placed on polylysine-coated slides and freeze cracked. Slides were fixed in MeOH at −20°C and rehydrated in an ethanol/PBS (phosphate buffered saline) series and blocked with bovine serum albumin plus normal goat and donkey serum (Jackson ImmunoResearch). After blocking, slides were incubated with the primary antibodies anti-GFP (diluted 1:100) and MH27 (anti-AJM-1;

specific for epidermal adherens junction, (a kind gift from the McGhee Lab) (FRANCIS and WATERSTON 1991; DING *et al.* 2004) (1:200) overnight at 4°C. After washing in PBS, slides were incubated for 1 hour at 37°C with the two secondary antibodies: anti-mouse Alexa Fluor 488 and anti-rabbit Alexa Fluor 568 (Invitrogen) (each diluted 1:400). Slides were washed in PBS containing 5 mg/ml 4', 6-diamidino-2-phenylindole (DAPI, a fluorescent stain for the nucleus as it binds strongly to A-T rich regions in DNA) and mounted in a drop of ProLong® Gold Antifade Mountant (Invitrogen). Embryos were examined with a Zeiss Axio Imager 2 microscope. Images where taken by AxioCam camera and collected with Axiovision software (Carl Zeiss).

Isolation of RNA and RT-PCR

Gravid hermaphrodites were treated with alkaline hypochlorite using standard protocols and embryos were collected using a sucrose suspension (SHAI 2006). Total RNA was isolated from both gravid adults and embryos using the TRIzol® Plus RNA Purification System (Invitrogen). Reverse transcription PCR (RT-PCR) was carried out using the Pure High Capacity cDNA Reverse Transcription Kit (Applied Biosystems®). Two sets of primers were designed at the N-terminus and C-terminus of *fhod-1* cDNA (Table 1). To clone the full cDNA of *fhod-1*, I designed three sets of PCR primers that cover the whole length of the predicted cDNA (Table 1). Embryonic lysate was tested for expression of adult-specific *vit-2* to assess contamination from adult RNA. PCR products of the appropriate size were extracted from gels and were sequenced to confirm their identity. Sequences were compared to the available *fhod-1* sequence at Wormbase.org.

Sequence analyses

Sequence alignments of FHOD proteins from different organisms were carried out using Clustal2.1 tools (www.ebi.ac.uk/Tools/msa/clustalo/). The amino acid sequence of the novel *C. elegans fhod-1* short isoform was predicted using Sequence Translation tool (http://www.ebi.ac.uk/Tools/st/). Protein domain predictions were carried out using InterPro tool (http://www.ebi.ac.uk/interpro/). NCBI protein search tools and other free bioinformatic tools were used to identify protein domains.

Table 1. Primers used in PCR and RT-PCR experiments for *fhod-1* isoform cloning

Primer	Sequence	Experiment
Nterm-F	ACGACGACGACACATTCACC	(prime.set#1) & N-terminus identification
Nterm-R	CTCTCCACCACCACCTTCC	N-terminus identification
Cterm-F	CAATAAGACACGTGGAAAGATATGG	C-terminus identification
Cterm-R	CTCTACGTCGTTGATCTCTTGG	C-terminus identification
FhdNR.3	CACTCTCGTCGGTTTCTTTCG	(prime.set#1)
Shrt.1F	CCGATTCAGTTGGTTCAGGA	(prime.set#2)
Shrt.1R	ATTCCCATCGCAACTTTGAA	
Shrt.2F	CTTCGTCTTTGGCTATTCACC	(prime.set#3)
Shrt.2R	TAGTAGTTTGTTTCGAGCTGTCCA	
vit2-F	GCCAGAAGAACCAGAGAAGCC	*vit-2* identification
Vit2-R	TGTTGTTGCTGCTCGACCTC	
wGFP-R	CCATCTAATTCAACAAGAATTGGG	Validating the *fem-2::gfp* construct
wGFP-F	GAGTTTGTAACAGCTGCTGGG	

Constructing the fem-2::gfp expressing strain

The *fem-2::gfp* fosmid construct was supplied by TransgeneOmics (www.mpi-cbg.de). The transgene was validated following the provided protocol (SAROV *et al.* 2006). The primers wGFP-R and wGFP-F were designed to confirm the presence of the GFP tag in the isolated clone by sequencing. The GFP positive clones were injected into the N2 wild-type strain at 20 ng/µL along with 50 ng/µL of the dominant Roller marker pRF4 (*rol-6(su1006)*) (MELLO *et al.* 1991) and 30 ng/µLpBlueScript II SK (+). Worms of mixed stages were mounted with 25 mM levamisole (anesthetizing solution) on 2% agar pads, sealed with a cover slip and examined immediately. Embryos were dissected out of hermaphrodites and mounted on agar pads and examined by time lapse with a Carl Zeiss Axio Imager 2 microscope. Images where taken by AxioCam camera and collected with Axiovision software (Carl Zeiss).

fem-2 cDNA constructs for rescuing experiments

All PCR products and enzymatic digestion fragments were gel purified and confirmed by sequencing. The ligation orientation was confirmed by diagnostic digestion with relevant restriction enzymes. Sequence information available at www.wormbase.org (WS244 data freeze) was used to design primers for cloning of the *fem-2, elt-3, ceh-16* and *myo-3* promoters and the *unc-54* 3'UTR (Table 2). The *fem-2* cDNA pDP#DH014 plasmid (pGEX-Sal vector) was a kind gift from D. Pilgrim (PILGRIM *et al.* 1995; HANSEN and PILGRIM 1998). The full-length cDNA was amplified out of the vector by PCR using the two primers *fem*2-F and *fem*2-R, which introduce the cut sites of *PstI* and *NotI*, respectively. The PCR product was digested with *PstI/NotI* and then ligated into pBS II (SK+) previously digested with same set of enzymes. The *3'-UTR* of *unc-54* was

cloned from genomic DNA using unc54-F and unc54-F primers (Table 2), which introduce *NotI* and *SacII* restriction sites, respectively, and introduced to the 3'end of the *fem-2* cDNA in the pBS II (SK+) vector. Incorporation of 3'UTR regions generally enhance the transgenic expression in various systems (BUCHMAN and BERG 1988; CHOI *et al.* 1991; BRUNET *et al.* 2003). Promoters of *fem-2*, *elt-3, ceh-16* and *myo-3* were amplified by PCR from genomic DNA and digested by *KpnI* and *PstI,* which cut on sites introduced by the two primer sets (Table 2) and then ligated separately into the pBS II (SK+) vector that had the *fem-2* cDNA and *unc-54* 3' UTR.

Each of the four constructs was injected into the *fem-2; fhod-1* mutant strain at 2 ng/µL, together with 20 ng/µL of the gut-specific reporter (*elt-2::GFP::LacZ)* (FUKUSHIGE *et al.* 1998), 50 ng/µL of the dominant Roller marker pRF4 (*rol-6(su1006)*) (MELLO *et al.* 1991), and 48 ng/µL pBS II (SK+). For every *fem-2* cDNA plasmid, two transgenic lines were isolated from independent injections. Chi-squared analysis was carried out to determine significance of changes of phenotype frequencies between the strains that carry rescuing *fem-2* cDNA constructs.

Table 2. Primers used for construction of rescuing plasmids

Primer	Sequence	Product size	Enzymes
fem2-F	tttctgcagATGGAAAAAGTAAACGAGGAGC	1350bp	PstI/NotI
fem2-R	tttgcggccgcTTATTCCTCATCAGTGACATCG		
femPr-F	tttggtaccTTTTTGATCCATTTTTGATTTGATAA	299bp	KpnI/PstI
femPr-R	tttctgcagGTATTTTTCCAGTTTTAAAACC		
elt3-F	tttggtaccCGTTAAATGCTCCAATAAAGTTT	1900bp	KpnI/PstI
elt3-R	tttctgcagTTGAATTCTGTAACTGAAAATTTG		
ceh16-F	tttggtaccCCACAAGTTTTTGGCCGA	2900bp	KpnI/PstI
ceh16-R	tttctgcagCCCCGCTCTAAGGAAGCT		
myo-F2	tttggtaccTGTGTGTGATTGCTTTTTCAC	1994bp	KpnI/PstI
myo-R2	tttctgcagTGGATCTAGTGGTCGTGG		
unc54-F	TTTGCGGCCGCGTCCAATTACTCTTC	304bp	NotI/SacII
unc54-R	tttccgcggGTGTGCGGTTTTTTCTATGATG		

Chapter Three: **GENETIC ANALYSIS OF THE M1 NEURON AXON EXTENSION**

"*Work presented in this chapter was published in (REFAI et al. 2013), unless otherwise stated. It was written by me (Osama Refai) and edited by my supervisor (Paul E. Mains). Experiments were mainly designed by me, with my previous supervisor (Jeb Gaudet) and my current supervisor (Paul E. Mains). Patricia Rohs, a previous undergraduate student in the Gaudet Lab, participated in the cell ablation experiments*."

BACKGROUND

During development, axons navigate towards their final targets in a highly dynamic and precisely regulated process. Correct axon targeting requires the combined action of a variety of conserved signaling molecules sensed by the growth cone (CHISHOLM and TESSIER-LAVIGNE 1999; YU and BARGMANN 2001; DICKSON 2002). Some signaling molecules act as long range repellents or attractants (DICKSON 2002; ARAUJO AND TEAR 2003). Other signaling molecules act locally to break the distance travelled by the axon into a series of shorter trajectories, causing the axon to change direction at specific choice points. Also known as guidepost cells or intermediate targets, such choice points may be provided by neuronal support cells, non-neuronal cells or pioneer neurons (BATE 1976; BENTLEY and CAUDY 1983; COLAMARINO and TESSIER-LAVIGNE 1995; HIDALGO and BOOTH 2000; ARAUJO and TEAR 2003; HIDALGO 2003; HUTTER 2003; COLON-RAMOS and SHEN 2008; RAPER and MASON 2010).

The last several decades have witnessed great progress in the identification of mechanisms necessary for axon pathfinding, yet known pathways still cannot explain all of the complexity required to build nervous systems (SCHMITZ *et al.* 2007; O'DONNELL *et*

al. 2009). Thus additional axon guidance mechanisms almost certainly remain to be identified. C. *elegans* proved to be an excellent model for the discovery of key axon guidance cues and regulators, which are commonly conserved amongst invertebrates and vertebrates (CULOTTI and MERZ 1998; CHISHOLM and TESSIER-LAVIGNE 1999). In addition to being amenable to large-scale genetic screens, the transparent worm allows *in vivo* visualization of living neurons using fluorescently tagged proteins (HUTTER 2004).

The *C. elegans* pharynx has a very simple nervous system that consists of only 20 neurons, each with a stereotyped trajectory. This system develops independently from the rest of the nervous system, and thus may use unique pathfinding mechanisms. Neurons elsewhere in the body usually grow between basement membranes laid down by epidermis and muscles. In contrast, pharyngeal neurons lie within the pharyngeal muscle folds (ALBERTSON and THOMSON 1976; AVERY and THOMAS 1997; GRAHAM *et al.* 1997; PILON and MORCK 2005). The pharyngeal nervous system is organized into one dorsal nerve cord, two subventral nerve cords, and a pharyngeal nerve ring. As individual ablation of most of these neurons has no visible effect, pharyngeal neurons are thought to act redundantly to regulate the rhythmic contractions of the pharynx (AVERY and HORVITZ 1989; AVERY 1993; AVERY and THOMAS 1997; PILON and MORCK 2005). Therefore, severe defects in many pharyngeal neurons should result in a viable and fertile, an advantage for analysis of mutant phenotypes.

The unique morphology of each of the 20 pharyngeal neurons raises the possibility that different neurons may use distinct mechanisms to establish their trajectories. Previous analysis of the axon guidance of two left/right pairs of pharyngeal neurons, NSML/NSMR and M2L/M2R, revealed that they use known guidance

mechanisms, such as Netrin and Slit/Robo, and the genes *unc-51* and *unc-119* that have growth cone function, but in different ways from each other (MORCK *et al.* 2003; AXANG *et al.* 2008; PILON 2008). Indeed, the genetic requirements differ between the different processes of the NSM neurons (AXANG *et al.* 2008). As with other examples of axon guidance in *C. elegans*, the extension of the NSM and M2 axons is robust, with mutations in genes with guidance cue and growth cone functions generally having incomplete penetrance.

The NSM and M2 pharyngeal neurons also use unusual growth cone independent mechanisms (MORCK *et al.* 2003; AXANG *et al.* 2008; PILON 2008), extending for part of their journeys using the "fishing line" paradigm (BRAY 1984; ZHENG *et al.* 1991; HEIDEMANN *et al.* 1995; CHADA *et al.* 1997). In this model, the neuron soma ("the fish") may pull out the axon ("the line") as the cell body moves away from an initial attachment point. Alternatively, the cell body may remain stationary with the axon drawn out by an attachment to a migrating neighbor (BRAY 1984; PILON 2008). This concept was demonstrated experimentally by applying mechanical tension to the short axonal processes of cultured neurons. In response to mechanical stimuli, rat embryonic dorsal root ganglia neurons increase their length and rate of growth (PFISTER *et al.* 2006; SMITH 2009; LOVERDE *et al.* 2011). *Drosophila* larval optic nerves, and possibly the cerebellar granule cells in mammals, use similar mechanisms to extend their axons (JAN *et al.* 1985; KOMURO and YACUBOVA 2003; YACUBOVA and KOMURO 2003). In *C. elegans*, morphogenesis of the pharynx as a whole is thought to provide the motive force for the fishing line to draw out the M2 and NSM axons (MORCK *et al.* 2003; MORCK *et al.* 2004; MORCK *et al.* 2006; PILON 2008).

Here we explore axon guidance in the *C. elegans* pharynx by analyzing axon extension of the pharyngeal motor neuron M1. Unlike the previously studied pharyngeal neurons, the M1 axon spans nearly the whole length of the pharynx, navigating through several different pharyngeal compartments (ALBERTSON and THOMSON 1976). Similar to the M2 and NSM neurons, M1 may use growth cone independent mechanisms to build the initial part of its trajectory. Additionally, we found that M1 relies partially on the adjacent non-neuronal g1P gland cell to navigate the distal portion of its trajectory, using genes implicated in growth cone function. Unlike the M2 and NSM neurons, the M1 axon is not affected by mutations in the Netrin and Sax/Robo guidance pathways but it uses the semaphorin system to a small extent. However, phenotypes for mutations affecting growth cone and axon guidance are incompletely penetrant, indicating redundant mechanisms likely mediate M1 axon extension. Finally, a genetic screen for M1-defective phenotypes identified nine mutations for M1 development, including a mutation that may affect neuronal differentiation or cell fate specification. We suggest that the M1 system provides an important new model for the study of axon guidance.

RESULTS FOR THE M1 AXON GUIDANCE ANALYSIS

glr-2::gfp allows visualization of the M1 neuron

The four anatomical structures of the pharynx are, from anterior to posterior, the procorpus, metacorpus, isthmus and terminal bulb (Figure 9A). Each of the 20 *C. elegans* pharyngeal neurons has a unique morphology. We chose to focus on the M1 neuron, which has its cell body located in the terminal bulb. Electron microscopy reconstructions indicate that the M1 axon has four components to its trajectory, as outlined on Figure 9E (ALBERTSON and THOMSON 1976). First, the M1 axon extends anteriorly from its cell

body in the terminal bulb through the isthmus to the metacorpus (the "proximal trajectory"). Second, when the M1 axon reaches the pharyngeal nerve ring in the metacorpus, it deflects dorsally to join the dorsal nerve cord and contacts the projection of the g1P gland. Third, the M1 axon runs anteriorly along the g1P gland projection (the "distal trajectory"). Near the anterior end of the procorpus, the M1 axon splits into two projections, which synapse on the anterior-most pharyngeal muscles, pm1 and pm2. Fourth, the M1 axon reflexes ventrally and posteriorly to reach the two subventral pharyngeal nerve cords.

To monitor M1 axon migration, we used the marker *glr-2::gfp* that is expressed in M1 motor neuron (Figure 9B). This transgene is also expressed in a number of neurons outside the pharynx, in the nerve ring and ventral nerve cord. These cells are easily distinguished from M1 based on position (BROCKIE *et al.* 2001; ARONOFF *et al.* 2004). M1 is born at ~330 min post-fertilization (SULSTON *et al.* 1983). *glr-2::gfp* expression was first observed at 550 minutes (BROCKIE *et al.* 2001), when the developing embryo has lengthened to three times that of the eggshell (3 fold stage) (CHISHOLM and HARDIN 2005). The M1 axon is fully extended by this time, and so we cannot use this marker to directly observe M1 axon migration before the 3 fold stage (the early pan-neuronal markers *rgef-1::gfp* (ALTUN-GULTEKIN *et al.* 2001) or *unc-119::gfp* (MADURO and PILGRIM 1995; KNOBEL *et al.* 2001) were not useful as we could not distinguish M1 from other pharyngeal neurons, even when the adjacent g1P gland cell (see below) was also marked).

Like M1, the gland g1P cell body is located in the terminal bulb and sends a projection anteriorly, within the pharyngeal nerve cord, and terminates near the anterior

limit of the pharynx (Figure 9C) (SMIT *et al.* 2008). Using *phat-1::wCherry*, *hlh-6::yfp* or *hlh-6::mTomato* to mark g1P (SMIT *et al.* 2008), we observed that the distal trajectory of the M1 axon extends along the g1P projection (Figure 9B-D) as previously noted by electron microscopy (ALBERTSON and THOMSON 1976).

Figure 9. *glr-2::gfp* allows visualization of the M1 neuron

Anatomy of the pharynx showing the M1 neuron and the g1P gland in L4 or young adult. (A) Nomarski image of the *C. elegans* pharynx. (B) Fluorescence micrographs of M1 marked by the *glr-2::gfp* reporter (arrowhead). Other non-pharyngeal green cells are part of the nerve ring (long arrow) and can be distinguished from M1 by position. Note the M1 projection into the procorpus (short arrows). (C) Fluorescence micrographs of the pharyngeal gland cells marked by the *phat-1::wCherry* reporter. The g1P cell body (arrowhead) is located in the terminal bulb and extends a projection to the procorpus (arrow). Other gland cells are also marked with this reporter (star). (D) Double transgenic animals with a gland-expressed *phat-1::wCherry* and the *glr-2::gfp*. Arrowhead indicates the M1 cell body. Arrow denotes the nerve ring. (E) Diagram of the *C. elegans* pharynx (outlined in gray), with the M1 neuron (green) and g1P gland (red). The different portions of the M1 axon trajectory are numbered from 1-4 (see text). Panel E is modified from (ALBERTSON and THOMSON 1976). Scale bar in (B) = 10 µm.

Figure 9. *glr-2::gfp* allows visualization of the M1 neuron

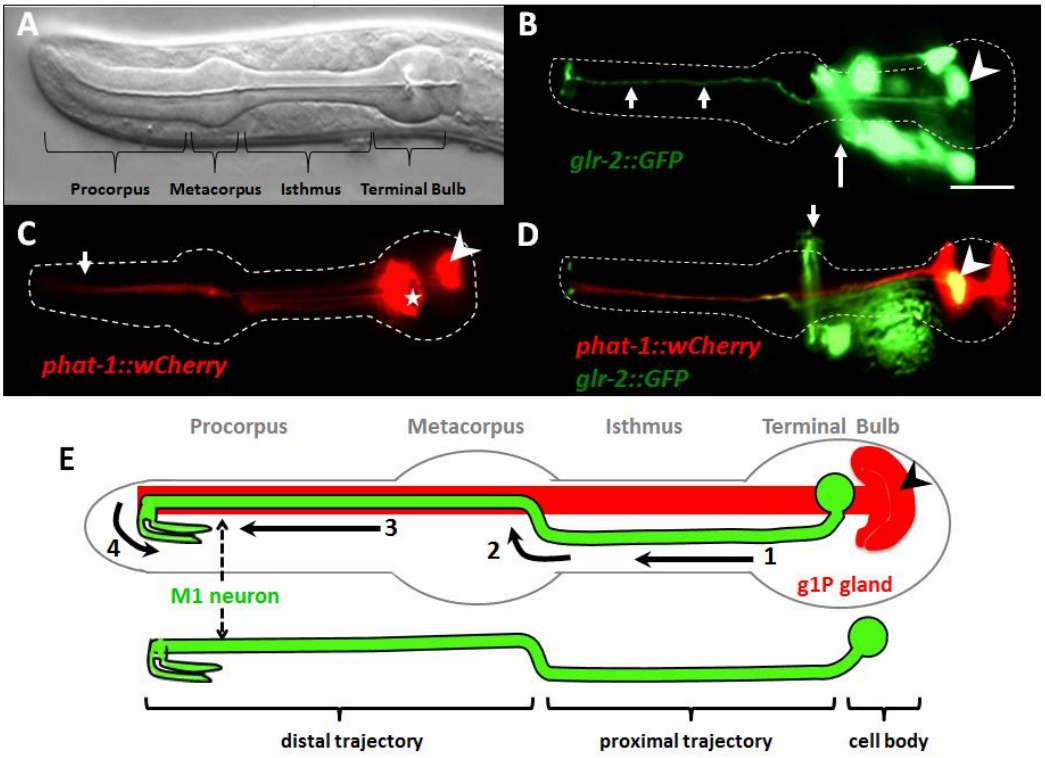

Genetic ablation of the g1P pharyngeal gland cell affects the distal, but not the proximal, trajectory of the M1 axon

To examine whether the adjacent g1P gland projection is necessary for the M1 axon extension in the procorpus, we genetically ablated the gland cells. The gland-specific *hlh-6* promoter (SMIT *et al.* 2008), which is first expressed at the "bean" stage (380 min), was used to drive expression of the pro-apoptotic gene *egl-1* (CONRADT and HORVITZ 1998) in g1P shortly after its birth at ~360 min. We found that the majority of such animals exhibited M1 axon abnormalities within the procorpus. Of gland-ablated worms (n = 140), 35% showed premature axon termination in the procorpus, frequently with extra small branches (Figure 10B, C, Table 3). Another 21% extended beyond the procorpus but followed abnormal trajectories (Figure 10D). Notably, the proximal trajectory of the axon from the M1 cell body to the procorpus was normal in all animals. While other gland cells were killed, none sends projections into the metacorpus or procorpus, so they are unlikely to be involved in M1 guidance. Furthermore, no major structural defects in the other pharyngeal tissues were detected (data not shown).

Figure 10. Genetic ablation of the g1P pharyngeal gland affects the M1 axon guidance

M1 axon phenotypes (marked with *glr-2::gfp)* in gland-ablated *hlh-6::egl-1* (B-D) or in I3 neuron-ablated *ceh-2::egl-1* transgenics (E). Arrowhead denotes the M1 cell body and the long arrow in wild type (A) indicates the nerve ring in these at L4 or young adults. Short arrows highlight M1 defects (B-D). In 56% of gland-ablated transgenics, the M1 axon is either truncated (B) with abnormal branching in the metacorpus and procorpus (C), or follows an abnormal trajectory in the procorpus (D). (E) In 7% of I3 ablated animals, the M1 axon in the procorpus exhibits an abnormal shape with GFP swellings (arrows) although the axon always extended fully. Scale bar in (A) = 10 µm.

Figure 10. Genetic ablation of the g1P pharyngeal gland affects the M1 axon guidance

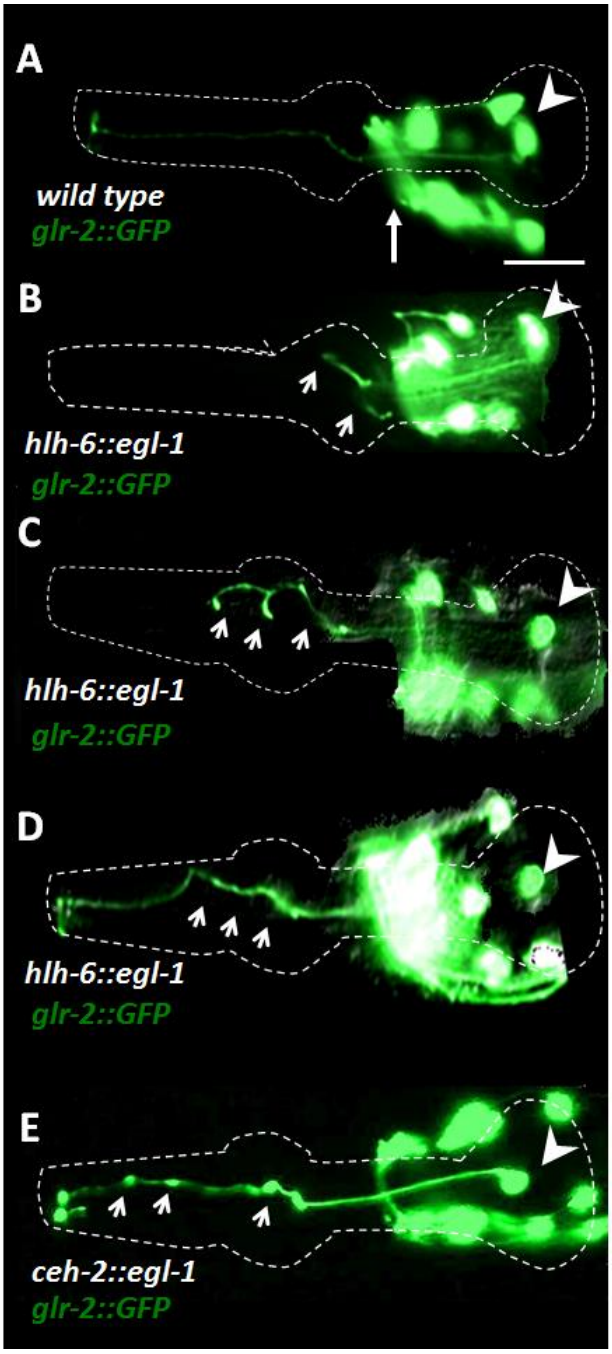

Examining the efficiency of gland ablation

The incomplete penetrance of the M1 phenotype in the gland-ablated *hlh-6::egl-1* transgenics could reflect incomplete or delayed gland killing. Therefore, we performed a time course analysis to score killing efficiency (Figure 11). Using the *hlh-6::yfp* gland reporter (SMIT *et al.* 2008), we observed that the g1P appeared to initiate its projection at the 1.5 fold stage, shortly after the gland birth (Figure 11B; J. Kormish and J. Gaudet, unpublished). Additionally, we noted that the g1P projection was always fully formed by the late 2 fold or early 3 fold stage (~500 min) in the normal embryos (Figure 11E, H; J. Kormish and J. Gaudet, unpublished). However, only 2% of the gland-ablated embryos had normal glands (n =70), indicating that poor transgene expression or mosaicism for the unintegrated array cannot explain the incomplete penetrance. YFP was completely absent in 38% of those embryos between 1.5 fold and 3 fold (430–520 min). Residual YFP (likely remnants of apoptotic cell corpses) was apparent in the remaining 60%, but no distinct gland projection or cell bodies were observed. Therefore, the gland was efficiently killed before it developed its projection.

The fact that 44% of the gland ablated worms apparently had a normal M1 axon implies that M1 uses more than one mechanism to extend in this region. Furthermore, the initial outgrowth of M1 is independent of the gland cell, indicating that different (or perhaps overlapping) mechanisms are used during the different phases of the journey. Thus, we genetically ablated the I3 interneuron that bundles with the M1 axon and g1P projection in the procorpus (ALBERTSON and THOMSON 1976). I3 apoptosis was induced using a transgenic array with the *ceh-2* promoter (ASPOCK *et al.* 2003) driving *egl-1* as well as *gfp* to mark the cell. I3 was eliminated in 97% of animals (n = 63). Using this

construct, the M1 axon always reached its final target with a normal trajectory. We occasionally (7%, n = 50) observed swellings of the M1 axon in the procorpus (Figure 10E, Table 3). Moreover, double ablation of I3 and g1P was not additive, resulting in 42% normal M1 axons (n = 14, the strain was unhealthy and difficult to maintain) compared to 44% for the g1P single ablation. These data suggest that distal M1 axon outgrowth relies on the presence of the g1P projection in the procorpus, in concert with other elements.

Figure 11. Time course measuring the efficiency and timing of the gland killing in *hlh-6::egl-1* transgenics

Examples of 1.5 fold (first row), 2 fold (second row) and 3 fold (third row) embryos are shown. First column (A, D, G) shows Nomarski images, second column (B, E, H) shows wild-type glands visualized using the *hlh-6::yfp* reporter and the third column (C, F, I) represents *hlh-6::egl*-1 transgenics at similar developmental stages. Note the absence of the *hlh-6::yfp* reporter in the glandless embryos in (C, F, I). Arrow indicates gland cell bodies and arrowheads indicate the g1P projection. Stars indicates intestine expressing *elt-2::tdCherry* transgene marker. Scale bar in (G) = 5 µm.

Figure 11. Time course measuring the efficiency and timing of the gland killing in *hlh-6::egl-1* transgenics

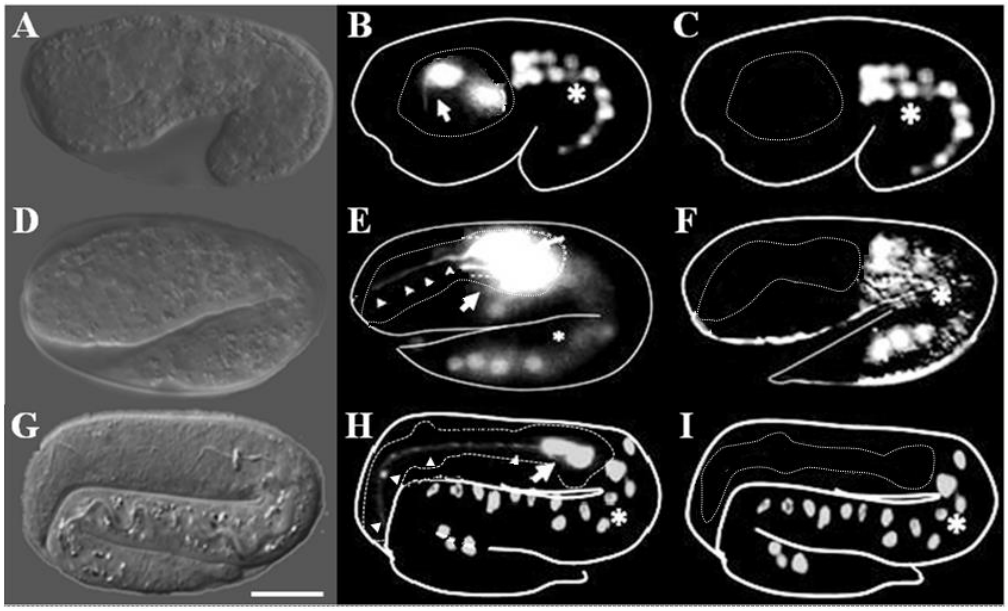

Table 3: Summary of M1 phenotypes

Quantification of M1 axon phenotypes are shown for mutants or after cell ablation. All values are in percent, and for each category a cartoon showing representative examples of the axonal phenotypes is shown. Footnotes on the figure areas follows. (A) All strains included *glr-2::gfp*, except as noted. Some neurons had multiple abnormalities and therefore some genotypes sum to100%. (B) M1 showed abnormal trajectories in the procorpus. (C) Axons showed swelling or small ectopic projections in the procorpus. (D) Independent *glr-2::gfp* transgenes were made for each of these strains. (E) This was the maternal genotype as *vab-1(e2); sax-3(ky123)* homozygous segregants arrest before the stage when M1 can be scored. Note that two thirds of scored progeny will be *vab-1/+; sax-3*. (F) These *rpm-1*alleles were identified independently of this screen. (G) M1 neuron was absent as scored by the absence of *glr-2::gfp*.

GENOTYPE [a]	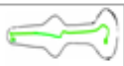 WILD TYPE	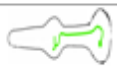 DISTAL TRUNCATION	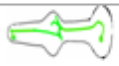 METACORPAL ECTOPIC PROJECTIONS	 OVER-EXTENSION	 IPSILATERAL OUTGROWTH	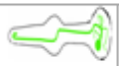 CELL BODY BRANCHING	OTHER	N
Wild type	100%							300
glr-2::GFP	100%							200
hlh-6::elg-1	44%	35%					21% [b]	140
ceh-2::egl-1	93%						7% [c]	50
ceh-2::egl-1; hlh-6::elg-1	42%	35%					21% [b] 7% [c]	14
Genes with guidance and growth cone functions								
unc-119(e2498)								
L4	1%	99%	76%		40%			182
L4 + 72 hrs	1%	99%	81%		66%			182
unc-51(e369)	50%	50%	20%				5% [c]	270
unc-51(e369); hlh-6::elg-1	40%	57%	23%				21% [b] 6% [c]	21
unc-34(e315)	38%	62%	35%		3%	5%		140
unc-34(e315); hlh-6::elg-1	30%	69%	55%		3%	5%	21% [b]	14
unc-115(e2225)	80%						20% [c]	130
unc-115(e2225); hlh-6::elg-1	44%	35%					21% [b] 23% [c]	15
ced-10(n1993)	98%						2% [c]	45
mig-2(mu28)	99%						1% [c]	42
ced-10(n1993); mig-2(mu28)	98%						2% [c]	120
unc-69(e587)	96%		4%				1% [c]	100
unc-73(e936)	97%		3%					100
unc-76(e911)	93%		7%				1% [c]	120

Table 3 (continued)

GENOTYPE [a]	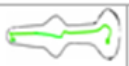 WILD TYPE	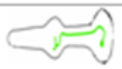 DISTAL TRUNCATION	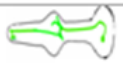 METACORPAL ECTOPIC PROJECTIONS	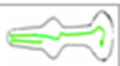 OVER-EXTENSION	 IPSILATERAL OUTGROWTH	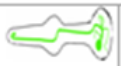 CELL BODY BRANCHING	OTHER	N
Genes with guidance functions								
smp-1(ev715)[d]	99%		1%					100
smp-2(ev709)[d]	94%		6%					180
smp-1(ev715); smp-2(ev709)[d]	85%		11%	3%			7% [c]	100
mab-20(bx24)[d]	95%		2%	5%				140
plx-1(ev724)[d]	91%		9%	2%				180
plx-2(ev775)[d]	97%		2%	3%				180
unc-6(ev400)	99%		1%					180
unc-6(e78)	99%		1%					180
unc-40(e271)	99%		1%					160
unc-5(e53)	96%		4%					178
unc-129(ev554)	88%		12%					130
slt-1(eh15)[d]	99%		1%					60
sax-3 (ky123)	99%		1%					100
vab-1(dx31)[d]	98%					2%		100
egl-20(hu105)[d]	99%	1%	1%					100
lin-17(n3091)[d]	100%							120
pry-1(mu38)	100%							150
egl-15(n484)	97%						3% [c]	50
plx-1(ev724); unc-129(ev554)	82%	1%	18%			1%	3% [b]	100
unc-5(e53); unc-129(ev554)	87%		15%					42
unc-51(e369); unc-129(ev554)	46%	50%	33%				5% [c]	60
unc-51(e369); unc-5(e53)	47%	50%	23%				7% [c]	55
unc-115(e2225); egl-15(n484)	80%						20% [c]	56
vab-1(e2)/+; sax-3(ky123) [c]	98%					5%		100

Table 3 (continued)

GENOTYPE [a]	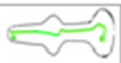 WILD TYPE	 DISTAL TRUNCATION	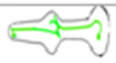 METACORPAL ECTOPIC PROJECTIONS	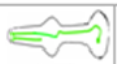 OVER-EXTENSION	 IPSILATERAL OUTGROWTH	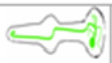 CELL BODY BRANCHING	OTHER	N
vab-1(e2)/+; sax-3(ky123) [e]	98%					5%		100
Genes with adhesion functions								
fmi-1(rh308)	93%						7% [c]	100
cdh-4(ok1323)	100%							60
rig-5(hd48); rig-6(gk376); rig-4(hd47); rig-1(hd15) wrk-1(hd45) rig-3(hd51) syg-1(hd18 ncam-1(hd49)	100%							100
Mutants from the M1 defect screen								
unc-51(iv84)	49%	51%	20%					200
rpm-1(iv78)	34%			66%				180
rpm-1(iv79)	47%			53%				170
rpm-1(iv80)	65%			37%				120
rpm-1(iv81)	55%			45%				140
rpm-1(js317) [f]	56%			44%				70
rpm-1(ur299) [f]	48%			52%				60
mnm-6(iv88)	75%		1%	25%				160
mnm-7(iv77)	40%			7%		60%		100
mnm-7(iv90)	48%			12%		52%		100
mnm-8(iv82)	5%						95% [g]	200

The distal, but not proximal, trajectory of M1 axon is affected by mutations that impair growth cone function

To test whether M1 axon outgrowth may employ a growth cone-dependent mechanism, we examined a set of mutations with impaired growth cone function. We either crossed *ivIs26[phat-1::wCherry glr-2::gfp pRF4(rol-6(su1006)]* into these backgrounds or extrachromosomal *glr-2::gfp* arrays were created by injection into the strains (see Table 3).

unc-119 functions in axon elongation, guidance, branching and fasciculation (MADURO and PILGRIM 1995; MADURO *et al.* 2000; KNOBEL *et al.* 2001; MATERI and PILGRIM 2005). Human UNC119, which can rescue the *C. elegans* mutation, functions as a receptor-associated activator of signal transduction for G protein-mediated trafficking and appears necessary for growth cone function (GORSKA *et al.* 2004; ZHANG *et al.* 2011a). In 99% (n = 182) of *unc-119* mutants, the M1 axon was truncated in the metacorpus (Figure 12B, C, Table 3). Additionally, M1 frequently exhibited ipsilateral outgrowths within the isthmus and ectopic outgrowths from the cell body (Figure 12C). The frequency of these latter phenotypes increased as animals aged from L4 to 3 days post L4 adults.

unc-51 encodes a conserved serine/threonine kinase involved in growth cone membrane dynamics (OGURA *et al.* 1994; ASAKURA *et al.* 2010; OGURA *et al.* 2010). In 50% (n = 270) of the *unc-51* mutants, the M1 axon was truncated at either the anterior bulb with a few ectopic branches, or within the procorpus (Figure 12D, Table 3). As revealed by GFP, defective axons also showed swellings along the distal trajectory (Figure 12E). These structures may represent remnants of stalled growth cones, similar to

those observed for the axons of pharyngeal M2 motor neurons in the metacorpus of *unc-51* mutants (MORCK *et al.* 2003).

unc-34 encodes an Enabled/VASP actin-binding protein that controls growth cone filopodia formation in parallel to the Rac pathway (YU *et al.* 2002; GITAI *et al.* 2003; WITHEE *et al.* 2004; SHAKIR *et al.* 2006; NORRIS *et al.* 2009)**.** The M1 axon prematurely terminated at the procorpus or metacorpus in 62% (n = 140) of *unc-34* mutants (Figure 12F, Table 3). The abnormal axons that terminated in the metacorpus usually had short branches. We occasionally (5%) observed ipsilateral branches that ran in parallel to the original axon in the isthmus, in addition to short projections from the M1 cell body.

UNC-115/abLIM is an actin-binding protein that controls formation of lamellipodia and filopodia, and is thought to be regulated by Rac (STRUCKHOFF and LUNDQUIST 2003; YANG and LUNDQUIST 2005; DEMARCO and LUNDQUIST 2010). *unc-115* mutants did not show truncations, but (20%, n = 130) exhibited minor defects of the M1 axon within the procorpus such as swellings, similar to those found in *unc-51* (Figure 12G, Table 3). Mutants of genes that are regulated by Rac GTPases usually exhibit defects in axon outgrowth, likely as a result of impaired growth cone navigation (GALLO and LETOURNEAU 1998; BISHOP and HALL 2000; YANG and LUNDQUIST 2005). Mutants for the Rac GTPases *ced-10* and *mig-2,* as well as the double mutant, exhibited similar M1 axon defects at the procorpus, albeit with much lower frequencies (2%, Table 3). Similarly, mutants of the growth cone expressed genes *unc-69, unc-73* and *unc-76* exhibited minor, low penetrance defects of the M1 distal axon trajectory, such as short ectopic projections and swellings (Table 3).

The defects we observed among all mutants known to have growth cone phenotypes were restricted to the distal trajectory of M1. The initial proximal trajectory of M1 in the isthmus was always normal, suggesting that M1 uses two distinct mechanisms to build its trajectory.

Figure 12. M1 axon abnormalities in growth cone defective mutants in L4 or adult stages

The M1 neurons express the *glr-2::gfp* reporter. The pharynx is outlined in each panel, arrowheads indicate the M1 cell body and arrows highlight M1 defects. Other neurons visible in the figure are non-pharyngeal. Note that with the exception of *unc-119*, all mutations show incomplete penetrance (Table 3). (A) Wild-type M1 neuron. (B) *unc-119* young adult exhibits axon truncation in metacorpus with abnormal branching. (C) Older *unc-119* animals (L4 + 72 hrs) exhibit axon truncations, bilateral branches in the isthmus and abnormal branches from the cell body. *unc-51* mutants exhibits axon truncations in metacorpus (D) or procorpus (E). (F) *unc-34*mutants with a truncation of the M1 axon at the metacorpus accompanied with short branches. (G) *unc-115*animals exhibit swelling of M1 axon throughout the procorpus and metacorpus. Scale bar in (A) = 10 µm.

Figure 12. M1 axon abnormalities in growth cone defective mutants in L4 or adult stages

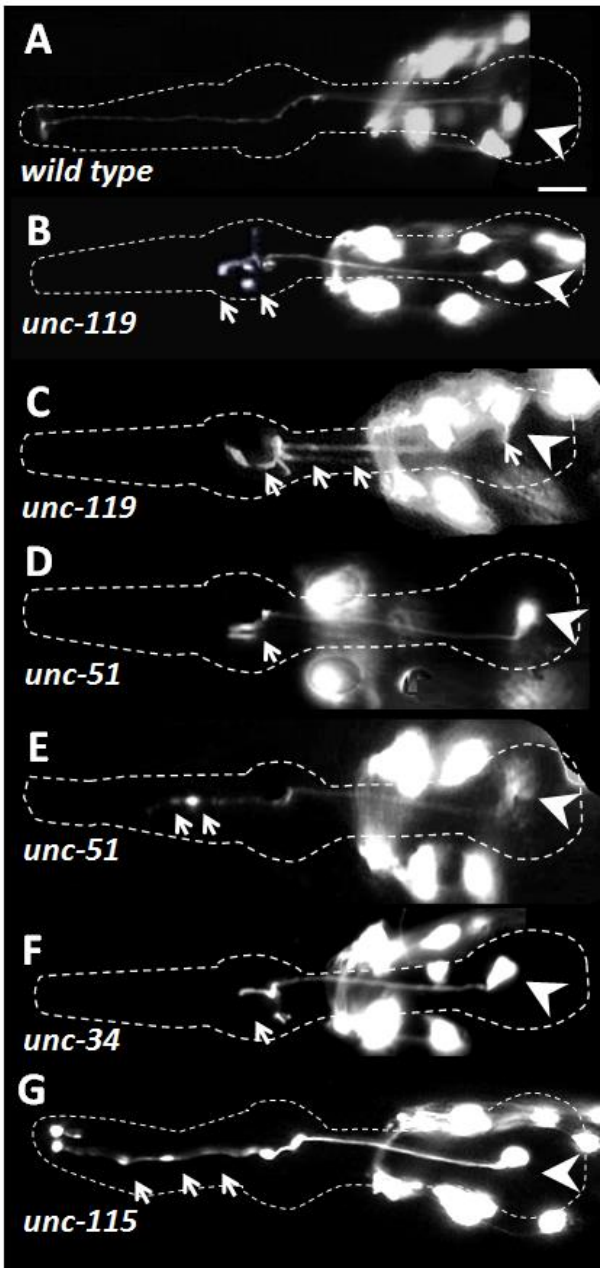

The gland cell may provide cues for growth cone-mediated guidance of the distal M1 axon

The M1 axon abnormalities scored in several mutants with growth cone defects phenocopied gland removal. However, neither these mutants (with the exception of *unc-119*) nor gland ablation resulted in 100% penetrance. Since we showed that gland ablation was up to 98% efficient, and because we used null or severe loss-of-function mutations, the incomplete penetrance of M1 defects suggests multiple mechanisms for distal M1 extension. To determine if the gland acts in parallel to the growth cone for M1 axon navigation, we examined M1 axons in glandless *hlh-6::egl-1* worms that also carried mutations in genes with growth cone phenotypes (Table 3). If the gland and growth cone act in parallel redundant pathways, removal of both would enhance the defects, while there would be no change if they acted together. The removal of the gland was at best weakly synergistic with the growth cone mutants tested, with a non-significant increase in the percentage of animal with M1 truncations ($p \geq 0.05$ in all cases). More specifically, the axon truncation phenotype was elevated from 50% to 57% for *unc-51* (n = 21) and from 62% to 69%for *unc-34* (n = 16, values are small because the strains grew very slowly). Gland removal in *unc-115* mutants, which has axon swelling rather than a truncation phenotype, exhibited 44% normal axons similar to gland ablation alone (n = 16), suggesting no additive effect. These observations suggest that the M1 growth cone may uses the gland projection for its navigation.

To test whether the M1 axon phenotype that we observed in *unc-51, unc-34* and *unc-115* mutants was a secondary result of defects of the g1P gland projection, we

examined gland shape in these mutants. *unc-51* exhibited a weak effect on the g1P projection, causing minor swellings (5%; n = 20, Appendix, Figure 40). *unc-34* mutants showed a higher frequency of swellings and ectopic projections along the g1P process (42%; n = 20), with 3% premature terminations near the pharyngeal tip. *unc-34* also affected other pharyngeal gland cells and the g1P cell body. *unc-115* mutants showed some ectopic g1P projections and swellings (25%; n = 20). Overall, the g1P phenotypes in these mutants were much less severe than those of the M1 axon, and in particular the gland projection always reached its final target (except in a few *unc-34* mutants). These results suggest that M1 axon defects in these mutants are unlikely the secondary consequence of g1P defects. Additionally, these data suggest that the g1P gland does not need M1 to establish its projection in the procorpus.

The distal trajectory of the M1 axon is only weakly affected by axon guidance mutations

The incomplete penetrance of the distal M1 axon phenotypes in the absence of the gland cell suggests that additional external guidance cues act redundantly with the g1P projection. To identify such genes, we tested mutations affecting the major axon guidance cues or their receptors. The four major guidance systems in both vertebrates and invertebrates include semaphorins and their plexin and neuropilin receptors (TESSIER-LAVIGNE and GOODMAN 1996; CASTELLANI and ROUGON 2002; GINZBURG *et al.* 2002), Netrins and their DCC and UNC5 receptors (HEDGECOCK *et al.* 1990; SHEKARABI and KENNEDY 2002; NORRIS and LUNDQUIST 2011), Slits and their Robo receptors (BROSE *et al.* 1999; HAO *et al.* 2001), and Ephrins and their Eph receptors (GEORGE *et al.* 1998; CHIN-SANG *et al.* 1999; RODGER *et al.* 2012).

C. elegans has two transmembrane semaphorins, SMP-1 and SMP-2, which signal through the PLX-1 plexin receptor (TESSIER-LAVIGNE and GOODMAN 1996; CASTELLANI and ROUGON 2002; FUJII *et al.* 2002). Worms also have one secreted Semaphorin, MAB-20(ROY *et al.* 2000), which signals through PLX-2 receptor (IKEGAMI *et al.* 2004; NAKAO *et al.* 2007). In *smp-2* mutants, ectopic outgrowths were observed occasionally in the M1 axon within the metacorpus and in the procorpus, with a frequency of 6% (n = 180) (Figure 13B, Table 3). Although the M1 axon showed only 1% defects (ectopic projections in the metacorpus) in *smp-1*, these abnormalities were seen in 11% (n = 100) of the *smp-1 smp-2* double mutants, suggesting that the two genes act redundantly ($p < 0.05$). *plx-1* mutants exhibited defects (9%, n = 180) similar to those of *smp-1 smp-2* double mutants. *mab-20* and *plx-2* had low frequencies of ectopic projections in the metacorpus and also occasional posterior overextension (Figure 13C, Table 3).

UNC-6 is the *C. elegans* Netrin, and it has two receptors, UNC-40/DCC and UNC-5 (HEDGECOCK *et al.* 1990; ISHII *et al.* 1992; CHAN *et al.* 1996; CULOTTI and MERZ 1998; LIVESEY 1999). M1 was apparently normal in *unc-6* (n = 180 for each of two alleles) as well as *unc-40* (n = 160) mutant backgrounds (Table 3). *unc-5* mutants exhibited minor ectopic projection from the M1 axon at the metacorpus, with a frequency of 4% (n =178). This is the position where M1 moves dorsally into the dorsal pharyngeal nerve cord (ALBERTSON and THOMSON 1976). The TGF-beta family ligand UNC-129 physically interacts with UNC-5 to regulate cellular responses (MACNEIL *et al.* 2009). *unc-129* animals had ectopic projections similar to those observed in *unc-5*, albeit with a higher frequency of 12% (n = 130, Figure 13D, Table 3).

SAX-3 acts with EVA-1 as Robo receptors for SLT-1, the only Slit protein in *C. elegans* (HAO *et al.* 2001; FUJISAWA *et al.* 2007). We observed that mutants of *slt-1* and *sax-3* had little or no effect on the M1 axon (n = 100 each). VAB-1 is the sole Ephrin receptor in *C. elegans,* which receives signals from the Ephrins EFN-1, EFN-2, EFN-3 and EFN-4 (GEORGE *et al.* 1998; ARVANITIS and DAVY 2008). *vab-1* did not show M1 defects beyond a few ectopic projections from its cell body (2%, n = 100) (Figure 13E, Table 3).

We also tested components of Wnt signaling, which regulate migration of growth cones and cells along the *C. elegans* anterior-posterior axis (FRADKIN *et al.* 2005; HILLIARD and BARGMANN 2006; MARO *et al.* 2009). Mutants for the Wnt ligand EGL-20 showed rare truncations of the M1 axon at the procorpus (1%, n = 100) (Table 3). The M1 trajectory appeared normal upon the loss of the Wnt receptor LIN-17 or the downstream target of Wnt signaling PRY-1.We also tested *egl-15,* which encodes the only worm Fibroblast Growth Factor receptor and plays a role in axon guidance and fasciculation in the ventral nerve cord (BULOW *et al.* 2004). We found 3% of M1 distal axons (n = 50) had ectopic swellings or branching (Table 3).

None of the null or strong loss of function mutants we used showed defects in initial M1 axon outgrowth, or resulted in distal M1 truncations. These results suggest that tested guidance cues play minor roles in M1 axon outgrowth. It is possible that these pathways/genes act redundantly to guide the M1 axon. We tested double mutants including *plx-1; unc-129* (whose individual mutants had the highest penetrance among guidance genes), *unc-5; unc-129, unc-51; unc-129, unc-51; unc-5, unc-115; elg-15* and *vab-1/+; sax-3* (*vab-1; sax-3* homozygotes arrest prior to the stage of *glr-2::gfp*

expression (GHENEA *et al.* 2005)). All combinations were essentially identical to the allele with the highest penetrance (Table 3, $p > 0.05$ in all cases), arguing against redundancy between the tested pathways.

The distal trajectory of the M1 axon is only weakly affected by known adhesion mutants

Since distal M1 axon outgrowth is influenced by loss of either glands or genes with growth cone functions, we examined adhesion molecules that the M1 axon might use to fasciculate to the g1P gland projection. We screened candidates known to be expressed in the pharynx, glands or neurons. The *C. elegans* flamingo-like cadherin, *fmi-1*, controls axon pathfinding, fasciculation and synapse morphology (STEIMEL *et al.* 2010; NAJARRO *et al.* 2012). *fmi-1* mutants exhibited occasional bright GFP swellings of the M1 axon in the procorpus (7%, n = 100), which could be fasciculation defects or aberrant synapses (Figure 13F, Table 3). We found no defects in mutants of the Fat-like cadherin CDH-4, which controls axon fasciculation and cell migration (SCHMITZ *et al.* 2008). The redundantly acting IgCAMs RIG-3 and RIG-5 are expressed in M1 and g1P, respectively (SCHWARZ *et al.* 2009). Thus, we tested the octuple mutant *rig-5; rig-6; rig-4; rig-1 wrk-1 rig-3 syg-1 ncam-1* (SCHWARZ *et al.* 2009) but observed no M1 defects (Table 3).

Figure 13. M1 axon phenotypes in L4 or young adult guidance and adhesion mutants.

The M1 neuron expresses the *glr-2::gfp* reporter. The pharynx is outlined in each panel; arrowheads indicate the M1 cell body and arrows highlight M1 defects. Other neurons visible in the figure are part of the nerve ring. Note that penetrance is low in all cases (Table 3). (A) Wild type (this is the same image as shown in Fig. 12A). (B) *smp-2* exhibits small projections at the procorpus and metacorpus. (C) *mab-20* shows over-extensions of M1 terminal branches beyond their normal targets. (D) *unc-129* has short projections and swellings of the M1 axon in the metacorpus. (E) *vab-1* mutant has an apparently normal M1 axon, but that exhibits abnormal minor branches from the cell body. (F) *fmi-1* mutantshows abnormal swelling of the M1 axon in the procorpus. Scale bar in (A) = 10 µm.

Figure 13. M1 axon phenotypes in L4 or young adult guidance and adhesion mutants.

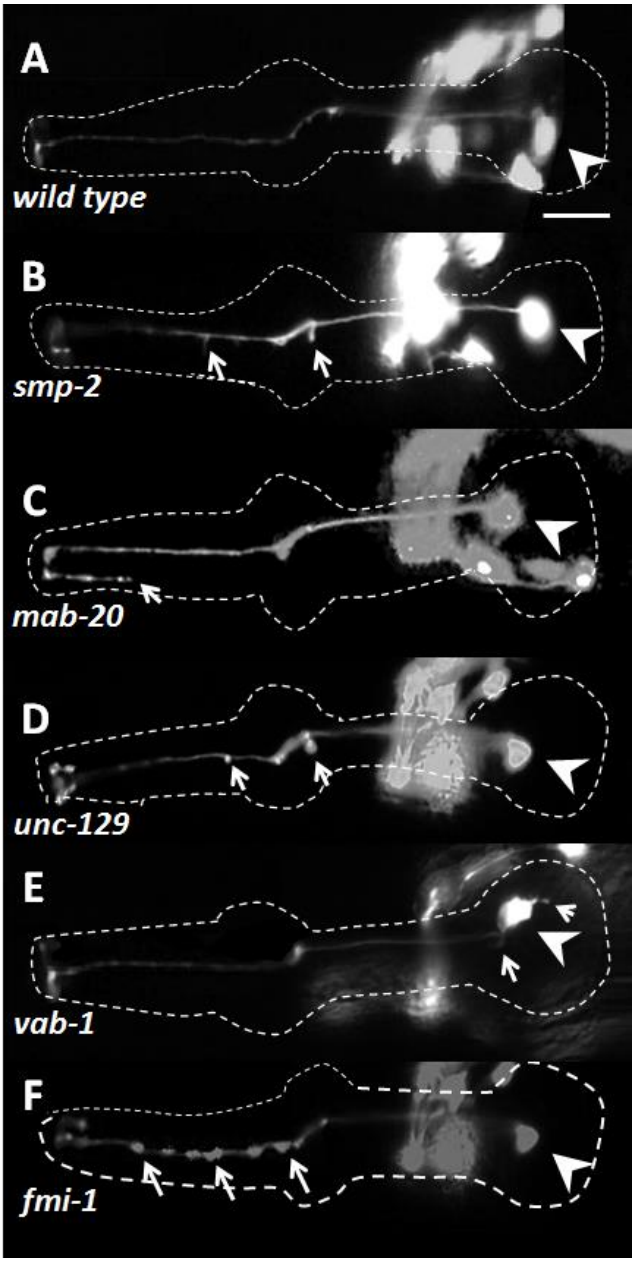

New mutations with abnormalities in M1 guidance and development

Because the M1 axon defects showed incomplete penetrance in all situations that we examined (with the exception of *unc-119*), M1 axon extension and guidance may involve novel genes. Thus we searched for viable mutants with M1 morphology or developmental defects using the integrated *glr-2::gfp* strain. In a screen of 5,000 mutagenized haploid genomes, nine mutations were identified that fell into four phenotypic classes: i) axon truncation, ii) axon over-extension, iii) ectopic branches at the cell body, and iv) M1 absent (Figure 14; Table 3). None affected the initial outgrowth of the M1 axon through the isthmus.

The truncation mutant *iv84* exhibited premature termination of the M1 axon in the procorpus or the metacorpus in 50% of animals (n = 200, Table 3). This mutant also has a severe Unc phenotype. *iv84* was mapped to the right arm of chromosome V and failed to complement *unc-51(e268)*. Identification of *iv84* in a gene known to be required for M1 axon extension serves as proof of principle for the effectiveness of the screen.

In the axon over-extension class, one or both of the terminal posteriorly facing M1 axon branches overshoots the final target, extending further posteriorly, sometimes as far as the anterior bulb (Figure 14B, Table 3). *iv78*, *iv79*, *iv80* and *iv81* mapped to the middle of chromosome V and failed to complement each other, as well as alleles of *rpm-1*. RPM-1, Regulator of Presynaptic Morphology-1, is an E3 ubiquitin ligase that contains a guanine nucleotide exchange factor domain. RPM-1 is a member of the conserved Pam/Highwire (PHR) protein family, which regulates axon termination and synaptogenesis (SCHAEFER *et al.* 2000; WAN *et al.* 2000; ZHEN *et al.* 2000; D'SOUZA *et al.* 2005; LI *et al.* 2008). As

expected, the previously identified alleles, *rpm-1(js317)* and *rpm-1(ur299*), showed the same axon phenotypes (Table 3). Thus, the formation of synapses on pm1 and pm2 may have a role in marking the termination of M1 axon extension. Another over-extension mutation, *iv88*, was also Unc, and this mutation mapped to the middle of chromosome IV. There were no obvious candidates in this region, and we assigned it the gene name *mnm-6* (M neuron morphology abnormal, (MORCK *et al.* 2003)).

The branching cell body mutations *iv77* and *iv90* have short, abnormal outgrowths from the M1 cell body and occasional axon over-extensions (similar to the over-extension class, Table 3). Nerve ring neurons that express *glr-2::gfp* are also affected, suggesting a general axon guidance defect. These two mutations failed to complement and both mapped to the right arm of chromosome III. There are no obvious candidates in the 2 cM region where they mapped. We assigned them the gene name *mnm-7*.

In the M1 missing mutation *iv82*, pharyngeal *glr-2::gfp* was absent in 95% of animals, where it was present in the nerve ring and ventral nerve cord. We will refer to *iv82* as M1 missing mutant (Figure 14E, Table 3). M1 was absent at high frequencies at all stages at which we could visualize the neuron (i.e., as early as 3 fold). This mutant also retained a fully penetrant protruding vulva phenotype after six outcrosses. *iv82* mapped to the right arm of chromosome I. The Wnt pathway gene *pry-1* (MALOOF *et al.* 1999; KORSWAGEN *et al.* 2002) maps to this region, but M1 is normal in both *pry-1/pry-1* and *pry-1/iv82*.*iv82* has been assigned the gene name *mnm-8.*

The absence of the M1 neuron in *mnm-8*could result from transformation of M1 into its sister MSpaapaap, which normally undergoes programmed cell death (SULSTON *et al.* 1983). Indeed, in *ced-3* mutants that block apoptosis (LETTRE and HENGARTNER

2006), we observed an additional M1-like cell, indicating that the undead M1 sister probably adopts an M1 like fate. However, in *mnm-8; ced-3* we observed neither cell, indicating that *mnm-8* affects both M1 and its putative sister rather than inducing apoptosis by transforming M1 into its dying sister. Thus *mnm-8* may affect either the generation of M1 or its ability to express the *glr-2::gfp* reporter (which is still expressed in other, non-pharyngeal neurons (Figure 14E)).

Figure 14. Phenotypes of mutants isolated from the forward genetic screen visualized in L4 or young adults.

M1 is marked with *glr-2::gfp*. Arrowheads indicate cell bodies and arrows denote defects, which are incompletely penetrant in all cases (Table 3). Other neurons visible in the figure are part of the nerve ring. Panels A'-E' represent a cartoon for each phenotypic class. (A) Wild type. (B) *unc-51(iv84)* shows axon truncation and an ectopic branch. (B) *rpm-1(iv78)* results in over-extension of M1 terminal branches beyond their normal targets. (C) *mnm-7(iv77)* shows ectopic branching from the cell body. (D) *mnm-8(iv82)* shows a 95% penetrant M1 missing phenotype while the other neurons that express the *glr-2::gfp* reporter are still present. Scale bar in (A) = 10 µm.

Figure 14. Phenotypes of mutants isolated from the forward genetic screen visualized in L4 or young adults.

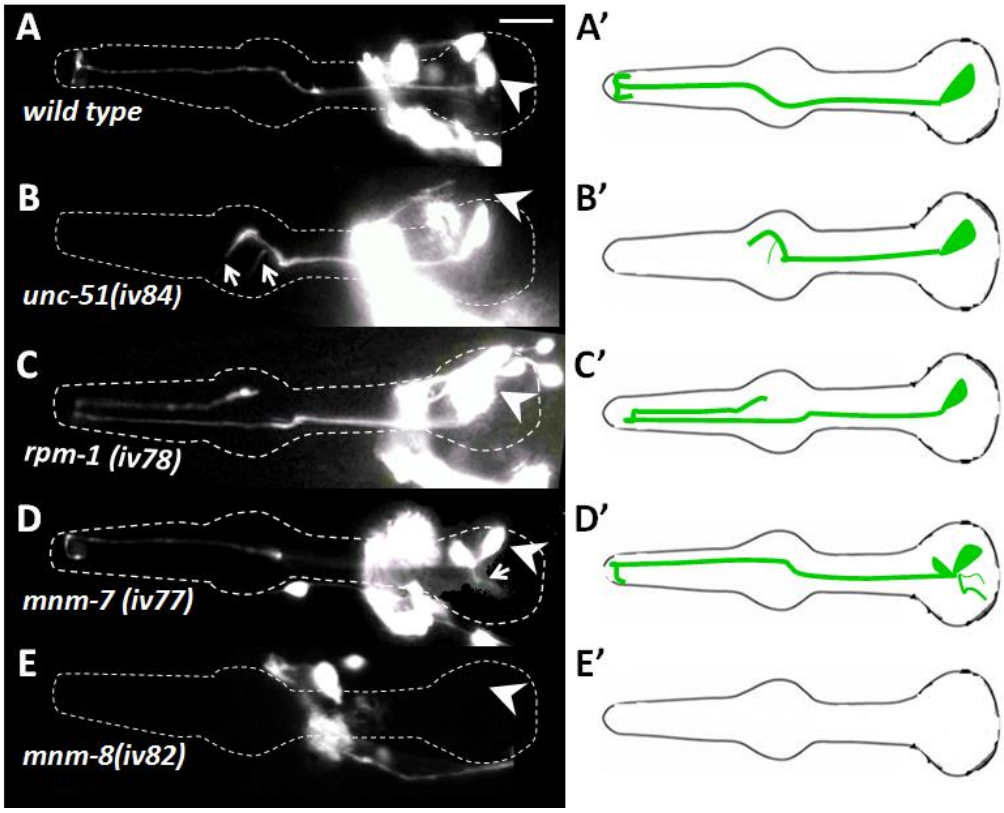

DISCUSSION AND FUTURE DIRECTIONS

DISCUSSION

In this work we explored the development of the *C. elegans* M1 motor neuron, which extends almost the entire length of the pharynx, as a model of how axons are extended within a simple structure, the pharynx. Our results indicate that axon extension in the pharynx appears to be robust and its proximal and distal outgrowth is mediated by two different mechanisms.

The proximal and distal phases of M1 axon extension employ distinct mechanisms

We demonstrated that the extension of the M1 axon occurs in two distinct phases. The first, proximal phase through the isthmus was always normal under all of the conditions we tested, not being affected by gland ablation, mutations that impair growth cone function or mutations in genes known to affect axon guidance or cell adhesion. Moreover, none of the mutants that we isolated from our screen for M1 defects exhibited abnormalities during the proximal phase of axon extension. In contrast, the subsequent distal phase of M1 axon extension through the metacorpus and procorpus was often abnormal after gland ablation, with mutations affecting growth cones, and to a lesser extent with mutations affecting axon guidance.

The proximal extension of the M1 axon appears similar to that described for outgrowth of the bilateral M2 and NSM pharyngeal neurons (MORCK *et al.* 2003; AXANG *et al.* 2008; PILON 2008). The M2 neuron growth cones appear only after the axon has extended through the nascent isthmus (RAUTHAN *et al.* 2007). Pilon and colleagues (MORCK *et al.* 2003; AXANG *et al.* 2008; PILON 2008) proposed that elongation of M2 axons and the minor processes of the NSM pharyngeal neurons is analogous to the

"fishing line" model (BRAY 1984) by attachment to a neighboring cell. The cells are later moved to opposite sides of the isthmus during pharyngeal morphogenesis, elongating the axon. During *C. elegans* embryogenesis, the pharynx primordium elongates from a ball-shaped cell mass to the bi-lobed shape of the mature pharynx as the embryo as a whole transforms from a spheroid to a tube (PORTEREIKO and MANGO 2001). This elongation likely provides the force for initial separation of the cell body from its axonal anchor point. Our results demonstrated that the M1 proximal trajectory is not affected by mutations in genes with growth cone functions, suggesting that M1 may use a similar mechanism to extend through the isthmus. However, we could not observe outgrowth directly due to the lack of a specific M1 marker expressed prior to axon elongation.

The pharyngeal gland g1P guides the distal trajectory of the M1 axon

M1 is the first studied pharyngeal neuron that extends its axon into the procorpus, which occurs during the second, distal portion of its outgrowth. The position of the non-neuronal pharyngeal g1P gland projection adjacent to the M1 axon in the procorpus (ALBERTSON and THOMSON 1976) prompted us to ask whether M1 uses g1P to establish its distal trajectory (Figure 9). Indeed, genetic ablation of the pharyngeal gland cells caused defects in the distal portion of the M1 axon, including truncations, abnormal branches and abnormal trajectories (Figure 10, Table 3). Abnormalities were never observed within the isthmus, where M1 does not contact the g1Pprojection. It is clear from our time course analysis that we killed the gland cells before g1P began extending its projection (Figure 11), and this occurred before the earliest time that we could observe the M1 axon. The early induction of gland cell death and the appearance of M1 axon

defects as soon as the neuron became visible argue against the possibility that phenotypes were caused by maintenance rather than initial guidance.

It is formally possible that M1 is influenced by gland cells other than g1P, which were also killed by *hlh-6::egl-1* (data not shown). However, M1 is never in contact with the other gland cells, which do not extend projections beyond the isthmus into the region of interest (ALBERTSON and THOMSON 1976; SMIT *et al.* 2008).

It is notable that we did not observe a reciprocal effect of M1 on the g1P projection. In most mutants that showed M1 extension defects, we never observed g1P truncation, and even minor structural defects of the g1P projection (e.g., ectopic branches or minor misroutes) were much less severe than for M1. Importantly, in mutants with frequent M1 truncations, the g1P projection was always able to extend fully (Appendix, Figure 40). In *mnm-8 (iv82)*, the g1P projection never failed to reach its final target although an M1-like (*glr-2::gfp* expressing) neuron was not present in 95% of animals (data not shown). Together these data indicate that the g1P gland does not need the M1 axon to establish its projection.

The incomplete penetrance of the M1 defects in gland-ablated animals could reflect redundancy between guidance by g1P and other cells that bundle with M1 in the pharyngeal dorsal nerve cord. However, ablation of such a cell, the I3 interneuron, alone or in combination with the gland cell ablation, did not appear to have additive effects on M1 guidance.

One possibility is that g1P acts as a pioneer neuron to which the M1 axon fasciculate. However, we failed to observe the M1 axon defects in multiple adhesion molecule mutants including *fmi-1* and mutations of other IgCAM genes that are

expressed in the pharynx and which could potentially mediate the M1/g1P fasciculation (Table 3). Thus, multiple cells or adhesive molecules may act redundantly to guide the M1 distal axon. Alternatively, g1P may act as a guidepost at the metacorpus to attract the M1 axon towards the dorsal nerve cord, after which the M1 axon is guided by other mechanisms. This role is analogous to that of the M2 neurons' sister M3, which is thought to send an instructive signal to guide M2 growth cones (RAUTHAN *et al.* 2007; PILON 2008). Another possibility is that g1P may function in a role usually carried out by neuronal supporting cells such as glia**.** Many studies have demonstrated that glial cells mark choice points for axon growth (SILVER *et al.* 1982; AULD 1999; HIDALGO and BOOTH 2000; PUCHE and SHIPLEY 2001; HIDALGO 2003; MCDERMOTT *et al.* 2005; SPINDLER *et al.* 2009), and this also occurs in *C. elegans* (BACAJ *et al.* 2008; YOSHIMURA *et al.* 2008; HEIMAN and SHAHAM 2009; OIKONOMOU and SHAHAM 2011).

Genes that function in growth cones guide the distal trajectory of the M1 axon

In contrast to the first phase of outgrowth, M1 axon extension within the isthmus was affected by mutations known to affect growth cone function, including *unc-34, unc-51, unc-115* and *unc-119.* However, defects were not fully penetrant in any of the conditions we examined (with the exception of *unc-119* mutants), suggesting that M1 uses multiple or overlapping mechanisms to establish its distal trajectory. It is likely that *unc-34, unc-51, unc-115* and *unc-119* act autonomously, within the M1 cell. These genes are normally expressed in worm neurons during their development and have been demonstrated to act cell-autonomously during the outgrowth of many neurons (LUNDQUIST *et al.* 1998; KNOBEL *et al.* 2001; LAI and GARRIGA 2004; MATERI and PILGRIM 2005; SHEFFIELD *et al.* 2007; FLEMING *et al.* 2010). There are examples of *unc-*

119 and *unc-51* acting non-autonomously during axon guidance of ASI and AVM neurons, respectively (MATERI and PILGRIM 2005; OGURA *et al.* 2010). If *unc-34, unc-51, unc-115* or *unc-119* were acting non-autonomously for M1 guidance, the most likely focus would be the neighboring I3 interneuron or the g1P gland. However, ablation of I3 had no effect on the M1 cell (Table 3). It also is unlikely that M1 phenotypes stem from the genes with growth cone functions acting within g1P rather than M1. The growth cone mutations had at best weak effects on g1P, and rarely prevented full extension of the g1P process (Appendix, Figure 40). Furthermore, the g1P projection does not extend by a process similar to axonal outgrowth, but rather is anchored in the anterior of the pharynx and is then drawn out as the cell body migrates posteriorly (J. Kormish and J. Gaudet, in preparation). It is possible that these genes influence signals M1 receives from adjacent muscle cells, but it seems unlikely that each of the four genes, with well characterized growth cone functions, are all acting a novel way. The most parsimonious model is that at least most, if not all, of the genes with growth cone functions act within an M1 growth cone. Ablating the gland cells in the growth cone defective mutants *unc-34, unc-51* and *unc-115* (Table 3) had at best weakly additive effects. This suggests that an M1 growth cone acts in concert with the g1P projection.

Genes known to affect guidance signaling pathways have modest roles in M1 axon extension

We examined mutations in genes that encode axon guidance ligands and receptors to find those that might act in parallel to the g1P in guiding distal M1 axon outgrowth. None of these genes showed a profound effect on M1 axon that was similar to the defects caused by gland ablation or mutations in genes with growth cone functions. For example,

mutants for the dorsal/ventral guidance pathway (HEDGECOCK *et al.* 1990; ISHII *et al.* 1992) had weak effects where M1 deflects towards the dorsal nerve cord. Mutants of the Netrin receptor gene, *unc-5*, and the TGF-beta family ligand, *unc-129* (MACNEIL *et al.* 2009), exhibited 4% and 12%, respectively, short ectopic projections in metacorpus (Table 3). UNC-129 interacts with UNC-5 to regulate cellular responses to UNC-6 (MACNEIL *et al.* 2009), but *unc-5; unc-129* double mutation had little additive effect on M1 (Table 3). Two *unc-6*/Netrin alleles resulted in only 1% defects suggesting that if there is a minor role for UNC-5, it could be independent of UNC-6. For the semaphorin system *plx-1* or the *smp-1 smp-2* double mutant had ~10% short ectopic branching in the metacorpus with *mab-20* and *plx-2* showing weaker effects (Table 3). Lastly, SAX-3/Robo receptor of the Slit/Robo pathway had no effect on M1 guidance. We were unable to detect redundancy between the guidance systems among *plx-1; unc-129, unc-5; unc-129, unc-51; unc-129, unc-51; unc-5, unc-115; elg-15* or *vab-1/+; sax-3* (Table 3).

Different pharyngeal neurons use overlapping and distinct mechanisms to extend their axons

M1 both shares and has unique axonal elongation mechanisms with the other two pharyngeal neurons that have been studies in detail, M2 and NSM (MORCK *et al.* 2003; RAUTHAN *et al.* 2007; AXANG *et al.* 2008; see Pilon (2008) for review). Both M1 and M2 are influenced by interactions with another cell (g1P and M3, respectively). The minor process of NSM and the proximal trajectories of the M1 and M2 axons extend independent of the genes with growth cone phenotypes *unc-34, unc-51, unc-115* and *unc-119.* The axonal extension phase that does depend on these genes differs between the three types of neurons, for example NSM extension does not require *unc-119,* whereas,

M1 and M2 require *unc-119* to suppress ectopic branching. M1 differs from M2 and the major NSM projections in showing only weak *unc-69*, *unc-73* and *unc-76* phenotypes. The most dramatic difference is that M1 shows only weak phenotypes for mutations in the major guidance pathways. While both M1 and NSM show phenotypes for semaphorin and *unc-129* mutations, the defects were much weaker for M1. M1 also differs from the other two neurons by not showing dependence on the Netrin and Slit systems. A similarity between the three neurons is that none responded to Ephrin mutations. Extension of the three types of pharyngeal neurons, for mutants that do have phenotypes, and indeed most *C. elegans* neurons, nearly always showed incompletely penetrant phenotypes, highlighting the robustness of the process.

New mutations affecting M1

Because all situations tested resulted in incomplete penetrance for distal M1 extension, novel molecules might be involved in M1 guidance. We thus carried out a forward genetic screen for abnormal M1 morphology using the integrated *glr-2::gfp* maker and identified nine mutations resulting in axon truncation, abnormal branching or termination defects. This screen isolated new *unc-51* alleles (demonstrating the utility of the screen), and *rpm-1*. We also identified mutations in three novel genes, *mnm-6*, *mnm-7* and *mnm-8*.

The RPM-1 (Regulator of Presynaptic Morphology-1) protein functions in synaptogenesis and axon termination in different organisms (SCHAEFER *et al.* 2000; WAN *et al.* 2000; ZHEN *et al.* 2000; D'SOUZA *et al.* 2005; LI *et al.* 2008). In *C. elegans*, RPM-1 acts cell autonomously in the PLM mechanosensory neuron and DA/DB motor neurons to regulate axon termination, guidance and synapse formation (GRILL *et al.* 2007; LI *et al.*

2008; TRUJILLO *et al.* 2010; TULGREN *et al.* 2011). Consistent with these observations, the *rpm-1* mutants, including both existent alleles and those isolated in our screen, exhibited failure of the M1 terminal process to stop at their final destination. Rather, they extend posteriorly, overshooting their normal targets. This is the first case to describe a role for *rpm-1* in the pharyngeal nervous system.

The Unc phenotype of the *mnm-6* overextension mutant may indicate that the gene functions in guiding other neurons. Since *mnm-6* shows a stronger phenotype than any of the axon guidance null mutants we tested, it may function independently of the guidance pathways that we tested. *mnm-7* also has general effects on axon guidance since other *glr-2::gfp* neurons outside the pharynx show overextension and abnormal-branching. *mnm-8* results in the absence of M1 neuron in 95% of animals while other *glr-2::gfp* expressing neurons were present. *mnm-8* likely affects some aspect of M1 specification or differentiation that leads to absence of the *glr-2::gfp* expression rather than transforming M1 to the fate of its sister, which normally undergoes programmed cell death (SULSTON *et al.* 1983). It will be interesting to see whether any other neurons that emerge from the pharyngeal primordium differentiate in a *mnm-8* dependent manner.

A simple model for M1 axon development involves two phases (Figure 15). In the first phase, M1 builds its proximal trajectory using mechanisms distinct from those used during the rest of the axon journey, and may be coupled to elongation of the pharynx as a whole. In the second phase, M1 uses multiple mechanisms to establish its distal trajectory, including growth cones and cues from the non-neuronal g1P gland cell. Incomplete penetrance under all the tested conditions suggests that this phase may use highly redundant, involve novel mechanisms or depend on mutations with lethal

phenotypes. Alternatively, the route of the M1 axon may be physically constrained by surrounding pharyngeal tissues such that the axon sometimes extends properly when normal guidance cues employing g1P or growth cone are compromised. The M1 system is a compelling model for axon guidance in the pharynx with similarities and differences from previously described models such as M2 and NSM neurons (MORCK *et al.* 2003; AXANG *et al.* 2008). Even though the pharynx represents a closed and limited environment of only 80 cells (ALBERTSON and THOMSON 1976), axon guidance in this simple structure is nevertheless a complex process.

Figure 15. Model for M1 axon guidance

M1 is shown in green, g1P in red. M1 development is divided into two steps. During “Phase 1”, M1 builds its proximal trajectory independent of genes affecting growth cones. In “Phase 2” M1 builds its distal trajectory, which is affected in growth cone-defective mutants and loss of the g1P cell. The regions where M1 axon phenotypes occur are shown for each gene. These genes are categorized in groups, which either act in metacorpus, procorpus and or at the anterior pharyngeal tip where the axon terminates. *unc-119* (which also acts for distal extension), *mnm-7* and *vab-1* are necessary for preventing ectopic branching in the isthmus or terminal bulb, rather than axon extension in those regions.

Figure 15. Model for M1 axon guidance

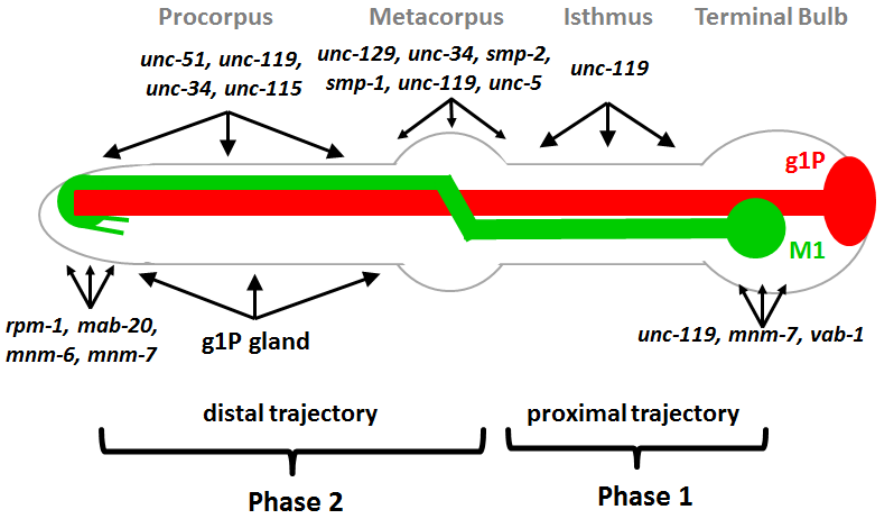

FUTURE DIRECTIONS (this was not part of the original manuscript)

The current work was successful in identifying mechanisms and molecules necessary for development of the pharyngeal neuron M1. The finding that most of the known axon guidance molecules had minor or no effect on M1 axon guidance suggest the involvement of novel or unknown guidance molecules. In a forward genetic screen for 5000 haploid genome, I identified nine mutations that result in M1 abnormalities, including mutations in new alleles for *unc-51* and *rpm-1* and may be three novel genes, *mnm-6, mnm-7* and *mnm-8*. However, there is a strong possibility that the genetic screening did not reach saturation. The isolation of more than one allele for a single gene, *rpm-1,* may be due to the relatively large size (more than 14.5kbp) of the gene. Additionally, it is possible that some mutations were not isolated due to their lethality. Thus, it is worth screening more animals in a forward genetic screen.

Fine mapping and cloning of the novel isolated genes *mnm-6, mnm-7* and *mnm-8* might be of a great interest of the future work. *mnm-8* appears to affect the neuronal specification or early differentiation of M1, therefore it may help the understanding of how M1 is specified. Furthermore, identifying the promoter of *mnm-8* may provide a new tool to drive specific gene expression in M1. Such a promoter can be used to visualize the early stages of M1 development and axon guidance if tagged with GFP. Moreover, it will allow the study of the first phase of M1 axon development, which is thought to be independent of guidance molecules.

UNC-119 appears to play an essential role in M1 axon guidance and maintenance. Mutants of *unc-119* were the only ones that showed almost complete penetrance of M1 defects. It is of great importance for future work to find out where *unc-119* functions

during M1 development. It is possible that *unc-119* is expressed in the g1P gland or pharyngeal muscles. Thus, making a construct to drive *unc-119* cDNA in these cells may help define the role of *unc-119*. Such experiments were successful in rescuing *unc-119* phenotypes, including defective axon outgrowth (MADURO and PILGRIM 1995; MADURO *et al.* 2000; KNOBEL *et al.* 2001; MATERI and PILGRIM 2005). The pharyngeal gland-specific promoter *hlh-6* (SMIT *et al.* 2008) can be used to drive *unc-119* cDNA expression in g1P gland. Pharyngeal muscle-specific expression of *unc-119* can be achieved using the *myo-2* promoter (OKKEMA *et al.* 1993). A caveat to this experiment might be the lack of an M1 neuron specific promoter that is expressed early in embryogenesis. The available *glr-2* promoter is expressed relatively late in development (see Results).

Chapter Four: **THE EMBRYONIC ELONGATION**

BACKGROUND

During *C. elegans* embryonic development, the worm embryo undergoes dramatic changes to elongate from a spheroid into a long, thin worm. This process is known as embryonic elongation, where the embryo reduces its circumference by a factor of three and increases in length by a factor of four during the elongation process (Figure 16) (CHISHOLM and HARDIN 2005). Embryonic elongation starts approximately 350 minutes after first cleavage and is completed by about 600 minutes. Interestingly, these morphogenetic events take place without a change in cell number or cell size and the process is mainly initiated in a single cell layer that surrounds the embryo, the epidermis (sometimes referred to as the hypodermis in nematodes) (PIEKNY and MAINS 2003; LIU *et al.* 2007).

The development of the epidermis is crucial for the whole process of embryonic morphogenesis. Epidermis is a single epithelial layer that surrounds the embryo and its morphogenesis involves cell-cell interactions that determines the final shape of the animal. As demonstrated by laser killing experiments, the integrity of the epidermal sheet is necessary for the elongation of the embryo (PRIESS and HIRSH 1986; CHISHOLM and HARDIN 2005). In fact, embryonic elongation reflects the epidermal cell elongation along the anterior-posterior axis, where the circumferential epidermal surfaces shorten around the animal while elongating in the orthogonal direction (PRIESS and HIRSH 1986; CHISHOLM and HARDIN 2005).

Figure 16. Overview of the embryonic elongation

During elongation, the embryo reduces its circumference by a factor of three and increases in length by a factor of four. (I) Schematic diagram illustrates the timing of the embryonic elongation. Elongation occurs in two phases: the early elongation phase starts at about 360 minutes after the first cleavage and extends to the 2 fold (twice the length of the eggshell) embryonic stage. The late elongation phase, which starts right after the 2 fold stage and continues until the embryo hatches into the worm-shape larva. (II) DIC photographs for the early elongation phase (panels A-E) and the late elongation phase (E-I).

Figure 16. Overview of the embryonic elongation

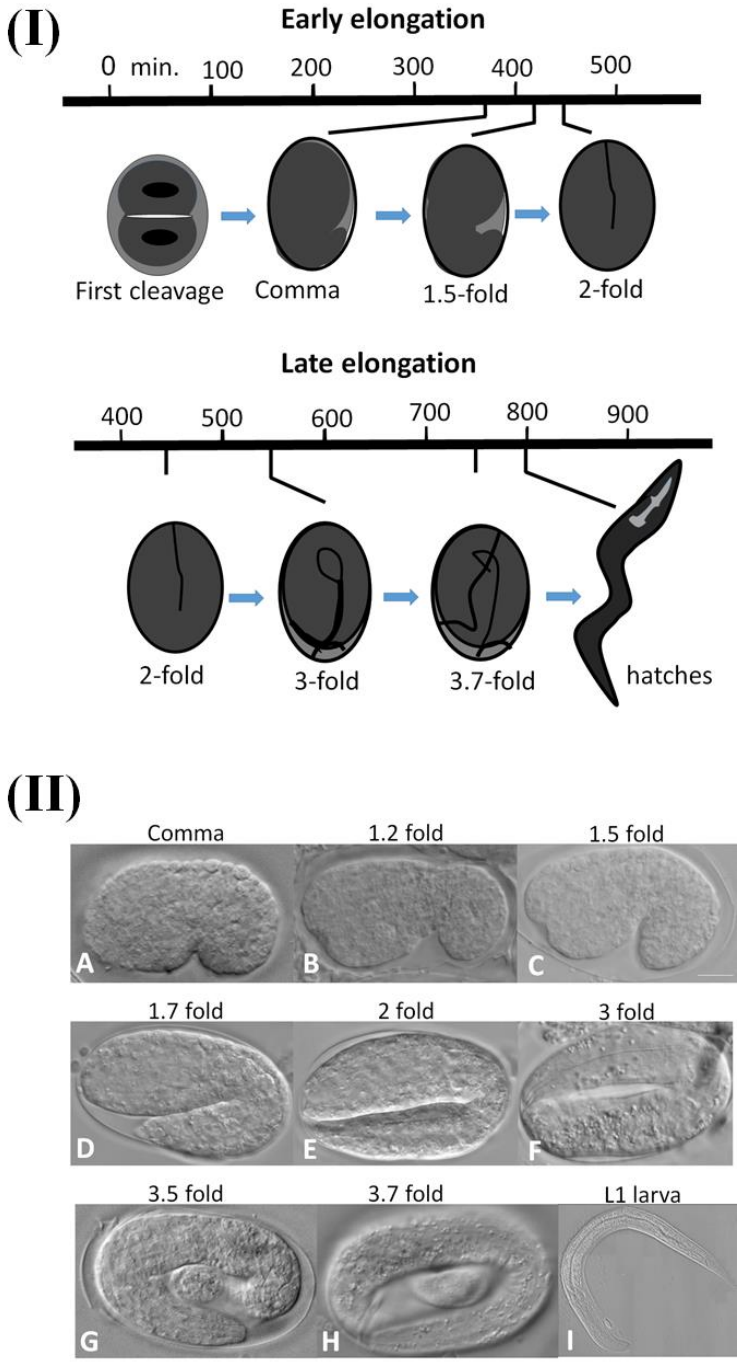

Prior to the start of embryonic elongation, epidermal cells encase the entire embryo as described in Chapter One. These are organized in three major groups: (1) one row of dorsal epidermal cells straddling the dorsal midline along the anterior-posterior axis; (2) two rows (one on each side of the embryo) of lateral epidermal cells (also known as seam cells); and (3) two rows of ventral epidermal cells meeting each other across the ventral midline. Lateral epidermis has the ability to initiate and generate the contractile forces need for epidermal elongation (DING *et al.* 2004; DIOGON *et al.* 2007; AAMODT and CULOTTI 1986; PRIESS and HIRSH 1986; PIEKNY and MAINS 2003). Embryonic elongation can be divided into two main phases. First is the "early elongation" phase that occurs between comma (Figure16, IIA) and two-fold stages (Figure16 IIE, "fold" stages refers to the length of the embryo relative to the long axis of the egg). Upon completion of the first phase, the "late elongation" phase starts and continues until the embryo becomes fully elongated. The early elongation phase is mainly controlled by epidermis, while the late elongation phase depends on function of muscle cells. These two phases are discussed below.

Early elongation phase (epidermis driven elongation)

Epidermal elongation is a reflection of the overall changes in the epidermal cytoskeleton, extracellular matrix and adhesion junctions. The epidermal cytoskeleton, which includes the contractile system of early elongation, is a highly organized structure of three major cytoskeletal filament systems, which are essential for epidermal elongation. These structures are actin microfilaments (MF), microtubules (MT), and intermediate filaments (IF) (DING *et al.* 2004). At the onset of elongation, both actin MFs and MTs become highly organized in a striking circumferential pattern within the

epidermal cells (COSTA *et al.* 1997; WILLIAMS-MASSON *et al.* 1997; COSTA *et al.* 1998; PRIESS and HIRSH 1986; DING *et al.* 2004). The actin MFs are organized in circumferential bundles (CFBs) in all epidermal cells. Thus, the actin cytoskeleton encircles the embryo, and become attached to the cell-cell adherens junctions of adjacent epidermal cells (COSTA *et al.* 1997; WILLIAMS-MASSON *et al.* 1997; COSTA *et al.* 1998). Most importantly, epidermal actin filaments appear unordered up to an hour after elongation begins and right after elongation is complete, implying that CFBs are required only transiently during elongation (PRIESS and HIRSH 1986; DING *et al.* 2004). Drugs that destroy actin filaments, such as cytochalasin, disrupt CFBs and in turn block elongation, indicating that it is essential for elongation (PRIESS and HIRSH 1986).

There are many lines of evidence that the actomyosin-based contractile machinery is primarily active in the lateral epidermal cells. The dorsal and ventral epidermal cells may only passively respond to waves of contractile forces produced by their adjacent seam cells, rather than being contractile themselves (PRIESS and HIRSH 1986; DING *et al.* 2004; GALLY *et al.* 2009). Transmission of the contractile forces from the seam cells to the dorsal/ventral epidermis is via CFBs and cadherin-catenin junctions (CHISHOLM AND HARDIN 2005).

MFs of the dorsal and ventral epidermis are circumferentially arranged and associated with the apical membrane of the epidermis. However, circumferential filaments in the lateral epidermis appear not to be associated with the apical membrane (Figure 17) (PRIESS and HIRSH 1986). Such architecture allows the seam cells to generate their smooth muscle-like actin/myosin contraction, which will be subsequently

transmitted to dorsal and ventral epidermal cells through connections with adherens junctions, which anchor the CFBs (PRIESS and HIRSH 1986).

Figure 17. Overview of epidermal cells organization during elongation

DIC images of wild type *C. elegans* embryos (upper row) at early elongation (1.5 fold), mid-elongation (2 fold), and late elongation (3fold). Epidermal elongation involves arrangement of epidermal cells (middle row), outlined by *ajm-1::gfp* (which marks cell borders) fluorescent images at the three stages in the above row. Schematic drawing of the epidermal cell elongation (lower row), with dorsal cells are coloured pink, lateral cells are green, ventral cells are red. The yellow arrow in the bottom row highlights the lengthening of lateral epidermal cells.

Figure 17. Overview of epidermal cells organization during elongation

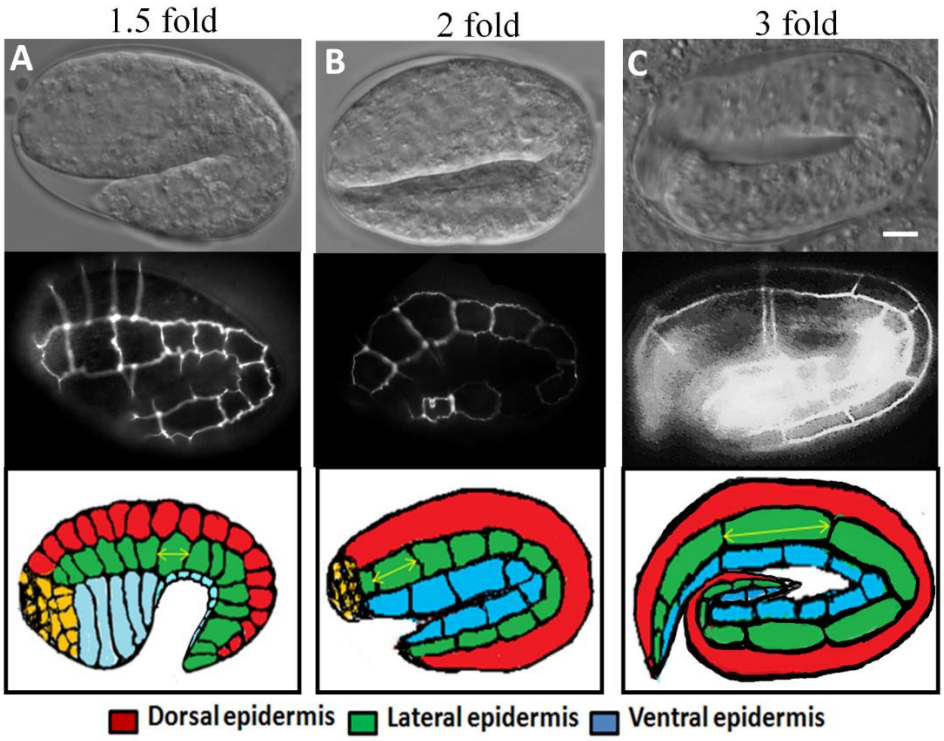

Similar to actin MFs, lateral epidermal MTs appear randomly oriented before and after elongation. The MTs in the dorsal and ventral epidermal cells become circumferentially oriented with the start of elongation. Moreover, MTs in the lateral cells are also not associated with the apical membrane and remain arranged in a meshwork (WISSMANN *et al.* 1997b; SOMLYO and SOMLYO 2000; SIT and MANSER 2011). Although the role of MTs in elongation is not well characterized, they are thought to function in distributing the contractile force. Indeed, MT inhibitors cause incomplete elongation and epidermal deformations (PRIESS and HIRSH 1986).

Adherens junctions, which are connected to the actin cytoskeleton, are necessary to transfer the contractile force generated in lateral epidermal cells to the rest of the epidermis. Mutations in the junction related HMR complex and transmembrane protein VAB-9, result in epidermal defects and elongation defects (PRIESS and HIRSH 1986). Moreover, embryos lacking other junctional complex proteins, such as the Discs-large homolog DLG-1 and the apical junction molecule AJM-1do not elongate properly (SIMSKE and HARDIN 2001; SIMSKE *et al.* 2003). The *C. elegans* genome encodes 11 cytoplasmic intermediate filaments, at least three of which have been implicated in epidermal morphogenesis (KOPPEN *et al.* 2001; SIMSKE *et al.* 2003).

Genetic regulation of the early elongation

Although the events of cytoskeletal changes that occur during elongation are well studied, less is known about the mechanisms by which the CFBs form in an ordered fashion (DING *et al.* 2004). Genetic analysis of *C. elegans* elongation revealed several redundant pathways that produce the force that acts on the CFBs (Figure 18) (CHISHOLM and HARDIN 2005): (i) one pathway includes *let-502* Rho-binding kinase and *mel-11* myosin phosphatase; (ii) a second pathway involves the sex-determination gene *fem-2*, which encodes a PP2c phosphatase and PAK-1 (p21 kinase); and (iii) a third pathway involves the muscle genes, which act predominantly in late elongation phase. The *let-502/mel-11* and *fem-2/pak-1* pathways are responsible for the early elongation.

let-502/ROCK/Rho-binding kinase and mel-11/MYPT myosin phosphatase pathway

As stated earlier, small GTPases are responsible for morphogenetic processes by regulating signal transductions that control the actin cytoskeleton (PIEKNY *et al.* 2000). The Rho-binding kinase (ROCK), a Rho GTPase effector, and two of its targets, the myosin regulatory light chain (rMLC) and the myosin-binding phosphatase regulatory subunit (MYPT) of myosin light chain phosphatase (MLCP) are necessary for several morphogenetic processes, including smooth muscle contraction (VAN AELST and SYMONS 2002; BURRIDGE and WENNERBERG 2004).

Once activated, ROCK can activate myosin II by phosphorylating the rMLC, which is necessary and sufficient for contraction (Figure 18) (YOUNG *et al.* 1993; WISSMANN *et al.* 1997a; WISSMANN *et al.* 1999; PIEKNY and MAINS 2002; PIEKNY *et al.* 2003; DIOGON *et al.* 2007). MLCP dephosphorylates rMLC, counteracting ROCK. However, ROCK can also inactivate MLCP by phosphorylating its targeting subunit,

MYPT, and thus trigger contraction (VAN EYK *et al.* 1998; TOTSUKAWA *et al.* 2000). Thus, ROCK is able to promote actin-myosin contraction by either activation of myosin or inhibiting the myosin inhibitor, MLCP/MYPT.

Genetic analysis revealed that expression of *C. elegans* ROCK homolog LET-502 is essential for embryonic elongation. Loss of function mutations of *let-502* reduce contraction (hypocontraction) and result in elongation arrest. Conversely, loss of the LET-502 target MEL-11, the homolog of MYPT, results in the opposite phenotype, "hypercontraction" as result of myosin II hyperactivity and embryos arrest and often burst (WISSMANN *et al.* 1997a; PIEKNY and MAINS 2002; PIEKNY *et al.* 2003; DIOGON *et al.* 2007). Thus, it is clear that LET-502 and MEL-11 are antagonistic to each other. LET-502 and MEL-11 were found to be expressed at high levels in the cytoplasm of seam cells; however, due to LET-502 activity, MEL-11 becomes restricted to the cell periphery and the cell-cell junctions at the onset of elongation, effectively moving it away from the contractile apparatus (PIEKNY *et al.* 2003). Additionally, rMLC/MLC-4is highly expressed in seam cells, acting as a target for LET-502 (WISSMANN *et al.* 1997a; PIEKNY and MAINS 2002; PIEKNY *et al.* 2003; DIOGON *et al.* 2007). Indeed, *mlc-4* mutants exhibits an elongation arrest similar to that of *let-502* mutants. This implies that MLC-4 and LET-502 promote the actomyosin contraction of the seam cells and thereby their elongation. The two non-muscle myosin heavy chains, NMY-1 and NMY-2 are thought to be regulated by MLC-4, as their mutations exhibit a similar elongation arrest (i.e., hypocontraction phenotype) (SHELTON *et al.* 1999b; PIEKNY *et al.* 2000; GALLY *et al.* 2009). Additionally, new components of the known pathway were identified, such as the formin FHOD-1, which is thought to act downstream of LET-502/MEL-11 pathway

(VANNESTE *et al.* 2013). The *mel-11/let*-502 pathway mainly controls the early stage of elongation between 1.2 and 2 fold stages by controlling actin/myosin contractions (WISSMANN *et al.* 1997a; SHELTON *et al.* 1999b; PIEKNY and MAINS 2002; PIEKNY *et al.* 2003; DIOGON *et al.* 2007).

The incomplete penetrance of the *let-502*; *mel-11* double mutant phenotype is evidence for redundancy and has led to identification of parallel pathways (PIEKNY *et al.* 2000). That is, when both *let-502* and *mel-11* are eliminated, embryos often elongated and grow to adulthood, albeit animals are sterile and have abnormal body shapes. Components of such parallel pathways may include calmodulin and MLCK (myosin light chain kinase), as identified in mouse smooth muscle (SMITH *et al.* 1987); however, no obvious MLCK homolog is known in *C. elegans* (BATCHELDER *et al.* 2007).

The fem-2 PP2C phosphatase and p21 kinase pak-1 in elongation

In addition to the *let-502/mel-11* pathway, two proteins were identified as components of the redundant pathway(s): FEM-2 (PP2c phosphatase) and PAK-1 (p21 kinase). These two genes act together in parallel to *let-502* to mediate contraction (BATCHELDER *et al.* 2007). The *C. elegans fem-2* gene encodes a protein phosphatase of the type 2c (PP2c phosphatase), which has a well-established essential function in sex determination (KIMBLE *et al.* 1984; HODGKIN 1986; PILGRIM *et al.* 1995; CHIN-SANG and SPENCE 1996; HANSEN and PILGRIM 1998). Mutations in *fem-2* enhance the near-normal elongation of *let-502; mel-11* as triply mutant animals, which arrest with little elongation, indicating that *fem-2* acts in a parallel, early elongation pathway. Genetic analysis indicated that function of *fem-2* in elongation appears to be independent of its role in sex

determination as no other sex determination genes function during elongation (PIEKNY *et al.* 2000). However, it is not known where FEM-2 acts during elongation.

The p21 kinase PAK-1 is a CDC42/RAC-effector and has a role in early elongation (GALLY *et al.* 2009; MARTIN *et al.* 2014). PAK-1 appears to be acting redundantly with other two kinases, LET-502/ROCK and MRCK-1 to regulate myosin II during elongation. The combined loss of function mutations of LET-502, PAK-1 and MRCK-1 resulted in a complete embryonic arrest at 1.2 fold stage, suggesting that the elongation was completely blocked (GALLY *et al.* 2009). PAK-1 was shown to be associated with intermediate filaments (IFA2 and IFA3) in all stages and is required more specifically in the dorsal/ventral cells for mechanotransduction signalling later in embryogenesis (ZHANG *et al.* 2011). The CDC42/RAC-specific GEF, PIX-1, is an activator of PAK-1 and was shown to control early embryonic elongation in parallel with *let-502/mel-11*(MARTIN *et al.* 2014). *pix-1*is thought to be mostly required in the anterior part of the embryo, along with *pak-1,* to control the elongation of the head of the embryo. *let-502* function is required throughout the anterior/posterior axis to control embryonic elongation (MARTIN *et al.* 2014). Despite identification of some of its components, details of the *pak-1/fem-2* elongation pathway is not well characterized. *fem-2* appears to be within the *pak-1* elongation pathway (VANNESTE *et al.* 2013).

Figure 18. Gene interactions controlling embryonic elongation

Diagram illustrating genetic interactions during elongation, which involves several redundant pathways, showing the different activities in the lateral vs. dorsal ventral cells. Boxed genes are (inactivated)while circled genes are (activated) in the indicated cells. Some genes are expressed differentially in the epidermal cells. The *let-502* Rho-binding kinase plays a central role in embryonic elongation, by promoting the actomyosin contraction of the lateral epidermal cells. The *mel-11* myosin phosphatase plays an antagonistic role by blocking contraction. In addition to the *let-502/mel-11* pathway, there are other redundant pathways, including the *fem-2/pak-1* pathway.

Figure 18. Gene interactions controlling embryonic elongation

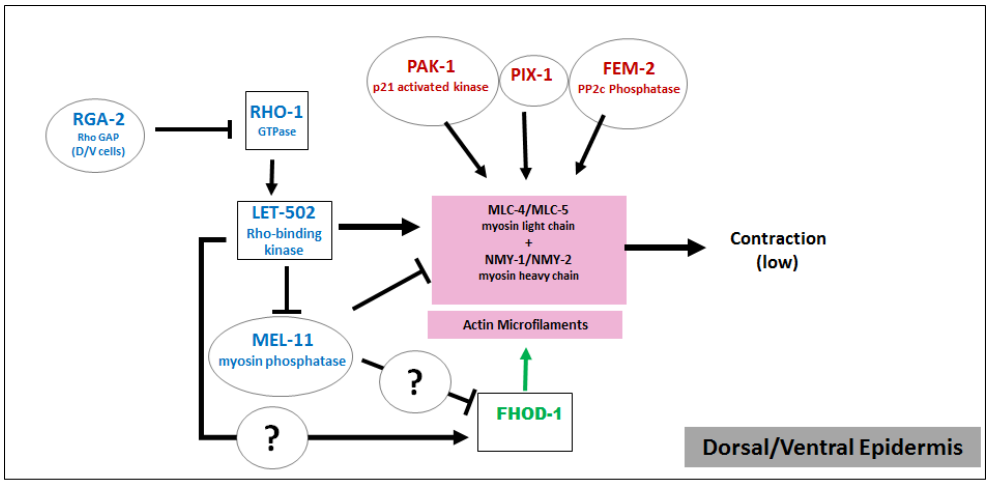

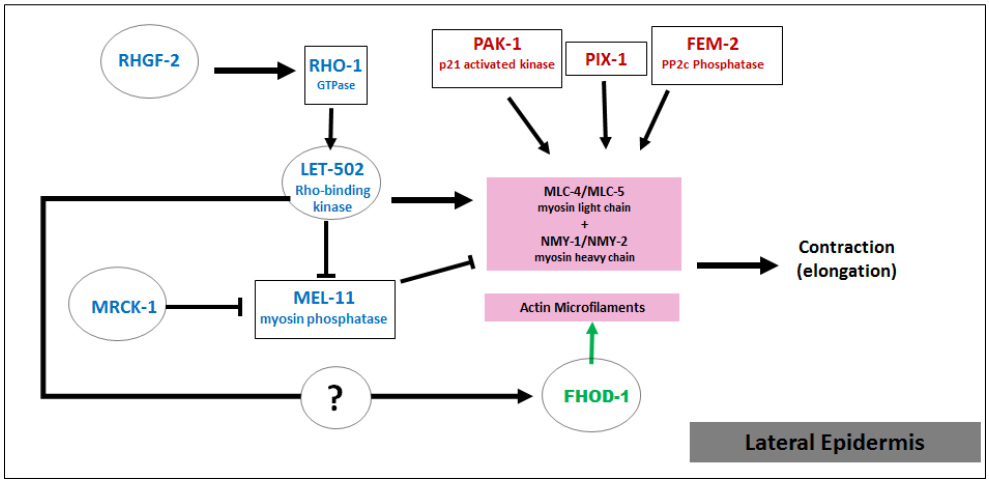

Late elongation phase (muscle driven elongation)

The epidermal elongation mediated by contraction of the lateral epidermal cells is complete by the 2 fold embryonic stage (Diogon et al., 2007), beyond which additional molecular mechanisms and contractile machinery is required to finalize the embryonic elongation (DING *et al.* 2004). This phase is predominantly controlled by muscle cells. Mutants that have complete muscle dysfunction fail to elongate. In these mutants elongation is apparently normally until the 2 fold stage. This is called the Pat phenotype (paralyzed arrest at two-fold) (WILLIAMS and WATERSTON 1994). Mutation of *myo-3*, which encodes the minor muscle MHC, results in a Pat phenotype (GETTNER *et al.* 1995; MACKINNON *et al.* 2002; LIN 2003; CHISHOLM and HARDIN 2005).

Muscle contraction force is transmitted to the embryonic sheath via trans-epidermal attachments, originally named fibrous organelles (FRANCIS and WATERSTON 1991; DING *et al.* 2004). Muscle attachment structures are thought to interact with the epidermal CFBs, MT bundles or other components of the epidermal cytoskeleton, to induce epidermal shape changes. Defects of epidermis/extracellular matrix attachment to muscles result in elongation arrest about the 2 fold stage, for example mutants of *pat-4*, which encodes an integrin-linked kinase (GETTNER *et al.* 1995; MACKINNON *et al.* 2002; LIN 2003; CHISHOLM and HARDIN 2005). However, it is not clear whether these elongation defects are due to lack of epidermal attachment structure components or whether they reflect a potential role for muscle contractions in epidermal elongation, i.e., independent of attachment structures (DING *et al.* 2004).

The epidermis produces the cuticle of the first larval stage after the end of the late elongation phase. From then on, the shape of the epidermal cells is held in place by the

cuticle. Defects in cuticle structure can cause late elongation defects (PRIESS and HIRSH 1986; MCMULLAN *et al.* 2003).

The arp2/3 complex

Actin related proteins (ARP-2/3) are composed of seven evolutionarily-conserved subunits that have the ability to nucleate actin Y-branched arrays by binding the sides of an existing actin filaments, but the mechanism is not understood (WELCH *et al.* 1997). The action of ARP-2/3 enables the formation of branched actin networks at the leading edge of migrating cells that results in a dense F-actin meshwork such as seen in lamellipodia (GOODE and ECK 2007; POLLARD 2007). The *C. elegans* genome encodes seven Arp2/3 complex subunit genes, *arx-1, arx-2, arx-4, arx-5, arx-6* and arx-7 (SWAN *et al.* 1998; SEVERSON *et al.* 2002; SAWA *et al.* 2003; NEIDT *et al.* 2008). Mutation in Arp2/3 subunits result in gastrulation defects and embryonic lethality (SWAN *et al.* 1998; SEVERSON *et al.* 2002; NEIDT *et al.* 2008). Arp2/3 complex is also required for embryonic ventral enclosure and excretory cell migration in *C. elegans* (SWAN *et al.* 1998; SEVERSON *et al.* 2002; SAWA *et al.* 2003; NEIDT *et al.* 2008). The function of the Arp2/ 3 complex requires the activity of the Arp2/3 nucleation promoting factors, including Wiskott-Aldrich Syndrome protein (WASP) and three WASP and verprolin homologs (WAVEs) (WELCH *et al.* 1997).

The formin multigene family

The formin protein family is an eukaryotic innovation, and these proteins are necessary for several dynamic cellular processes, including determination of cell shape (CHALKIA *et al.* 2008; CHESARONE *et al.* 2010). The formin family of proteins control the assembly and elongation of unbranched actin filaments and thereby regulate a wide range

of actin-based cellular processes (HIGGS 2005; HIGGS and PETERSON 2005; FAIX and GROSSE 2006; GOODE and ECK 2007; CHESARONE *et al.* 2010). Also, several formins are involved in other actin modulatory functions such as filament bundling or de-polymerization, in addition to their role in actin nucleation (HARRIS *et al.* 2006; HARRIS *et al.* 2010; SCHONICHEN *et al.* 2013). Formins bind to the growing (+) end of the actin filament and act as a progressive cap to stabilize the initial actin dimer during actin nucleation and prevent the filament termination by inhibiting capping proteins (WATANABE and HIGASHIDA 2004). Due to their importance in cell biology, some studies link aberrant formin function and expression to disease pathogenesis (DEWARD *et al.* 2010). For instance, knockdown of Diaphanous Related Formin 3 was reported to enhance metastasis and tumour growth in human prostate cancer (DI VIZIO *et al.* 2009).

Formins are long, multidomain proteins of more than 1000 amino acids and are categorized by their conserved formin homology domains FH1, FH2 and FH3 (Figure 19) (SCHONICHEN and GEYER 2010). The FH1 domain enhances the recruitment of new actin monomers onto the growing filaments by binding to the actin monomer binding protein profilin (HIGGS 2005) (Figure 19). The FH2 domain, which consists of about 400 residues and binds actin monomers (WESTENDORF *et al.* 1999; KOKA *et al.* 2003; TOJO *et al.* 2003; HIGGS and PETERSON 2005; GOODE and ECK 2007; CHESARONE *et al.* 2010), is involved in actin nucleation by forming homodimers of the formin in a ring-like structure around the nascent actin filament and enhances its elongation (HIGGS 2005). The FH3 domain, also known as the Diaphanous Inhibitory domain (DID), is responsible for the formin dimerization and localization in the cell (PETERSEN *et al.* 1998; ALBERTS 2001; KATOH *et al.* 2001;LI and HIGGS 2003). The N-terminus DID domain interacts with

another domain, the C-terminal Diaphanous Autoregulatory Domain (DAD), to keep formin in an inactive state (ALBERTS 2001; LI and HIGGS 2003). Another formin regulatory domain is the GTPase-binding domain (GBD), which interacts with the Rho-GTPases (Rho, Rac) that act as a molecular switch to activate formin by blocking the DID/DAD interaction (ALBERTS *et al.* 1998). Some other formins depend on kinases such as ROCK for phosphorylation of their DAD domain to active the protein (GOODE and ECK 2007; POLLARD 2007). Deletion or mutation of either of the DID or DAD domains results in a constitutively active protein that can nucleate actin filaments (GASTEIER *et al.* 2003; KOKA *et al.* 2003; TAKEYA and SUMIMOTO 2003; SCHONICHEN *et al.* 2006; BAARLINK and GROSSE 2008; HANNEMANN *et al.* 2008a; SCHULTE *et al.* 2008; TAKEYA *et al.* 2008). Domain structure varies between formin family members, including domains that are not highly conserved, such as the coiled-coil domain (CC) and the dimerization domain (DD) (GOODE and ECK 2007).

Figure 19. Typical domain structure of formin proteins and factors necessary for their function

Diagram shows the domain organization of most of the formin proteins. Starting at the N-terminus and ending at the C-terminus, as following: GTP-binding domain (GBD; gray), diaphanous inhibitory domain (DID; green) (also known as the FH3 domain), dimerization domain (DD; blue), coiled-coil domain (CC; dark blue), formin homology domain 1 (FH1; light blue), the formin homology domain 2 (FH2; red) and the diaphanous autoregulatory domain (DAD; yellow). Autoinhibition (black arrow) occurs by the interaction between the DID and DAD domains that keep the protein in an inactive state. Activation of formins usually depends on binding of GTP-bound Rho protein (GTP Rho) to the GBD domain. Formins control of actin filament assembly is initiated by the FH2 domain binding and stabilizing of actin dimers or trimers. During the filament's elongation, the FH2 domain remains associated with the barbed end and adds more units. Profilin bound actin (P-actin) acts as an activator that enhances the filament elongation by interacting with the FH1 domain.

Figure 19. Typical domain structure of formin proteins and factors necessary for their function

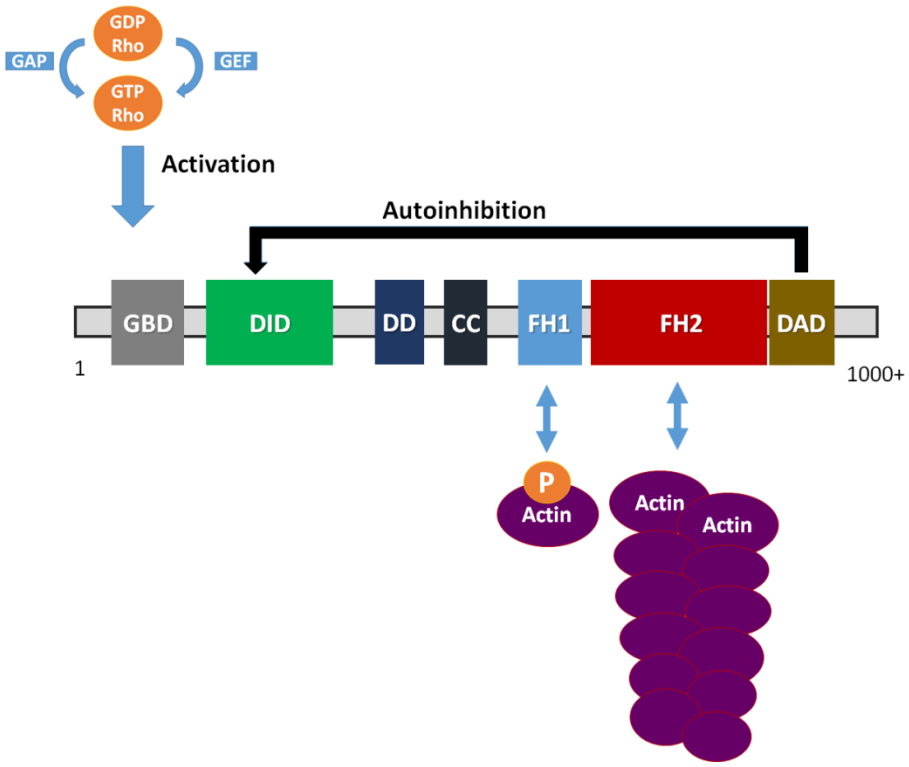

C. elegans formins

Bioinformatic studies classified mammalian formins (15 genes) based on their FH2 domains into seven groups or subfamilies (Table 4). These groups include, the Diaphanous Formins (DIA), Formin-Related proteins identified in Leucocytes (FRL), the Disheveled-Associated Activators of Morphogenesis (DAAM), Delphilin, the "inverted" formins (INF2), the original "namesake" formins (FMN) and the Formin Homology Domain-containing proteins (FHOD) (HIGGS 2005; HIGGS and PETERSON 2005; MI-MI *et al.* 2012).

The number of formin genes varies between species as some of the formin groups are completely absent, for instance *D. melanogaster* and *C. elegans* have no Delphilin genes (CHALKIA *et al.* 2008). The *C. elegans* genome encodes seven formins covering five of the formin subfamilies, *cyk-1, daam-1, fozi-1, frl-1, inft-1, inft-2,* and *fhod-1*, and so the worm represents a simple system to study formin functions (HIGGS 2005; HIGGS and PETERSON 2005; MI-MI *et al.* 2012). Cytokinesis defective-1 *(cyk-1)* is homologous to *Drosophila* diaphanous and human DIAPH1. *cyk-1* is known for its essential role in embryonic cytokinesis, where it is necessary for actin nucleation and contractile actin ring assembly (SWAN *et al.* 1998; SEVERSON *et al.* 2002; NEIDT *et al.* 2008). *cyk-1* is also required for striated muscle growth and maintenance (MI-MI *et al.* 2012). *daam-1* is a member of the DAAM subfamily and encodes an ortholog of *Drosophila* and human DAAM. DAAM-1 mediates Wnt signaling required for the asymmetrical division of the *C. elegans* B cell (ASPENSTROM *et al.* 2006; WU and HERMAN 2006). The formin-like, formin homology domain/zinc finger-1 (*fozi-1*) encodes a highly divergent nuclear protein that has a vestigial FH2 domain, which does not polymerize actin but can only

dimerize it, and is required in cell fate specification (JOHNSTON *et al.* 2006). *frl-1* encodes the sole *C. elegans* homolog of human FMNL1, 2, and 3 that are required for the asymmetric B cell division (FAVARO *et al.* 2003; WU and HERMAN 2006). *C. elegans* has two inverted formins (INF), *inft-1* and *inft-2* that are homologous to the mouse mINF-1 and mINF-2 (MI-MI *et al.* 2012). *fhod-1* is the sole *C. elegans* FHOD subfamily member and is homologous to the human and mouse FHOD1 and FHOD3. FHOD1 was reported to be associated with stress fibre formation and actin assembly in many systems, including human, mouse and *Drosophila* (ISKRATSCH *et al.* 2010; ISKRATSCH *et al.* 2012; ISKRATSCH *et al.* 2013; SCHONICHEN *et al.* 2013; DWYER *et al.* 2014). Human FHOD1 acts as an actin bundling factor with capping activity toward the filament barbed end and was found to selectively associate with actin arcs and stress fibres (SCHONICHEN *et al.* 2013). In *C. elegans*, FHOD-1 is expressed in striated body wall muscles and is localized near sarcomere Z lines, which anchor the actin filaments barbed ends (MI-MI *et al.* 2012). Additionally, a proportion of embryos that carry a mutation in *fhod-1* arrest at early elongation and exhibit actin defects specific to the lateral epidermal cells (VANNESTE *et al.* 2013). It is not known whether the other six formins have a role in embryonic elongation. My work will focus on the function of the seven formins in the *C. elegans* embryonic elongation.

Table 4. Mammalian formins are grouped in seven subfamilies

Formin groups	**Description**	**Examples for Member Genes**	***C. elegans* Homologs**
DIA	Diaphanous Formins (DIA)	mDia1, mDia2, and mDia3	*cyk-1*
FRL	Formin-related proteins identified in leucocytes (FRL)	mFRL1, mFRL2, and mFRL3 (also called formin- like FMNL1, -2, and -3)	*frl-1*
DAAM	The disheveled-associated activators of morphogenesis (DAAM)	mDAAM1, mDAAM2	*daam-1*
Delphilin	Delphilin formins	mDelphilin	---
INF	The “inverted” formins (INF)	mINF1 and mINF2	*inft-1 and inft-2*
FMN	The original “namesake” formins (FMN)	mFMN1 and mFMN2	---
FHOD	The formin homology domain-containing proteins (FHOD)	mFHOD1 and mFHOD3	*fhod-1*

THE ROLE OF FORMINS IN EMBRYONIC ELONGATION

Background: fhod-1 is involved in early elongation

Previous genetic analysis showed that the formin *fhod-1* is involved in the early stage of *C. elegans* embryonic elongation. FHOD-1 is thought to be necessary for epidermal actin organization between 1.2 fold (lima bean) stage and the 2 fold stage (VANNESTE *et al.* 2013). Actin nucleation is the rate limiting step of actin filament polymerization (CHESARONE *et al.* 2010; SIT and MANSER 2011). Thus, FHOD-1 may play a role in the initial contraction that take place in early elongation by controlling actin filaments. Indeed, *fhod-1* mutant embryos exhibit low penetrance defects in actin organization of their lateral epidermal cells, which are responsible for the first wave of elongation contraction (Figure 20). Moreover, *fhod-1* is likely acting downstream of the two major players that controls early elongation; *let-502* and *mel-11* (VANNESTE *et al.* 2013). Since *let-502* and *mel-11* act antagonistically, and they have opposite phenotypes, and *fhod-1* has a hypo-elongation phenotype similar to that of *let-502*, *fhod-1* potentiates contraction. Lack of LET-502/ROCK results in embryonic failure to elongate and arrest between 1.5 fold to 2 fold stage (WISSMANN *et al.* 1997b; PIEKNY *et al.* 2003; GALLY *et al.* 2009). Loss of *let-502* along with components of the redundant elongation pathway that includes *pak-1, pix-1* and *fem-2* results in elongation arrest as early as 1.2 fold stage (PIEKNY *et al.* 2000; PIEKNY *et al.* 2003; GALLY *et al.* 2009). The absence of MEL-11/myosin phosphatase causes embryos to die between the 1.2 and 2 fold stages, as a result of hypercontraction (WISSMANN *et al.* 1999). Loss of *let-502* or *fhod-1* can rescue

mel-11. Additionally, *fhod-1* was shown to act redundantly with the sex determination gene *fem-2* that has a low penetrance elongation arrest between 1.5 and 2 fold stages.

Figure 20. *fhod-1* is involved in early elongation

Wild-type 3 fold embryo (A). *fhod-1* mutants (B) exhibits a low penetrance elongation arrest similar to that of *let-502* (C). Actin filaments are normally organized in parallel arrays in lateral and dorsal/ventral epidermis (white triangle and empty triangle respectively) of wild-type embryos (D). The *fhod-1* mutant (E) exhibits defects in actin organization of lateral epidermal cells (star), as visualized with VAB-10::GFP. (F) *fem-2* mutant showing the low penetrance elongation arrest phenotype (D and E were provided by P. Mains).

Figure 20. *fhod-1* is involved in early elongation

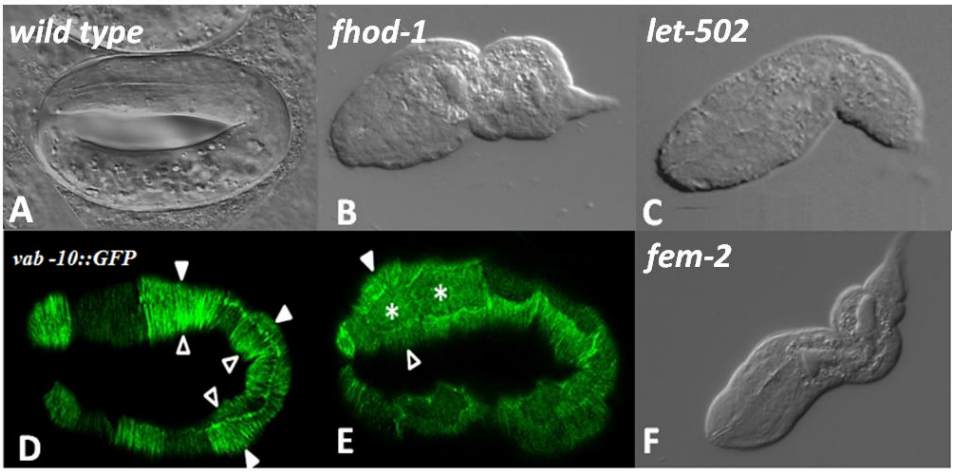

Investigating the role of formin genes in C. elegans embryonic elongation

Previous work demonstrated that less than 25% of *fhod-1* mutant embryos exhibit elongation arrest and I found that a minority (34%; n = 50) showed defects in actin organization as visualized by *lin-26p::ABD$_{vab-10}$::GFP* (WISSMANN *et al.* 1997b; PIEKNY *et al.* 2000; GALLY *et al.* 2009). The incomplete penetrance of *fhod-1* phenotypes suggests redundancy with other genes that regulate elongation. In addition to *fhod-1*, the *C. elegans* genome encodes six other formin genes, *daam-1, inft-1, inft-2, frl-1, fozi-1,* and *cyk-1*, which have the FH2 domain and probably are playing a role in actin organization (MI-MI *et al.* 2012). Thus, I examined these genes as well as genes from the Arp2/3 actin nucleation pathway for elongation defects and genetic interaction with *fhod-1.*

Elongation arrest phenotypes in the following experiments were categorized into four groups, according to the time of arrest in the worm life cycle based on dissection microscope phenotypes (Figure 21): (i) Unhatched embryos, which in the case of *fhod-1* previously were found to arrest before hatching at the 1.5 – 2 fold stages when examined in the compound microscope (VANNESTE *et al.* 2013). Some rare embryos arrested as a ball of cells right before the start of elongation, at 1.2 fold stage or earlier, likely due to earlier defects unrelated to elongation. (ii) Early larval arrest, where embryos hatch but had undergone elongation only to the 1.5 - 2 fold stages. Although fully-defective elongation arrest would be at 1.2 fold, these embryos arrest between the 1.5 - 2 fold stages, as observed for incompletely penetrant mutations such as the *let-502(sb118)* temperature-sensitive (*ts*) allele and *fhod-1(tm2363)* alone (VANNESTE *et al.* 2013). (iii) Late larval arrest, in which embryos hatch and pass the 2 fold stage but arrest with a

dumpy (Dpy) phenotype as L1 – L4 larva. (iv) Wild type, which grow normally to adult stage.

Figure 21. Elongation phenotypes

Normal embryonic elongation of 1.5 fold, 2 fold, 3 fold and 4 fold in (A-D), respectively. Elongation defects were categorized in the current study into four groups according to the stage of arrest: (i) unhatched embryos (E-H), which arrest before hatching at 1.5 – 2 fold stages, (ii) early larval arrest (I-L), which hatch but arrest at 1.5 – 3 fold, (iii) late larval arrest (Q-T), which arrest at larval stages (L1 – L4 larva), often with abnormal body shape. (M-P)Wild type development.

Figure 21. Elongation phenotypes

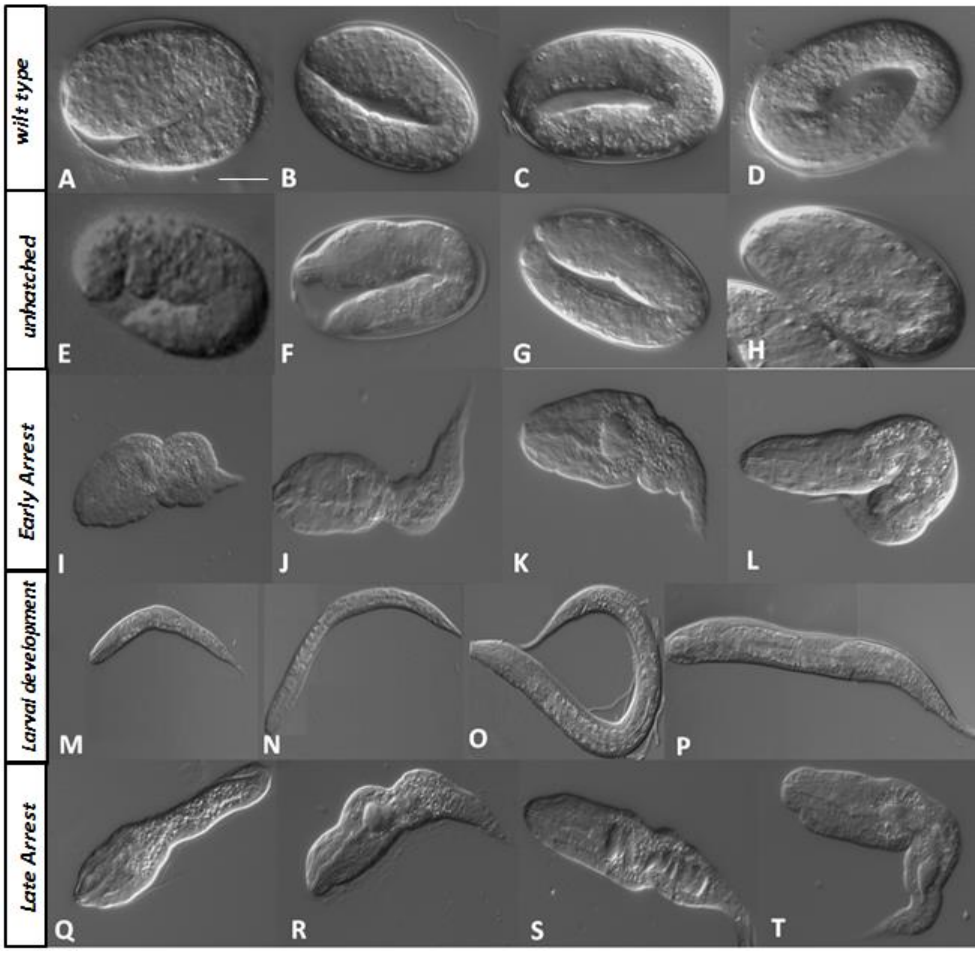

Mutants of formin genes have little or no effect on embryonic elongation

If any of the six formins has a role in embryonic elongation, their mutants are expected to exhibit phenotypes similar to that of *let-502* and *fhod-1*. Therefore, I examined the embryonic elongation of the six formin mutants, *daam-1, inft-1, inft-2, frl-1, fozi-1,* and *cyk-1* (n ≥300; Figure 22). All analyses were carried out at the 25ºC, except if otherwise stated. Homozygous strains for the formin alleles *fozi-1(ok1182), frl-1(ok460), inft-1(gk386)* and *inft-2(ok1296)* were examined as they are viable. Since homozygous alleles of *daam-1* and *cyk-1* are sterile, heterozygous strains *daam-1(tm2133)/+* and *cyk-1(ok2300)/+*, which segregates 25% homozygous embryos, were used. Notably, the products of all formin alleles used here are thought to be null for actin assembly activity, as they lack a functional FH-2 domain (MI-MI *et al.* 2012).

The *frl-1(ok460)* mutant allele appeared to have a wild-type hatching rate and had no apparent elongation defects (Figure 22). *fozi-1(ok1182)* mutants showed slightly higher rate of unhatched embryos, but no apparent elongation defects (Figure 22). In fact, FOZI-1 is a divergent nuclear protein that shows no ability to interact biochemically with F-actin and has its earliest expression in neuronal lineages at the 2 fold stage (JOHNSTON *et al.* 2006). Similarly, mutants of *daam-1, inft-2,* and *cyk-1* had no obvious elongation defects, with less than 10% unhatched embryos (Figure 22).

inft-1 is the only single formin mutant that showed a relatively high percentage of unhatched embryos that may be a result of elongation defect. About 25% of *inft-1(gk386)* mutants exhibited the unhatched phenotype, most of which arrested at the 1.5 to 2 fold embryonic stages, with a frequency of 20% of the total progeny (Figure 22). Only few of the unhatched embryos (<4%) arrested at later stages.

Figure 22. Embryonic elongation phenotypes of the seven formin mutants

Formin genes *inft-1* and *cyk-1* single mutants show about 5% elongation arrest phenotypes that are similar to *fhod-1*, with rest of embryos arresting early in elongation or before elongation starts (unhatched category), probably because of other developmental defects. The double mutants *fhod-1; inft-1* and *fhod-1; cyk-1* have higher elongation arrest frequencies than that of single mutants, but effects are additive rather than synergistic. *inft-2, fozi-1* and *daam-1* single mutants had no apparent elongation defects and hatching rates similar to that of wild-type.

Figure 22. Embryonic elongation phenotypes of the seven formin mutants

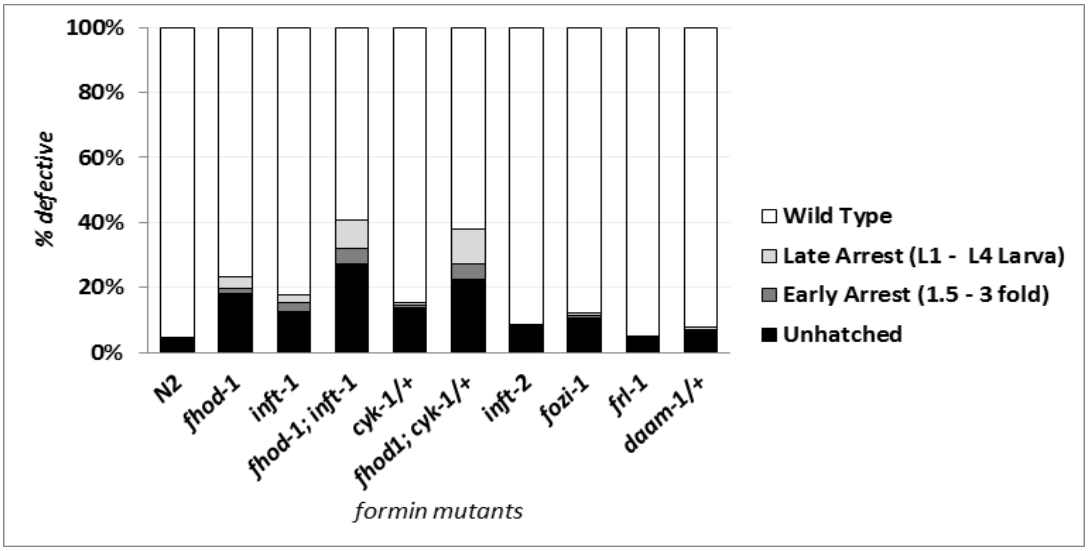

Formins inft-1 and cyk-1 have an additive effect on fhod-1 elongation phenotype

Many genes that control embryonic elongation were found to act in a redundant manner. For instance, *fhod-1* was found to act redundantly with *fem-2*: *fhod-1* and *fem*-2 single mutants have 25% and 5% elongation defects, respectively, whereas, knocking down both genes in the *fhod-1; fem-2* double mutant elevate the frequency of defective embryos to 78%, indicating that the two genes are acting synergistically to control embryonic elongation (VANNESTE *et al.* 2013). Similarly, *fem-2*, which has a low penetrance phenotype can induce a complete elongation arrest when combined with the nearly normal combination *let-502; mel-11* (i.e., in *let-502; mel-11; fem-2* show no elongation) (PIEKNY *et al.* 2000). Thus, knocking down more than one component of formins at the same time should result in a dramatic change on their elongation phenotype, if they are redundant.

For investigation of formin redundancy with *fhod-1*, I examined the available two double mutants: *fhod-1(tm2363); inft-1(gk386)* and progeny of *fhod-1(tm2363); cyk-1(ok2300)/+*. The elongation phenotype was exacerbated in both double mutants; however, it was not completely penetrant. Notably, adult worms of *fhod-1(tm2363); inft-1(gk386)* occasionally exhibit a Roller phenotype (~2%), which is occasionally seen with *let-502* hypomorphs (PIEKNY *et al.* 2000).

In *fhod-1; inft-1* the unhatched embryo category was increased from 15% in *inft-1* and 25% in *fhod-1* to 30% in the *fhod-1; inft-1* (Figure 22). To investigate whether the unhatched phenotype of the *fhod-1; inft-1* mutants is a result of elongation defect, these embryos were examined under high power (Figure 23). In fact, microscopic analysis showed that they exhibit complicated phenotypes, in addition to elongation defects, with

frequencies of 27% (n = 75). The most common phenotypes include arrest before elongation and embryos with relatively small sizes. Certain alleles of *let-502* and *mel-11* were found to regulate cytokinesis in the early *C. elegans* embryo (PIEKNY and MAINS 2002) and also give rise to these cytokinetic and small embryo phenotypes under certain circumstances. Moreover, the *fhod-1; inft-1* double mutant strain produces about 15% unfertilized eggs. Small brood size was reported in *let-502* mutants due to contractile defects in the sperm storage organ, the spermatheca (WISSMANN *et al.* 1999; PIEKNY *et al.* 2000; PIEKNY *et al.* 2003; GALLY *et al.* 2009). Overall, these data show that *inft-1* has an additive effect on *fhod-1* in regulation of the embryonic elongation. Thus, *fhod-1* and *inft-1* do not show the synergistic genetic interactions that would indicate pair-wise redundancy.

Despite its weak phenotype, *cyk-1* was previously found to have an overlapping role with *fhod-1* in body wall muscle development. *cyk-1(ok2300)* causes defects in movement and body wall muscle F-actin organization (MI-MI *et al.* 2012). It is possible that *cyk-1* may have a similar effect in the epidermal actin during embryonic elongation. *fhod-1; cyk-1/+* showed 30% elongation phenotypes among their progeny, in comparison to 25% in *fhod-1* single mutant (Figure 22). Microscopic analysis of the *fhod-1; cyk-1* unhatched embryos showed additional phenotypes other than elongation defects (17/25), such as possible cytokinesis defects, and undeveloped embryos (similar to those observed in *fhod-1; inft-1* embryos in Figure 23). Indeed, *cyk-1* was found to act downstream of *let-502* to control early embryonic cytokinesis (PIEKNY and MAINS 2002). These observations suggest a minor role of *cyk-1* in embryonic elongation that is likely additive rather than synergistic with *fhod-1*.

Figure 23. Elongation arrest phenotypes of *fhod-1; inft-1* and *fhod-1; cyk-1*

Microscopic analysis of the unhatched embryos of *fhod-1; inft-1* and *fhod-1; cyk-1* show that they exhibit abnormalities different from the *fhod-1* elongation phenotype (A), such as small size embryos (B; arrow), cytokinesis defects (C), incomplete development or failure of epidermal enclosure (D and E), and unusual larval arrest (F). Many *inft-1; fhod-1* (G-I) and *cyk-1; fhod-1* (J-L) show elongation arrest similar to that of *fhod-1*, but not at the elevated rates expected for redundancy.

Figure 23. Elongation arrest phenotypes of *fhod-1; inft-1* and *fhod-1; cyk-1*

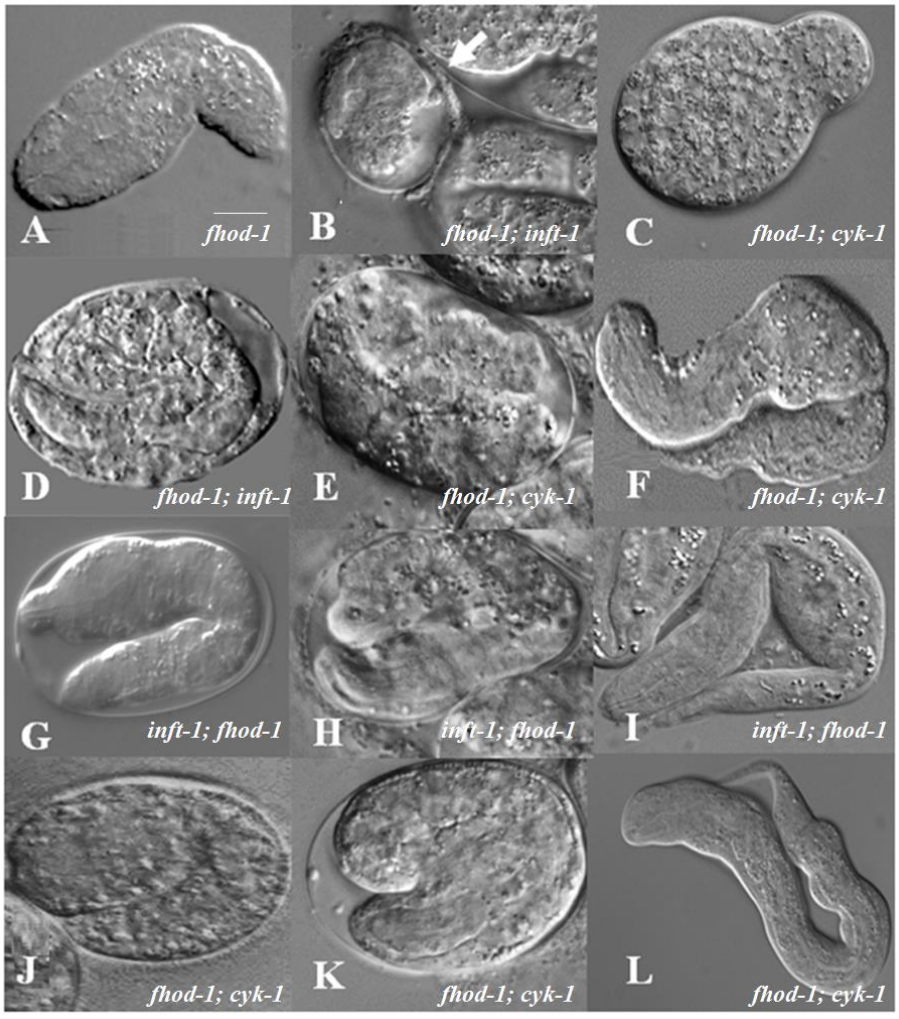

inft-1 and cyk-1 may act downstream of let-502 in embryonic elongation

My data suggest that two formins, *inft-1* and *cyk-1* have an additive effect on *fhod-1* mutants and so it is not clear that they act in a redundant manner with *fhod-1* during elongation. Genetic analysis previously showed that *fhod-1* enhances *let-502* and suppresses *mel-11* phenotypes, suggesting that *fhod-1* is acting in the same pathway as *let-502* (VANNESTE *et al.* 2013). Perhaps a more sensitive test for a role in elongation would be interactions between *inft-1* and *cyk-1* with *let-502* or *mel-11*. Here, *let-502(RNAi),* which has a strong effect on elongation of wild-type animals, will be used to test this hypothesis.

I tested RNAi knockdown of *let-502* on *fhod-1, inft-1* and *cyk-1/+*mutants to look for enhanced elongation arrest phenotypes (Figure 24). As expected, *let-502* RNAi showed a strong enhancement of *fhod-1* elongation phenotype as arrest phenotypes were elevated from 20% alone in *fhod-1*, 63% in *let-502* RNAi and 97% when combined. Feeding the *inft-1* single mutant *let-502* RNAi exhibited phenotypes similar to that of *fhod-1*, albeit in slightly lower frequencies of early arrest embryos. *inft-1; let-502(RNAi)* did have a large proportion of hatched with elongation arrest (47%), but this was not dramatically increased above *let-502(RNAi)* alone (34%). The *fhod-1; inft-1* double mutant strain fed *let-502* RNAi resulted in increases in unhatched embryos (~78%), but this was again additive rather than synergistic. Similarly, feeding of *cyk/+* strain on *let-502(RNAi)* showed about 86% unhatched embryos, whereas 5% had an early arrest phenotype and another 5% showed late arrest. *fhod-1; cyk/+; let-502(RNAi)* showed a slight decrease of the hatching rate at the expense of early and late arrest. The increase in

unhatched embryos in the double mutants were greater than additive, perhaps indicative of a strong genetic interaction. Again, using the DIC microscopy revealed that the unhatched phenotype include elongation arrest (n = 17/45) as well as other phenotypes such as cytokinesis defects, which were described for *fhod-1; inft-1* and *fhod-1; cyk-1* double mutants above (Figure 23). Thus, *inft-1* and *cyk*-1 may be partially acting in parallel with the *let-502/mel-11* pathway for pre-elongation defects, but at best are weakly redundant with *fhod-1* to regulate embryonic elongation. As expected, *let-502* knockdown by RNAi had little or no effect on *inft-2*, *fozi-1* and *daam-1/+* (data not shown).

Figure 24. *inft-1* and *cyk-1* show no strong interactions with*let-502(RNAi)* in embryonic elongation

let-502(RNAi) by feeding weakly enhances the elongation arrest phenotype of *fhod-1*,*inft-1* and *cyk-1*. The majority of *cyk-1* mutants that fail to hatch appear to arrest earlier than *fhod-1*or*inft-1* in the presence of *let-502(RNAi)* (see text).

Figure 24. . *inft-1* and *cyk-1* show no strong interactions with*let-502(RNAi)* in embryonic elongation

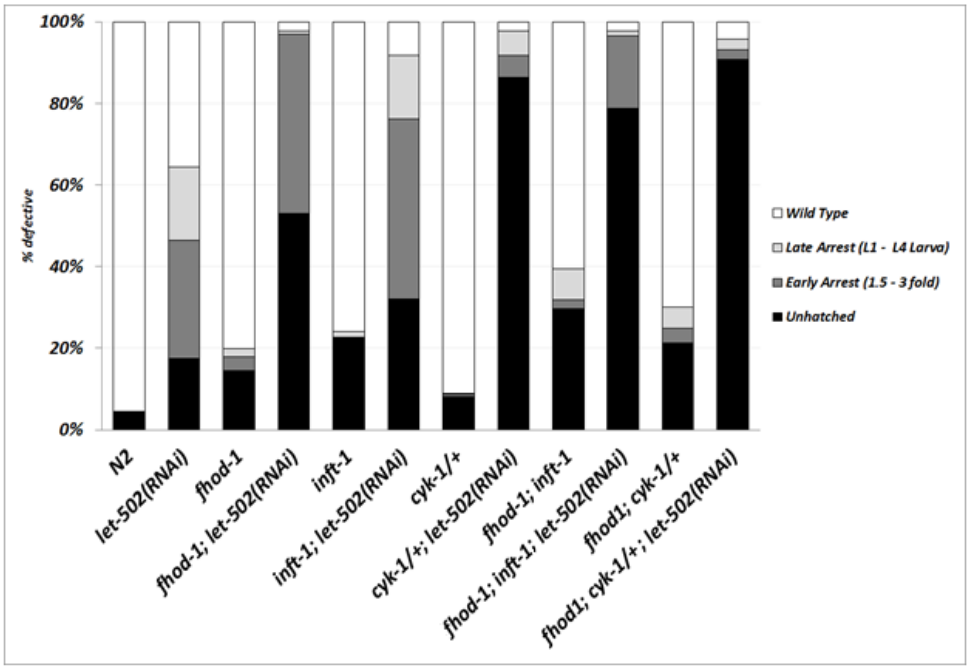

Formins knock down by RNAi had no dramatic effect on fhod-1 elongation

The *fhod-1; inft-1* and *fhod-1; cyk-1/+* double mutants showed a greater effect on elongation than any of the formin single mutants. Since not all double mutants are available, formins were knocked down using RNAi feeding in *fhod-1; inft-1* to search for triple redundancy (Figure 25A). Thus *fhod-1; inft-1* worms were separately fed on bacteria carrying RNAi clones of *cyk-1, inft-1, inft-2, fozi-1* and *daam-1*.

As expected, *fhod-1* RNAi and *inft-1* RNAi had no enhancement effect on the *fhod-1; inft-1* double mutant, since these alleles are functionally null. *cyk-1(RNAi)* caused significant decrease of the *fhod-1; inft-1* hatching rate, with the frequency of 70% unhatched, about 25% of which arrested before elongation when examined under high power (n = 12/50). Notably, *fhod-1; inft-1* was sick and almost completely sterile when feeding began at the L3-L4 stage on the *cyk-1* RNAi. To avoid this problem I used worms at late L4 and early young adult stages for the data in Figure 25. RNAi knock down of *fozi-1* and *daam-1* had no effect on wild type or of *fhod-1; inft-1* strains.

An attempt to feed the *fhod-1; inft-1* strain on a mixture of bacteria that carry the *cyk-1, inft-1, fozi-1* and *daam-1* RNAi clones showed no change (data not shown). Indeed, mixing more than two different RNAi significantly decreases the efficiency of the RNAi effect (FRASER *et al.* 2000; MIN *et al.* 2010). Similarly, *fem-2(RNAi)* had no effect on our positive control strain *fhod-1; fem-2(RNAi)* (Figure 25B). It is not clear why we did not see any effect on *fhod-1* and *inft-1* single or double mutants as expected; perhaps *fem-2(RNAi)* was not fully effective (although it did strongly enhance *cyk-1/+*).

Figure 25. Formins and *fem-2* RNAi had no dramatic effects on *fhod-1; inft-1*

(A) Formins RNAi knockdown had no dramatic effect on *fhod-1; inft-1* elongation. *cyk-1(RNAi)* feeding was carried on young adult worms, as the *fhod-1; inft-1* strain was sick and sterile when feeding began at the L3-L4 stage. (B) *fem-2(RNAi)* had no effect on formin mutant elongation.

Figure 25. Formins and *fem-2* RNAi had no dramatic effects on *fhod-1; inft-1*

A

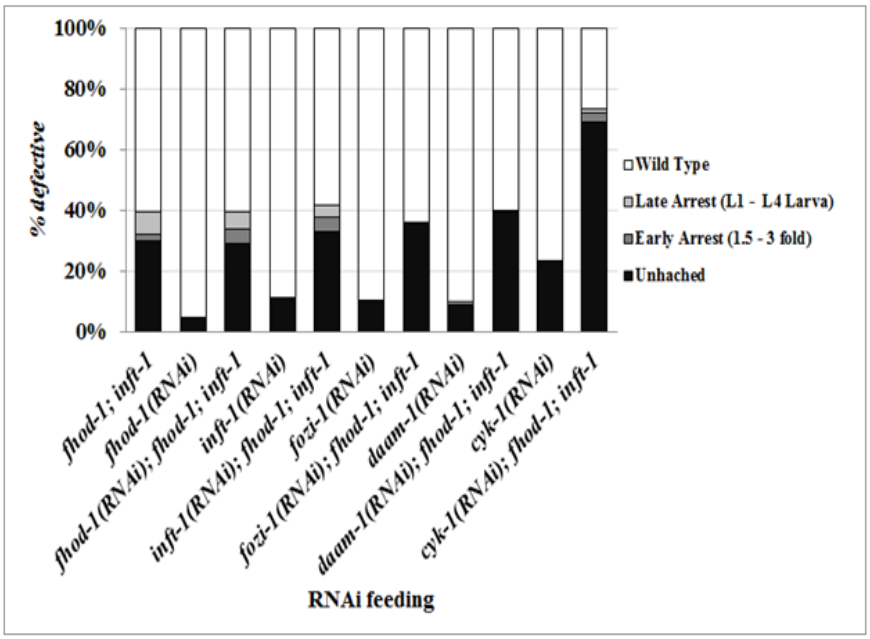

B

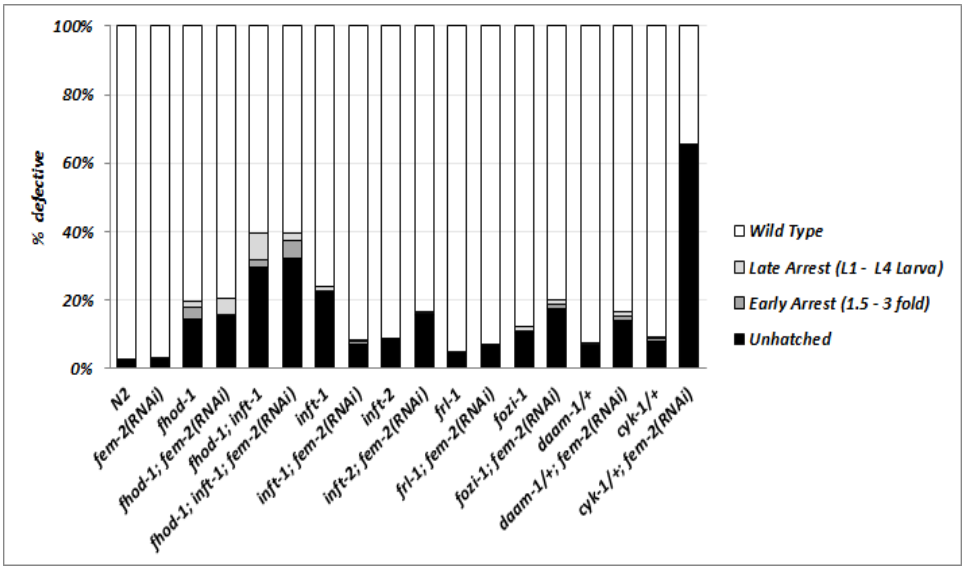

wve-1 and wsp-1activators of the ARP2/3complex had no effect on elongation

The ARP2/3 complex represent a pathway that potentially acts in parallel to formins to nucleate microfilaments during elongation. The Arp2/3 complex plays a major role in actin cytoskeleton organization, specifically the nucleation of branched actin filaments in *C. elegans* (GOODE and ECK 2007; POLLARD 2007). Thus, I examined the elongation phenotype of the two Arp2/3 complex activators; WVE-1/WAVE and WSP-1/WASP (SAWA *et al.* 2003). Progeny of *wve-1(ok3308)/+* and the viable *wsp-1(gm324)* allele were examined for elongation abnormalities. No elongation defects were observed. Moreover, *let-502(RNAi)* feeding had little or no effect on *wsp-1(gm324)* or *wve-1(ok3308)* elongation (Figure 26).

Figure 26. *wve-1* and *wsp-1* activators of the Arp2/3 complex had no effect on elongation

let-502(RNAi) knock down had no effect on *wve-1* or *wsp-1* embryonic elongation. Since *wve-1(ok3308)* null mutation is lethal, *wve-1(ok3308) I/hT2* balanced strain was used.

Figure 26. . *wve-1* and *wsp-1* activators of the Arp2/3 complex had no effect on elongation

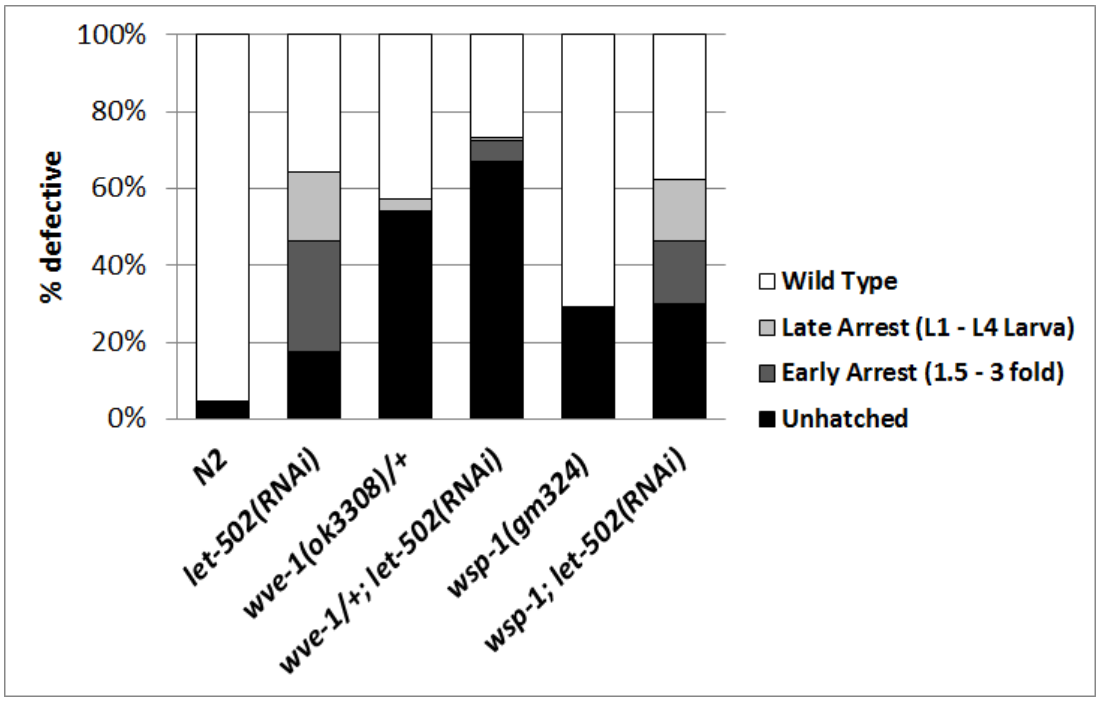

Conclusion

Using a series of experiments involved testing double mutants and RNAi knock down, I conclude that there are two formins, *cyk-1* and *inft-1,* that appear to have at best a weakly redundant role with *fhod-1*during embryonic elongation (Figures 22 and 24). Moreover, *inft-1* and *cyk-1* responded to *let-502* RNAi, somewhat similar to the response of *fhod-1* (Figure 25). Also, the pre-elongation arrest and gonad phenotype associated with the elongation arrest suggest that *inf-1* and *cyk-1* may be acting with *let-502* to regulate other functions in early morphogenesis.

The absence of complete penetrance in all cases suggests that the process of actin organization during embryonic elongation is triply (or more) redundant or there are other actin nucleators involved in the process. Such a third pathway is apparently not a component of the Arp 2/3 complex (Figure 26).

INVESTIGATING A ROLE FOR MUSCLE GENES IN EARLY ELONGATION

Background: muscles control the late elongation

Forces that drive embryonic elongation mainly come from two structural elements: epidermis, which regulates early elongation, and muscles, which regulate late elongation. Early elongation is controlled by the *let-502/mel-11* and *fem-2/pak-1* pathways, while late elongation depends on muscle genes (WISSMAN N *et al.* 1999; WILLIAMS and WATERSTON 1994).

The purpose of the following experiments is to investigate whether muscles play a role in early embryonic elongation of the *C. elegans*. As mentioned above, muscles are known to play a role in late elongation, most likely beginning around 2 fold stage (WILLIAMS and WATERSTON 1994). Genes such as *pak-1*, which is expressed in hemidesmisomes and intermediate filaments that span epidermis to the muscle, were found to affect elongation (VANNESTE *et al.* 2013; ZHANG *et al.* 2011; MARTIN *et al.* 2014). Moreover, CYK-1 was previously shown to interact with FHOD-1 in body wall muscles development in adult worms, and so perhaps elongation defects in *cyk-1* mutants could in part stem from muscle defects (MI-MI *et al.* 2012). In fact, my data (see above) show that *cyk-1* had a weak additive effect on the *fhod-1* elongation phenotype, again suggesting that muscle may have a previously overlooked role in early elongation that was not observed because of redundancy with the *let-502/mel-11* system.

To investigate the muscle's role in early elongation, genes encoding two biochemically different products were tested, *pat-4* and *myo-3*. Mutants of *pat-4* and *myo-3* have arrest at 2 fold stage with Pat phenotype (paralyzed at two fold). Despite their

relatively late phenotype (arrest at 2 fold stage), *pat-4* and *myo-3* expression start before the embryonic elongation (MILLER *et al.* 1983; HONDA and EPSTEIN 1990; MACKINNON *et al.* 2002). The *C. elegans pat-4* encodes an integrin-linked kinase (ILK), a focal adhesion protein necessary for muscle development (MACKINNON *et al.* 2002). *myo-3* encodes myosin heavy chain A, which is expressed in body muscle and is necessary for thick filament formation (MILLER *et al.* 1983; MILLER *et al.* 1986; HOPPE *et al.* 2003; KAMATH *et al.* 2003).

Muscle genes pat-4 and myo-3 show no interaction with mel-11/let-502 pathway in early elongation

If muscle has a previously undetected earlier role in elongation, muscle mutants should suppress *mel-11* hypercontraction, as do mutants of *let-502, fhod-1* and *fem-2. mel-11* mutants have a distinct phenotype, where the hypercontraction of the lateral epidermal cells during elongation cause the embryo to rupture before reaching the 2 fold stage. *mel-11*(*it26*) is a *ts* allele that is completely penetrant at 25^{o}C, with 2% to 18% hatching rate at 20^{o}C and 15^{o}C, respectively (WISSMANN *et al.* 1999). *pat-4* and *myo-3* arrest at the 2 fold stage and usually are able to hatch. If *pat-4* and *myo-3* were to suppress *mel-11*, progeny of the double mutants (*mel-11; pat-4* and *mel-11; myo-3)* should exhibit the Pat phenotype or perhaps show an increase in hatching rate. Additionally, *let-502(RNAi)* feeding was used in *myo-3* mutant. In the case of genetic interaction between *myo-3* and *let-502*, we should see enhancement of the *let-502* early arrest phenotype (i.e., between 1.2 fold and 1.5 fold).

I examined the elongation phenotype of the strains *mel-11(it26); pat-4(st551)/+* and *mel-11(it26); myo-3(st386)/+*. Embryos of both single and double mutants were

mounted in slides and examined microscopically under high power. *mel-11; pat-4/+* embryos only exhibited the *mel-11* mutant hyperelongation phenotype (n = 63), rather than the expected 25% Pat phenotype or increase in hatching rate (Figure 27). Indeed, knock down of *pat-4* by RNAi showed no increase in hatching rates of *mel-11* mutants (Cheryl Birmingham and Paul Mains, unpublished data). These observations revealed that *mel-11* was instead epistatic to *pat-4*, suggesting that *pat-4* is likely acting at a later stage in elongation and has no earlier interaction with *mel-11*. Similarly, the progeny of *mel-11(it26); myo-3/+* mutants exhibited the *mel-11* hypercontraction phenotype and blocked the expected 25% Pat phenotype (n = 100). These results were recapitulated by *let-502(RNAi)* knockdown by feeding in *myo-3* mutants, which resulted in no enhancement of the *let-502* arrest phenotype (Figure 27B). Thus, *mel-11* is epistatic to *myo-3* and so *myo-3* has no detectable interaction with the *mel-11/let-502* pathway at early embryonic stages (*i.e.*, before 2 fold stage). Together, these data imply that muscle does not participate in early elongation before the 2 fold embryonic stage.

Figure 27. The muscle genes *myo-3* and *pat-4* show no genetic /interaction with *mel-11* and *let-502*

(A) *myo-3* and *pat-4* Pat phenotype is masked by *mel-11* hyper-contraction phenotype in the progeny of *mel-11; pat-4/+;* and *mel-11; myo-3/+* double mutants. (B) *myo-3* showed no interaction with *let-502. myo-3* mutant exhibit Pat phenotype, but has no elongation defect before the 2 fold stage. No significant enhancement of the *let-502* phenotype was observed after feeding *myo-3/+* mutants *let-502(RNAi).*

Figure 27. The muscle genes *myo-3* and *pat-4* show no genetic /interaction with *mel-11* and *let-502*

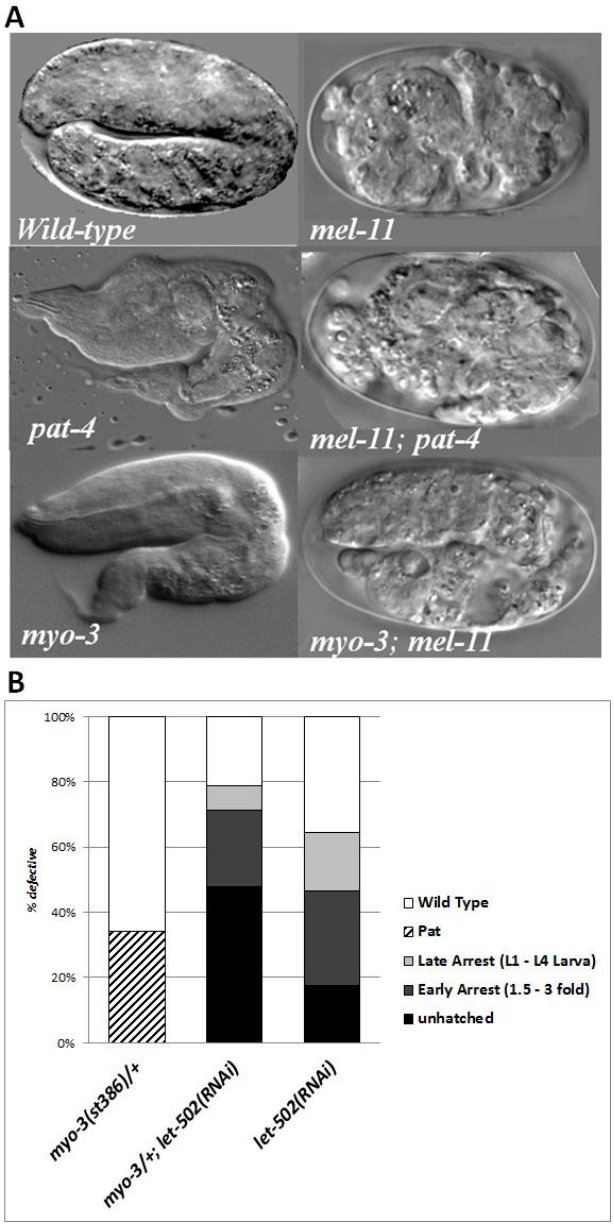

fhod-1 GENE EXPRESSION AND STRUCTURE

fhod-1::gfp expression

Background

The *C. elegans fhod-1*gene was thought to be expressed mainly in lateral epidermal cells (VANNESTE *et al.* 2013). Mutants of *fhod-1* exhibit elongation arrest phenotypes as early as the 1.2 fold stage and actin defects were restricted to lateral cells. However, anti-FHOD1 immunostain was detected only relatively late in elongation, about the 2.5 to 3 fold stage (VANNESTE *et al.* 2013). To determine the earliest expression of *fhod-1* I used a *fhod-1::gfp* integrated transgenic line, which has ~ 17 kbp genomic fragment containing the *fhod-1* gene and its promoter tagged to an in-frame C-terminal GFP fusion. This is potentially more sensitive than the antibody. The larval and adult expression of this fusion was described in details in (MI-MI *et al.* 2012), indicating that FHOD-1::GFP is associated with muscles and F-actin filaments.

Examining the expression pattern of fhod-1::gfp

Here, I am interested in studying the embryonic expression of FHOD-1::GFP to determine where and when it functions during the embryonic elongation. Although, the expression is very hard to detect under the dissecting fluorescent microscope, signal could be detected at higher power as early as the 1.5 fold stage (Figure 28A). The FHOD-1::GFP appeared to be expressed homogenously from 1.5 fold to 3 fold stage, often in puncta.

To determine the earliest expression of FHOD-GFP, I used the anti-GFP antibody to increase sensitivity. Indeed, FHOD-GFP expression was detected before the gastrula

stage (about the 26 cell stage) (Figure 28B). The expression was distributed ubiquitously in cytoplasm but was excluded from the nucleus.

Figure 28. The earliest expression of *fhod-1::gfp*

(A) FHOD-1::GFP expression can be detected between 1.5 fold and 3 fold embryonic stages. The expression appears to be homogenously distributed among cells, but excluded from the nucleus. (B) Using anti-GFP antibody staining (Green), the FHOD-1::GFP expression can be detected before the gastrula stage. The expression of FHOD-1::GFP appeared to be homogenous in all embryonic cells but excluded from the nucleus as shown by DAPI staining (blue) and the two merged colour images (Merge; right column). Images in A were taken with help from Dr. Jim McGhee.

Figure 28. The earliest expression of *fhod-1::gfp*

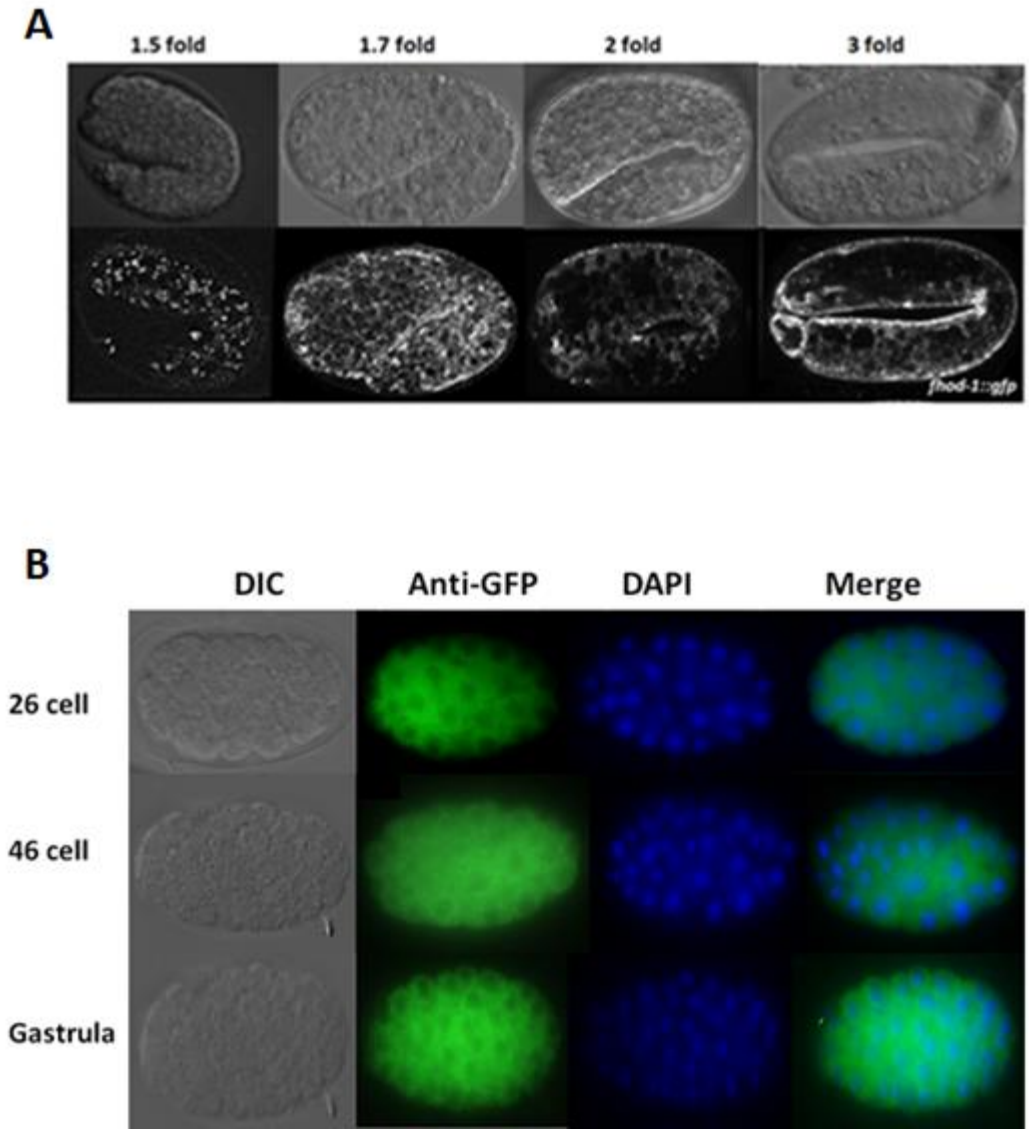

fhod-1::gfp is expressed homogenously in embryo

As shown in Figure 28, *fhod-1* appeared to be expressed homogenously before the start of embryonic elongation. Using time course analysis of *fhod-1* expression I found that this pattern appears to continue throughout the embryonic development (Figure 29). Considering its role in embryonic elongation, it is important to determine whether *fhod-1* is expressed in tissues necessary for embryonic elongation. Thus, I tracked the FHOD-1::GFP expression in the epidermal cells using the MH27 antibody co-staining of the epidermal cells' adherent junctions. FHOD-1::GFP expression was detected homogenously in all epidermal cells (i.e., dorsal, ventral and lateral cells), as determined by MH27 antibody. At the 3 fold stage, the signal appears to intensify in the lateral cells (Figure 29H), confirming previous observation of anti-FHOD-1 (VANNESTE *et al.* 2013).

Epidermal cells play an essential role in the early embryonic elongation, with lateral cells acting as the driving force behind epidermal elongation. It is possible that the results above are misleading and the *fhod-1::gfp* transgene might be expressed in places that the endogenous *fhod-1* is not expressed in, such as dorsal/ventral epidermal cells. It is also possible that *fhod-1* is expressed ubiquitously in epidermal cells, but mainly functions in the seam cells. Likewise, *let-502* was found to be expressed in all epidermal cells during elongation, but it functions specifically in seam cells to inhibit *mel-11* and promote actomyosin contraction of these cells (WISSMANN *et al.* 1997b; PIEKNY and MAINS 2002; PIEKNY *et al.* 2003; DIOGON *et al.* 2007).

Figure 29. *fhod-1::gfp* is expressed homogenously during elongation

Immunostaining for GFP shows that FHOD-1 is expressed homogenously in all tissue during embryonic development. DIC images for embryos is shown for embryonic stages from the start of gastrulation to the end of elongation at the three-fold stage. Embryonic stages shown are (A) pre-bean, (B) bean, (C) comma, (D) 1.4 fold, (E) 1.5 fold, (F) 1.7 fold, (G) 2 fold, (H) 3 fold. Anti-GFP antibody staining was used to visualize the expression of *fhod-1::gfp* genomic fusion (Anti-GFP; green). The anti-AJM-1 antibody (MH27; Red) was used to visualize the cell borders of the seam/lateral epidermal cells (star), and to a lesser extent the dorsal/ventral epidermal cells (arrow). The dual colour images (Merge; the far right column), indicate the expression of FHOD-1::GFP in all types of epidermal cells. The expression apparently intensified in the lateral epidermal cells at the 3-fold stage (H; star).

Figure 29. . *FHOD-1::GFP* is expressed homogenously during elongation

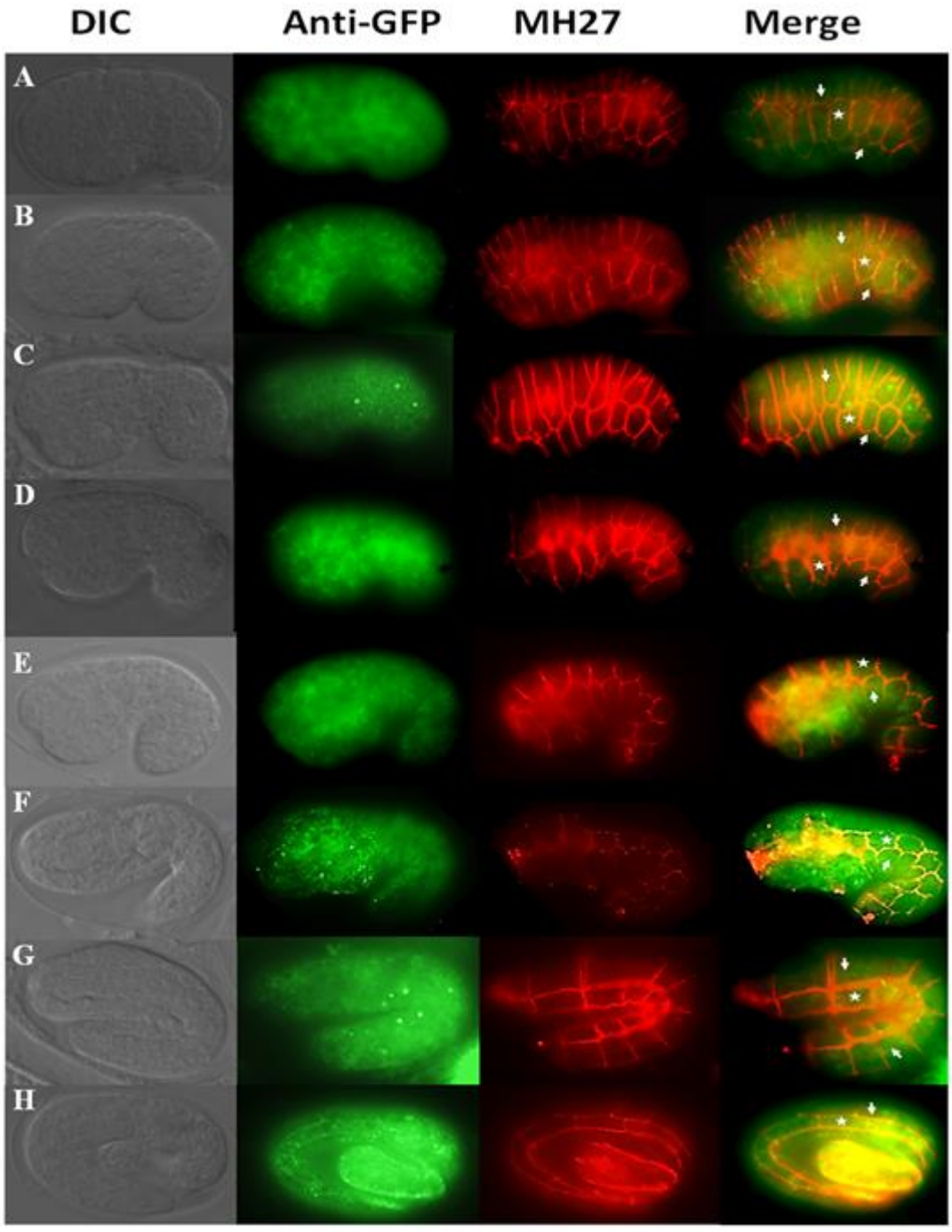

fhod-1::gfp can rescue the fhod-1 arrest phenotype

The FHOD-1::GFP genomic fusion was able to rescue the muscle defective phenotypes in adult worms (Mi-Mi *et al.* 2012). To determine whether the FHOD-1::GFP fusion is able to rescue the embryonic arrest phenotype of the *fhod-1* mutants, I crossed the construct into *fhod-1 let-502(sb118)*, a sensitized background for elongation arrest. *sb118* is a *ts* allele. The *fhod-1::gfp* fusion appear to fully rescue the *fhod-1* elongation arrest in *fhod-1 let-502(sb118).* The *fhod-1 let-502(sb118); fhod-1::gfp-1* strain had a phenotype very similar to *let-502(sb118)* alone (Figure 28), suggesting that FHOD-1::GFP-1 is expressed in a manner similar to the endogenous protein in the embryo.

Figure 30. *fhod-1::gfp* expression can rescue *fhod-1*arrest phenotype

The *fhod-1::gfp* genomic construct that was used to visualize *fhod-1* expression pattern and is able to rescue the *fhod*-1 mutant's elongation arrest phenotype. Using a sensitive background to detect elongation defects, the *fhod-1 let-502* double mutant, the strain that carries the integrated transgene (*fhod-1 let-502; fhod-1::GFP*) has an elongation phenotype similar to the *let-502* single mutant alone, indicating a full rescue of *fhod-1*. The experiment was carried out at the restrictive temperature of 25°C.

Figure 30. *fhod-1::gfp* expression can rescue *fhod-1*arrest phenotype

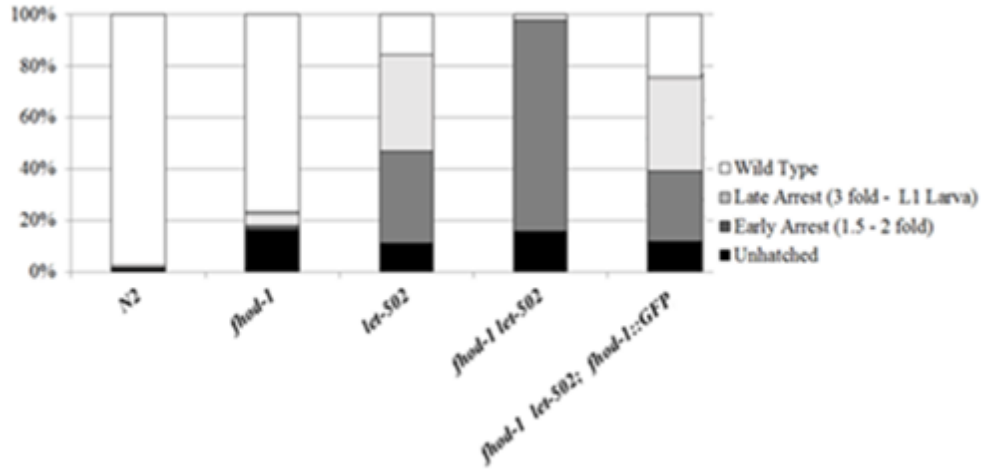

THE C. elegans fhod-1 GENE STRUCTURE AND ISOFORMS

Background

C. elegans FHOD-1 is highly similar to mouse and human FHOD-1 and FHOD-3 with more than 35% identity of its amino acid sequence (VANNESTE *et al.* 2013) (Figure 31 and Table 5). The conservation is much higher between specific domains. For instance the DAD and DID/FH3 domains of human FHOD1 and *C. elegans* FHOD-1 have 50% and 52% sequence identity, respectively (MI-MI *et al.* 2012; VANNESTE *et al.* 2013). Two *fhod-1* mutation alleles have previously been studied, *tm2363* and *tm3138* (Figure 31). The *tm2363* mutation deletes 377 bp from the region encoding the FH2 domain and introduces a frameshift mutation. This mutation is considered to be null and results in low penetrance embryonic elongation arrest (VANNESTE *et al.* 2013) and defects in adult body wall muscles (MI-MI *et al.* 2012). *tm3138,* which eliminates part of an intron and a portion of the DID-encoding exon, exhibits mild muscle defects (MI-MI *et al.* 2012).

To better understand the role of *fhod-1*, we must know the precise gene structure. The current release of the Wormbase.org (WS244 data freeze) shows *fhod-1* as a single gene form. However, an old release of Wormbase.org (WS170 data freeze) had listed two predicted isoforms of *fhod-1*, a short form that encodes 1078 amino acids and a long form that encodes 1346 amino acids. These two isoforms differ in the predicted protein start sites. Currently, the short form is considered as an obsolete gene model, with only the long form listed in Wormbase.org (WS244) (Figure 31).

Figure 31. *fhod-1* gene structure from Wormbase.org

(A) Current release (WS244 data freeze) showing *fhod-1* as a single isoform (*C46H11.11*) consisting of 17 exons. Red blocks indicate the location of the two deletion mutations described in this study. Note that 5' is to the right of the diagram. (B) An old release of Wormbase.org (WS170 data freeze) had listed two predicted isoforms of *fhod-1*, a short form and a long form. Red lines refer to N-terminus and C-terminus regions (not drawn to scale) that were amplified in the RT-PCR to verify the two isoforms. Currently, Wormbase.org lists this model as an obsolete gene model.

Figure 31. *fhod-1* gene structure from Wormbase.org

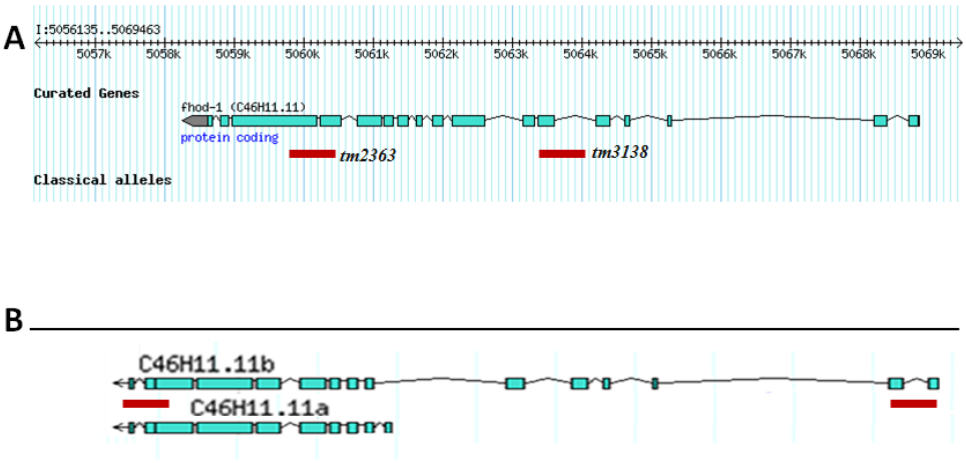

C46H11.11 is expressed in both adult and embryo

Previous work by C. Vanneste (Vanneste 2011; PhD Thesis, University of Calgary) predicted that the *C46H11.11* gene is SL1 *trans*-spliced using RT-PCR with an SL1 (splice leader) primer (CONRAD *et al.* 1993), and this form was detected exclusively in adult worms (Vanneste 2011; PhD Thesis, University of Calgary). This statement was based on RT-PCR data where he was able to amplify cDNA encoding the 5' end of *fhod-1* mRNA only from adult gravid hermaphrodite RNA, but not from the embryonic mRNA. In contrast, the cDNA encoding the *fhod-1* mRNA 3' end was successfully amplified from both embryo and adult cDNA pools, and it was assumed that this product might include the predicted short form that is common for both isoforms. Because the short form would lack critical regulatory regions, expression of only this form in embryos would have implications for FHOD-1 regulation and function. Curiously, *fhod-1(tm3138)*, which would not affect the suggested embryo-specific short isoform (Figure 31), shows no elongation phenotypes and does not suppress *mel-11* as does *fhod-1(tm2363)* (P. Mains, personal communication).

To determine whether an mRNA which could potentially encode the long form of the *C46H11.11* protein exists in the embryo, I used RT-PCR on both the embryonic and the gravid adult hermaphrodites RNA. Unfortunately, primers used in the previous study were not well documented, thus I designed new primers. Primers were designed based on the current Wormbase.org predicted *fhod-1*cDNA sequence to amplify 230 bp at the 5' end (staring right after the transcription start site) and the last 344 bp at the 3' end (Figure 32). The expected products were amplified successfully from both embryonic and the gravid adult. This indicates that the long form of *fhod-1* is expressed in both adults as

well as embryos. To confirm that the embryonic RNA does not have any contamination of adult RNA, RT-PCR was performed on the embryonic RNA samples to amplify a region of the adult specific gene *vit-2*. Vitellogenin genes, including *vit-2*, are well studied and known to be expressed solely in the adult hermaphrodite intestine (SPIETH *et al.* 1988; MACMORRIS *et al.* 1992; BROVERMAN *et al.* 1993; MACMORRIS *et al.* 1994). As expected, the desired product was successfully amplified from adult RNA sample, but not from the embryonic RNA sample (Figure 32). This confirms that the embryonic sample had no contamination from the adult RNA.

Figure 32. *fhod-1* (*C46H11.11*) is expressed in adult and embryos

(A) Schematic drawing of the *C46H11.11* gene and protein structure (upper diagram), with protein-coding exons colour-coded to match predicted product structural domains (not drawn to scale), including the FHOD-specific GTP-binding domain (GBD; gray), diaphanous inhibitory domain (DID; green), helical or coiled-coil (CC) regions (H; blue), formin homology domain 1 (FH1; light blue), the formin homology domain 2 (FH2; red) and the diaphanous autoregulatorydomain (DAD; purple). Red blocks indicate the location of the two deletion mutations described in this study. Blue lines indicate the two N-terminus and C-terminal regions (not drawn to scale) that were amplified by RT-PCR to confirm expression of *fhod-1*. (B, left) RT-PCR of the *fhod-1* mRNA that encodes N- terminus (N) and C-terminus (C) regions from graved adults and embryonic mRNA (duplicate samples). Expected bands were detected at the right size. Arrow indicates genomic DNA contamination (gDNA). N2 (wild-type) genomic DNA from mixed stages was used as a control, indicating that two forms were expressed. (B, right) RT-PCR on embryonic RNA to amplify a short region of the adult specific gene, *vit-2*. No product was detected from the embryonic cDNA sample, confirming that it has no contamination from the adult RNA.

Figure 32. *fhod-1* (*C46H11.11*) is expressed in adult and embryos

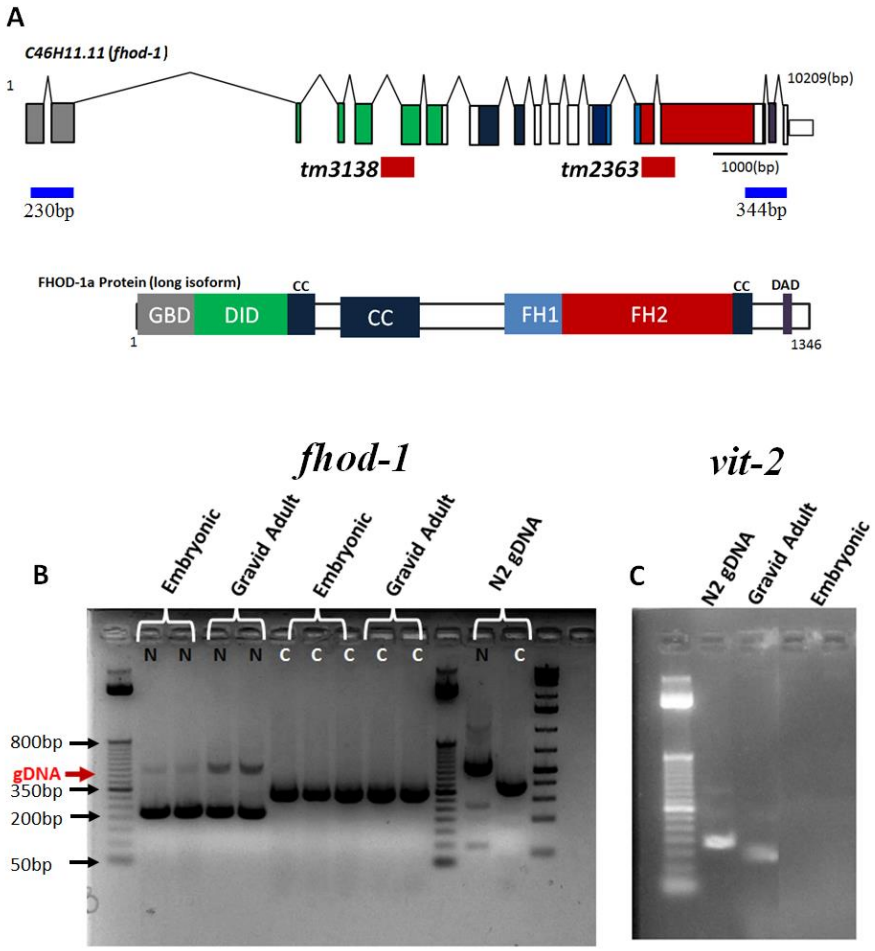

Identification of a novel short isoform of the C46H11.11 gene

Because FHOD-1 is the sole *C. elegans* formin with a clear function in the embryonic elongation, I decided to clone its full-length cDNA. Although, my RT-PCR data suggest that there is no variation on the *C46H11.11* mRNA encodes the N-terminal region of the protein, other variations might lie within the gene. To clone the full-length cDNA of *fhod-1,* I designed three primer sets to cover the whole length of its sequence (Figure 33; Table 1). All PCR bands showed the expected size, except for the primer set that amplifies the region from exon 1 to exon 11, where a novel lower band of 1.4 kbp was detected in both of the adult and embryonic samples in addition to the expected 1.8 kbp band. Sequencing showed that this product lacked the entire 474 bp of the exon 8, indicating an alternative splicing event that omitted this exon in a short isoform. Thus, the novel short *fhod-1* isoform consists of 16 exons and its cDNA is 3567 bp in length. The long isoform consists of 17 exons and its cDNA is 4041 bp in length. The two predicted proteins differ by 158 amino acids in length - the long isoform cDNA is translated into 1346 amino acids and the short isoform encodes 1188 amino acids (EMBOSS Transeq tool; http://www.ebi.ac.uk/Tools/st/emboss_transeq). The new isoform was named the *fhod-1b* while the longer current Wormbase.org isoform was named the *fhod-1a*.

Figure 33. *fhod-1* exon 8 is alternatively spliced

(A) Schematic view of the gene structure and primer sets used for the whole cDNA RT-PCRs. (B) RT-PCR for the whole cDNA of the *fhod-1*, showing a novel alternative splicing of exon 8. Primer set #1 produce two bands, the higher band was the expected 1.8 kbp product whereas the lower band represents the novel 1.4 kbp product. The lower band is smaller than the expected higher band by ~474 bp, the size of the omitted exon 8. Primer sets #2 and #3 produced the expected 1.2 kbp and 1.1 kbp products, indicating no other detectable variations for the rest of the cDNA. For every primer set, the right lane denotes gravid adult sample and left lane denotes the embryonic sample. The identity of all bands were confirmed by sequencing. (*) nonspecific products.

Figure 33. *fhod-1* exon 8 is alternatively spliced

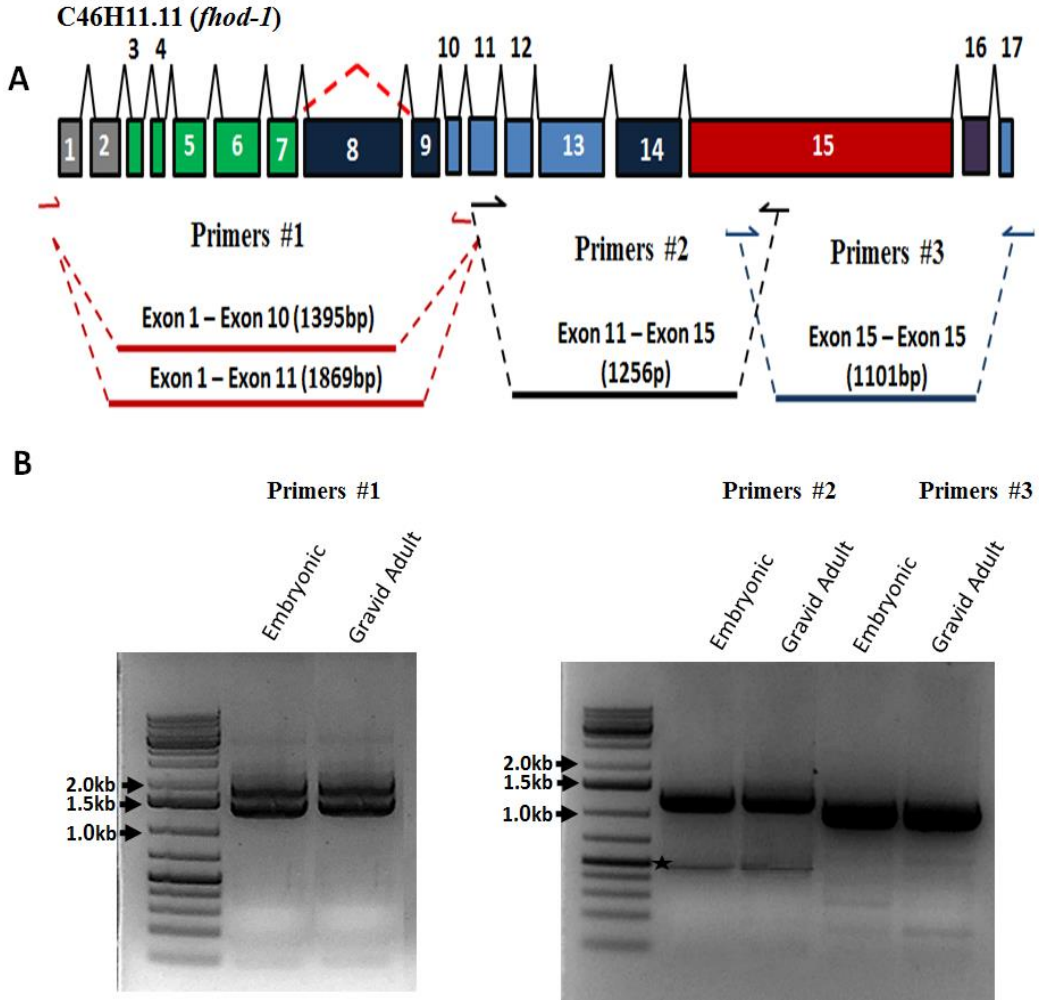

The spliced fhod-1 exon 8 is a nematode-specific sequence

The alternatively spliced exon of *fhod-1a* encodes a part of the coiled-coil domain. Using a protein domain predicting tool, the essential functional domains of FHOD-1 (i.e., FH2, FH3 and GTPase-binding domains), are not affected by the splicing event. However, the splicing event most likely affects the protein conformation, as the short isoform lacks a portion of the large coiled-coil region, according to COILS (a bioinformatics tool for prediction of the coiled-regions in proteins; http://www.expasy.org; (LUPAS *et al.* 1991) (See Appendix, Figure 42).

The amino acid sequence of exon 8 is not highly conserved, based on sequence alignment analysis carried out using Clustal2.1 (http://www.ebi.ac.uk/Tools/msa/clustalo/) between eight FHOD-1 orthologs, including human and mouse FHOD1 and FHOD3, fruit fly FHOS, and the FHOD-1 of the nematodes *C. remanei, C. briggsae* and *C. elegans* (Figure 34 and 35). Exceptions are a short sequence of three residues; one serine (S) and two arginine (R) at positions 1638 to 1640 are 100% conserved between seven orthologs. Also, a few single residues showed high conservation between at least five orthologs such as serine (S) at position 1623, 1642 and 1897, proline (P) at position 1670 and 1880, and glutamic acid (E) at 1946.

Sequence alignment analysis between these eight orthologs showed that exon 8 appears to be a nematode-specific sequence. Exon 8 has more than 76% sequence identity with *C. remanei* and 74% with *C. briggsae* (Table 5). However, sequence alignments showed that *C. elegans* FHOD-1a exon 8 has lower sequence identity (less than 29%) with *Drosophila* FHOS, mouse and human FHOD1/3 (Table 5). Interestingly, between the three nematode species, *C. elegans, C. remanei* and *C. briggsae,* there is an

evolutionarily highly conserved stretch of eight amino acids, six of which are encoded by exon 8 and two by exon 9, with 100% sequence identity (mainly with charged side chains). These eight amino acids are probably a part of a larger consensus sequence (about 25 amino acids) (Figure 35).

Figure 34. *fhod-1* exon 8 is not highly conserved

The alternatively spliced *C46H11.11* exon 8 encodes 157 amino acids (between red brackets) that are not highly conserved between eight orthologs, including the nematodes *C. elegans [Ce], C. remanei [Cre], C. briggsae [Cbr]* , the *fruit fly (D. melanogaster [Dm]), mouse (M. Musculus [Mm])* and *human (H. Sapiens [Hs]).* Alignment sequence analysis were carried out using the Multiple Sequence Alignment tool, Clustal Omega (www.ebi.ac.uk/Tools/msa/clustalo/). Residues are coloured in *Clustal X* according to their physiochemical properties, as following: red [basic residues (HRK)], blue [hydrophobic residues (AVFPMILW)], green [hydroxyl, sulfhydryl, amine residues (STNQY)], magenta [acidic residues (DE)], orange [the smallest amino acid, G], other colours denote unusual amino/imino acids, etc.

Figure 34. *fhod-1* exon 8 is not highly conserved

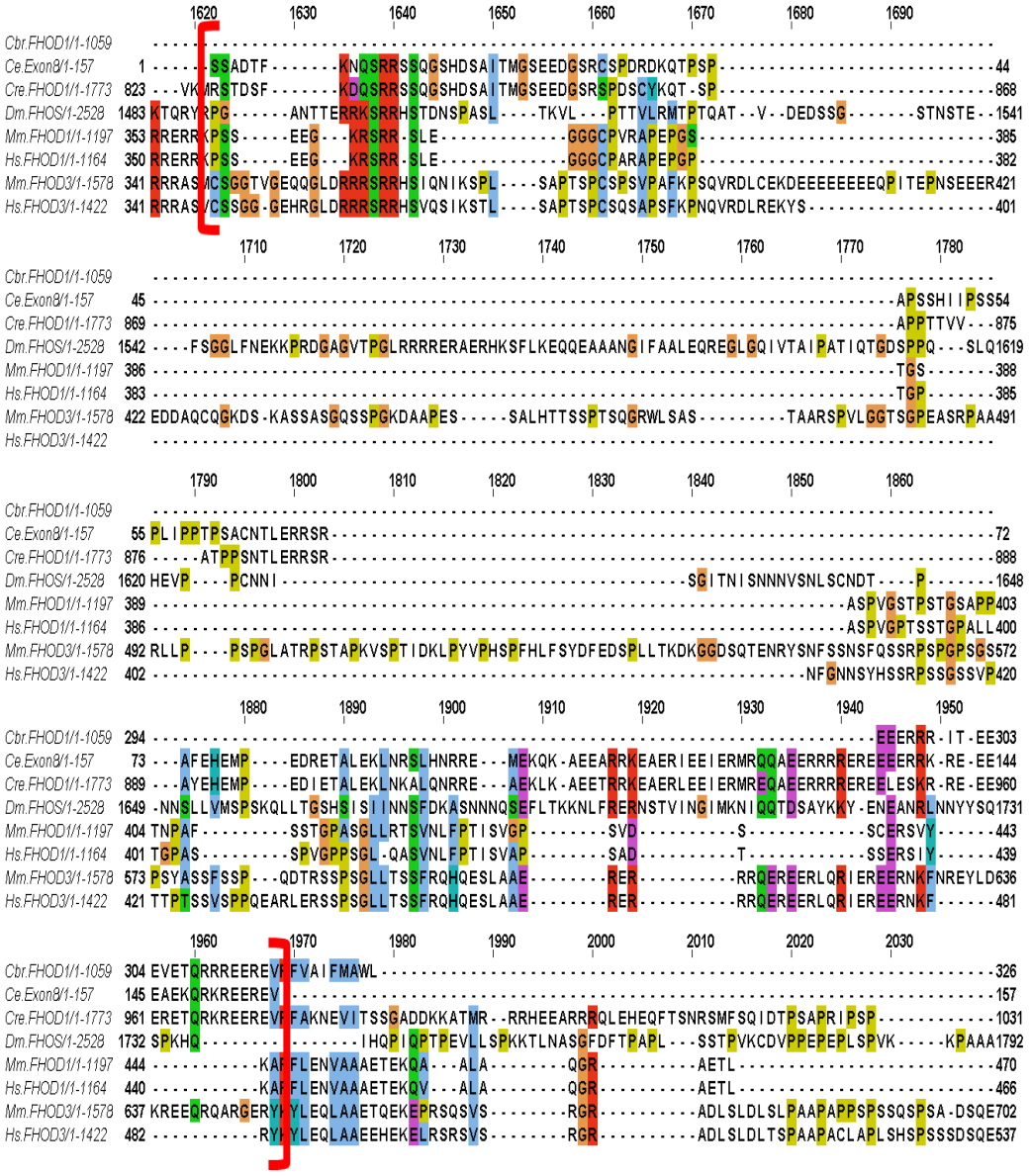

Table 5. FHOD protein sequence alignment analysis

Percent identity matrix was created by comparing the *C. elegans* FHOD1a and FHOD1b whole amino acid sequences and the 157 amino acids encoded by the alternatively spliced axon 8 to seven orthologs using Clustal2.1 (www.ebi.ac.uk/Tools/msa/clustalo/) for full-length proteins.

	C. elegans **FHOD-1a** **Percent Identity**	***C. elegans*** **FHOD-1b** **Percent Identity**	**FHOD1a Exon 8** **Percent Identity**
C. remanei **FHOD-1**	89	91	76
C. briggsae **FHOD-1**	88	88	74
Drosophila **FHOS**	35	37	18
Mouse **FHOD1**	37	38	22
Mouse **FHOD3**	37	38	29
Human **FHOD1**	35	37	18
Human **FHOD3**	37	38	28

The spliced fhod-1 exon 8 may encode a coiled-coil domain

The eight FHOD orthologs (human and mouse FHOD1 and FHOD3, fruit fly FHOS, the nematodes *C. remanei, C. briggsae* and *C. elegans* (examined here)) are predicted to have two or three regions encoding for coiled-coil domains, each of which is about 30 residues. However, sequence alignment analyses indicates that the primary sequence of the coiled-coil regions are not conserved between FHOD proteins (Figure 35B). *C. elegans* FHOD-1a (long isoform) is predicted to have three coiled-coil domains, involving a sequence of 29 residues at the N-terminus (between positions 309 and 337), a C-terminus sequence of 22 amino acids (between positions 1085 and 1106), and relatively large central region of 83 amino acids (from 429 to 511). The larger predicted coiled-coil region (of 83 amino acids) is mainly encoded by exon 8, which encodes positions 348 through 504 of the central coiled-coil. Additionally, this *C. elegans* predicted coiled-coil region has 51% sequence alignment identity with a conserved human and mouse FHOD3 coiled-coil domain, which consists of 33 residues and is 100% identical between the two mammalian species (Figure 35B). Moreover, the sequence alignment identity of the *C. elegans* 83 residues coiled-coil domain showed 32% alignment identity to the human FHOD1 predicted coiled-coil domain (38 amino acids).

Interestingly, the alignments fall at the region that contains the highly conserved stretch of eight amino acids and its larger consensus sequence (about 25 amino acids), suggesting that this nematode conserved sequence contributes to the function of the FHOD-1a coiled-coil domain. Together, these data suggest that the *C. elegans* FHOD-1a exon 8 encodes a large part of the protein's coiled-coil domain and the short form FHOD1b probably lacks this coiled-coil domain. Indeed, protein domain analysis for the

short FHOD-1b protein predicted only the two N-terminus and C-terminus coiled-coil domains, suggesting that the middle 83 coiled coil domain is absent.

Figure 35. *fhod-1* exon 8 is a nematode-specific sequence that may encode a coiled-coil domain

(A) *fhod-1* exon 8 encodes a nematode-specific protein sequence, showing a consensus sequence of about 25 amino acids (left panel; consensus), a part of that consensus sequence has an evolutionary high conserved stretch of eight amino acids (right panel; vertical bracket), two of which are encoded by the adjacent exon 9 (right panel; arrows). Residues are coloured in Clustal X according to their physiochemical properties, as following: red [basic –residues (HRK)], blue [hydrophobic residues (AVFPMILW)], green [hydroxyl, sulfhydryl, amine residues (STNQY)], magenta [acidic residues (DE)], orange [the smallest amino acid, G], other colours denote unusual amino/imino acids etc. Conservation and Quality are colour coded with bright yellow representing high degrees of conservation and quality and darker colour lower degrees. Conservation is scaled by numbers 0 – 9 with the highest (100%) conservation is denoted by a yellow star. (B) The *fhod-1* exon 8 involves a predicted coiled-coil domain (http://www.ebi.ac.uk/interpro/) of 83 amino acids (*Ce. Exon 8*), seven of which are encoded by the adjacent exon 9 (for simplicity, gaps between positions 10-40 and 50-60 are not shown). This region has 51% sequence identity with the conserved, 33 residues, human and mouse FHOD3 coiled-coil domains (*Hs. FHOD3_COIL* and *Mm. FHOD3_COIL*, respectively). Two short stretches of amino acids (4 residues each) are conserved between *C. elegans* FHOD-1, human FHOD3 and mouse FHOD3 coiled-coil domains (vertical brackets connected by dotted lines). (C) A schematic drawing showing positions of the predicted coiled-coil domains of *fhod-1*. The short isoform lacks the predicted 83 residue domain, which is mainly encoded by the alternatively spliced exon 8 (domains and exons are not drawn to scale).

Figure 35. *fhod-1* exon 8 is a nematode-specific sequence that may encode a coiled-coil domain

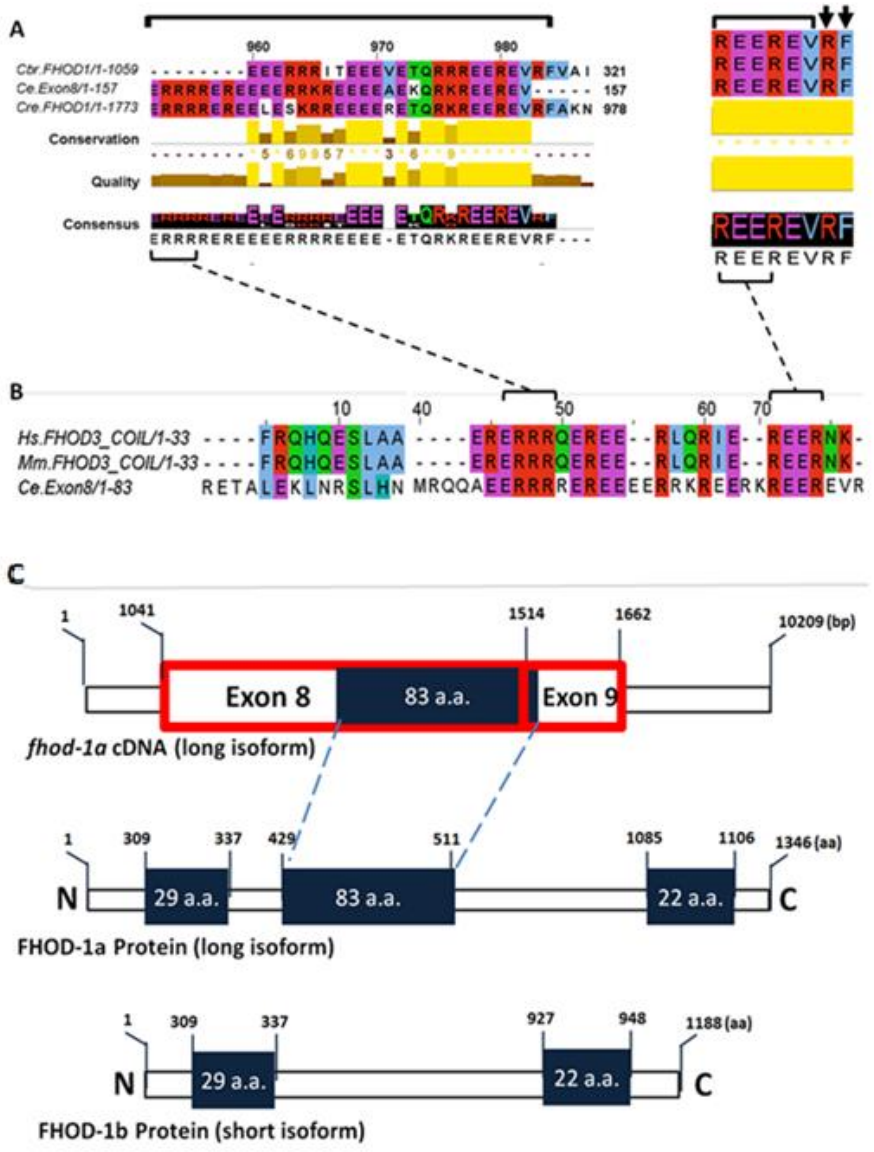

FEM-2 (PP2C PHOSPHATASE) IN EMBRYONIC ELONGATION

Background

The *C. elegans fem-2* has a well-established essential function in sex determination and encodes a protein phosphatase of the type 2c (PP2c phosphatase) (KIMBLE *et al.* 1984; HODGKIN 1986; PILGRIM *et al.* 1995; CHIN-SANG and SPENCE 1996; HANSEN and PILGRIM 1998). In addition to its role in sex determination, *fem-2* was found to function in embryonic elongation, in parallel to the formin *fhod-1*and the *mel-11/let-502*pathway (Figure 36) (PIEKNY *et al.* 2000; VANNESTE *et al.* 2013). The function of redundant pathways may guarantee the robustness of the *C. elegans* embryonic elongation (PIEKNY *et al.* 2000; VANNESTE *et al.* 2013). Function of *fem-2* in embryonic elongation is independent of its role in sex (PIEKNY *et al.* 2000).

Members of the *fem-2* elongation pathway include the CDC42/RAC-effector *pak-1* (p21 kinase) and its activator the CDC42/RAC-specific GEF, *pix-1* (Martin et al., 2014). *fem-2* does not enhance the *pak-1* phenotype, indicating that they act in the same pathway, but curiously, *pak-1* does not suppress *mel-11* as does *fem-2.* This implies that *pak-1(+)* is required for *fem-2* suppression of *mel-11* (VANNESTE *et al.* 2013). The enhancement of *fhod-1* by *pak-1* and *fem-2* may indicate that *pak-1/fem-2* could act on different cassettes of microfilaments than that of *let-502/mel-11* pathway. Thus, I sought determine where *fem-2* acts during elongation.

Figure 36. Genetic interactions involving *fem-2*, showing that *fem-2* acts with *pak-1* to control elongation

fem-2 may interact with *pix-1* since both appear to act in the same pathway as *pak-1*. *fhod-1* is acting in the *let-502/mel-11* pathway, in parallel to *fem-2*. Most of these interactions were discovered by genetic analysis and are consistent with biochemical interaction of the proteins in other systems (question marks indicate unknown an intermediate factor).

Figure 36. Genetic interactions involving *fem-2*, showing that *fem-2* acts with *pak-1* to control elongation

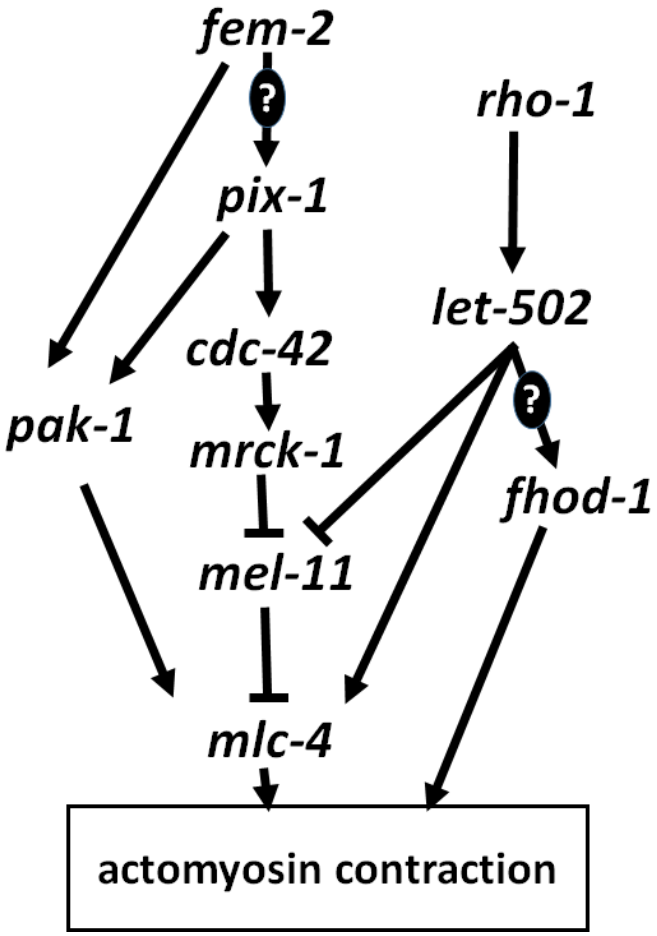

fem-2::gfp expression pattern

Lateral epidermis (seam cells) act as the driving force for epidermal elongation while the dorsal/ventral cells respond passively to the contraction wave coming from the lateral cells (PRIESS and HIRSH 1986). The difference between the lateral and dorsal/ventral epidermis may be explained by the difference in activity and expression of the genes that control the embryonic elongation. For instance, the inhibitory Rho GTPase-activating protein RGA-2 acts specifically in the non-contractile cells (DIOGON *et al.* 2007) and the Rho GEF RHGF-2 is required in the lateral cells (B. Chan , M.Sc. Thesis, University of Calgary) although both proteins are ubiquitously expressed. Moreover, zygotic LET-502 and MEL-11 are differentially expressed, with LET-502 being more highly transcribed in the seam cells and MEL-11 showing the opposite profile (WISSMANN *et al.* 1999). Although PIX-1::GFP is expressed homogenously in epidermis, it was proposed to be required at specific levels in the dorsal posterior cells to control the early elongation rate of the embryo (ZHANG *et al.* 2011; MARTIN *et al.* 2014). Later in elongation, *pix-1* is needed in ventral and dorsal epidermal cells for mechanotransduction signaling upon muscle contraction (ZHANG *et al.* 2011).

To date, it is not known where *fem-2* acts to regulate early embryonic elongation since there is no specific antibody available for immunostaining. Here I will use a genomic *fem-2::gfp* fosmid construct provided by TransgeneOmics (http://www.mpi-cbg.de) to examine the expression pattern of *fem-2*. Time course analysis of the *fem-2::gfp* expression were performed on embryonic, larval and adult stages. The onset of *fem-2::gfp* expression was detected at gastrula (Figure 37A).

FEM-2::GFP appeared to be expressed ubiquitously in early embryonic stages until 1.5 fold. At the 2 fold stage, the expression shifts toward the posterior of the embryo. It also appeared to be expressed in the intestine (this expression appears similar to autoflourescent gut granules, although the green florescent filter was used with short exposure time, which should decrease gut granule detection). Pharyngeal expression appeared at late 3 fold stage, along with continued intestine expression. At larval stages the expression can be detected in the intestine and the pharynx, but with lower intensity (Figure 37B). At adult stages, the expression became very strong in the pharynx as well as the vulva muscle cells. Also the intestine exhibited FEM-2::GFP expression. Additionally, very weak FEM::GFP expression was observed in the gonad. This expression may be restricted to the somatic cells surrounding the germline such as the gonadal sheath cells, which is a single layer that cover the germline components.

Figure 37. *fem-2::gfp* expression

(A) Embryonic expression of the translational fusion *fem-2::gfp* (a fosmid construct provided by TransGeneOmics). FEM-2::GFP appeared to be expressed ubiquitously in early embryonic stages until 1.5 fold, after which expression became more concentrated in the intestine (star). At the 3 fold stage, the expression started to appear at the pharynx as well (arrowhead). (B) FEM-2::GFP expression at larval and adult stages. At larval stages the expression appeared to be strongest in the pharynx (arrowhead) and intestine (star). In adult hermaphrodites, FEM-2::GFP expression was strong at both of the pharynx and the vulva muscles. The expression could also be seen in the intestine and the somatic cells of the germline.

Figure 37. . *fem-2::gfp* expression

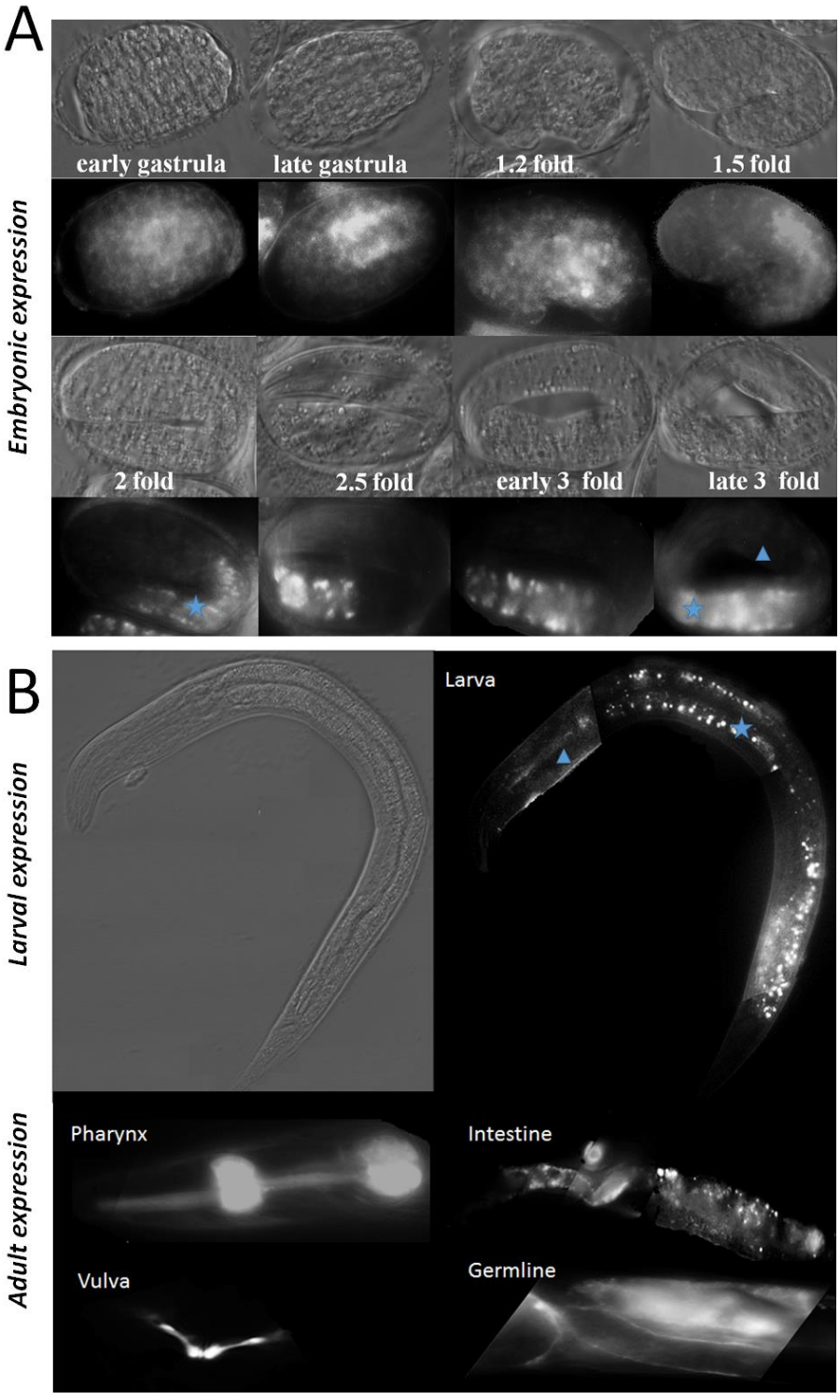

Where does fem-2 act in early elongation?

Although expression of FEM-2::GFP appeared ubiquitous during elongation, it is possible that FEM-2 is only needed for elongation in a subset of cells, as it is true for RHGF-2 and RGA-2 (CASSATA *et al.* 2005; DIOGON *et al.* 2007; GALLY *et al.* 2009) (B. Chan, M.Sc. Thesis, University of Calgary) even though RHGF-2 and RGA-2 are expressed equally in all epidermal cells. Thus, I expressed a *fem-2* cDNA construct (PILGRIM *et al.* 1995) under the control of tissue-specific promoters in lateral epidermal cells, dorsal/ventral epidermal cells or muscle cells. Driving *fem-2* cDNA in lateral epidermis (seam cells) was carried out using *ceh-16* promoter, which is active only in seam cells (CASSATA *et al.* 2005; DIOGON *et al.* 2007;GALLY *et al.* 2009). The *elt-3* promoter was used to drive *fem-2* cDNA in dorsal/ventral epidermal cells (GILLEARD *et al.* 1999; DIOGON *et al.* 2007; GALLY *et al.* 2009). Given the role of muscle in late elongation (WILLIAMS and WATERSTON 1994), I also drove the *fem-2* cDNA in muscles cells, using the *myo-3* promoter that is specific for body-wall muscle cells (OKKEMA *et al.* 1993). It is worth noting that these are well characterized *C. elegans* promoters and they were successfully used to rescue elongation defective phenotypes of *rga-2, mlc-4* and *rhgf-2* (DIOGON *et al.* 2007; GALLY *et al.* 2009) (B. Chan, M.Sc. Thesis, University of Calgary). As a control for this experiment, the *fem-2* endogenous promoter was used to drive *fem-2* cDNA. This promoter was characterized as 3 kb upstream of *fem-2* ATG and is able to rescue the *fem-2* feminization phenotype (PILGRIM *et al.* 1995; HANSEN and PILGRIM 1998).

fem-2 functions in dorsal/ventral epidermis to control elongation

Since the *fem-2* single mutant has a very low penetrance elongation phenotype, with a frequency of <5% (PIEKNY *et al.* 2000; VANNESTE *et al.* 2013), rescuing constructs were injected into the *fem-2; fhod-1* double mutant strain, which has elongation defects of more than 80% at 25°C and about 50% at room temperature (~23°C) (Figure 38). This strain included a *ts* allele, *fem-2(b245).* Two extragenic transgenic lines were tested for every construct and were examined at the two temperatures. The *Pelt-3::fem-2* construct could partially rescue the *fem-2; fhod-1* elongation phenotype at the 25°C and 23°C temperatures to an extent similar to that of the control *Pfem-2::fem-2* construct. The percent of worms that normally reached adulthood at 25°C was elevated from 16% in the *fem-2; fhod-1* parent strain to 45% and 43% in *Pfem-2::fem-2* and *Pelt-3::fem-2* transgenic strains, respectively. At 23°C, the percentage of wild-type adult worms was increased from 51% in the *fem-2; fhod-1* to 79% and 80% in *Pfem-2::fem-2* and *Pelt-3::fem-2* carrying strains, respectively. The changes were statistically significant ($p \leq 0.005$ for the experiment at 25°C, and $p \leq 0.001$ for the experiment at 23°C) using the chi-square test with 3 degrees of freedom. Notably, the *fem-2; fhod-1* mutants were rescued to about the *fem-2(+); fhod-1* single mutant's phenotype at 23°C, suggesting that *Pfem-2::fem-2* and *Pelt-3::fem-2* can fully rescue the *fem-2* elongation arrest phenotype. However, they only partially rescue the *fem-2* elongation defects at 25°C compared to *fhod-1* alone. In contrast, introducing *Pceh-16* and *Pmyo-3* constructs driving the *fem-2* cDNA in the *fem-2; fhod-1* mutant background had no significant effect in the elongation phenotype of these animals ($p > 0.05$). The percentage of *Pceh-16* and *Pmyo-3* animals that reached adulthood at 25°C were 25% and 26% respectively, vs. the control *fem-2;*

fhod-1 value of 16%). At 23°C the percentages of wild-type worms in strains carrying *Pceh-16* and *Pmyo-3* constructs were 59% and 56%, respectively, compared to 51% for the control *fem-2; fhod-1*. The values were not statistically different (p value = 0.3 and 0.2 respectively).

It is worth noting that *Pfem-2::fem-2* does not rescue the *fem-2(b245ts)* sex determination defective phenotype at 25°C (restrictive temperature), which can be scored as the self-sterility of XX hermaphrodites (PILGRIM *et al.* 1995). Extrachromosomal arrays in *C. elegans* are usually not expressed in germline (FIRE *et al.* 1990; HOPE 1991; MELLO *et al.* 1991; KELLY *et al.* 1997). In fact, one of the lines that carry *Pfem-2::fem-2* showed some swelling in the hermaphrodite tail, likely indicating weak masculinization due to excess *fem-2(+)* from the multi-copy transgenic array.

Figure 38. Transgenic *fem-2 cDNA* expression in the dorsal/ventral epidermal cells can rescue *fem-2* elongation defects.

(A) The *fem-2* cDNA driven by its native promoter is able to partially rescue the *fem-2* elongation arrest in the *fem-2; fhod-1* mutant background at the restrictive temperature of 25°C, albeit not to the level of *fem-2(+); fhod-1*. Expression driven in the dorsal/ventral epidermal cells by *Pelt-3::fem-2* showed partial rescue. Expression of *fem-2* cDNA in the lateral epidermal cells, under *Pceh-16* promoter control, or in the muscle cells under *Pmyo-3* promoter, had at best weak, if any, effect on *fem-2; fhod-1*. (B) The same strains shown in (A) were tested at room temperature. ** denotes significant differences between the group and the control *fem-2; fhod-1* strain using chi-squared and 3 degrees of freedom. $p \leq 0.005$ (for experiment at 25°C; A) and $p \leq 0.001$ (for experiment at 23°C; B). ns – not significant, $p > 0.05$.

Figure 38. Transgenic *fem-2 cDNA* expression in the dorsal/ventral epidermal cells can rescue *fem-2* elongation defects.

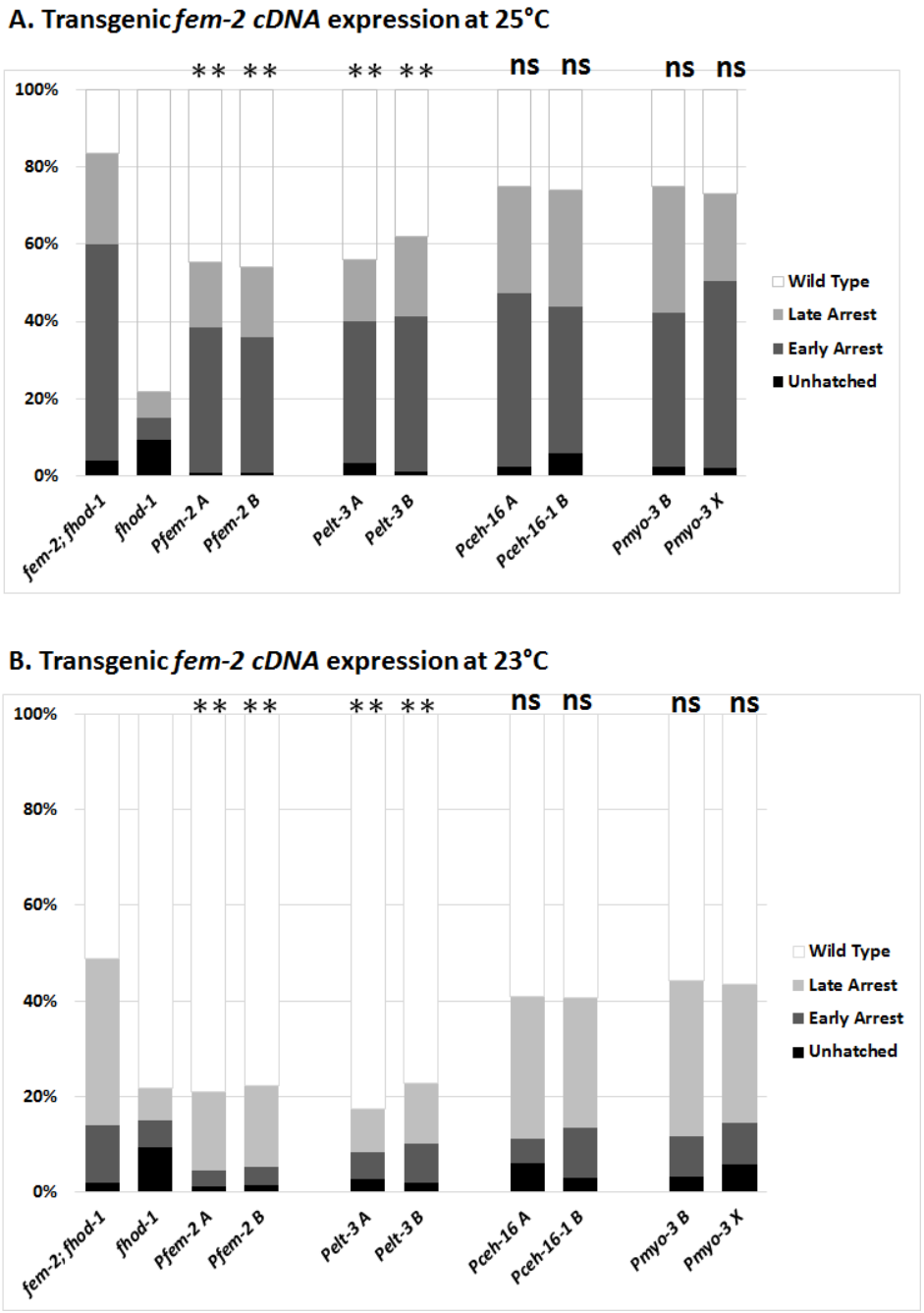

Conclusion

I conclude from these data that the expression of FEM-2 in the ventral and dorsal epidermal cells is at least partially sufficient to rescue the elongation defects caused by the *fem-2* loss-of-function mutation. Additionally, expression of FEM-2 in seam cells and body wall muscle cells might show, at best, weak rescue *fem-2* elongation defects, and so clearly are not necessary for elongation. Thus, *fem-2* likely acts mainly in dorsal/ventral epidermal cells, where it is likely necessary for interactions with *pak-1* (and *pix-1*), which also act in the dorsal/ventral cells (MARTIN *et al.* 2014). This interaction between *fem-2* and *pak-1* was shown genetically (VANNESTE *et al.* 2013). In mammalian cells, biochemical assays showed that PP2C phosphatase, the FEM-2 homolog, is a major biochemical inhibitor of PAK1 by dephosphorylation (CHAN *et al.* 2008). In these cells, PAK1 binds to PIX for targeting the focal adhesions during the hyperosmotic response pathway. My findings suggest that *fem-2* acts with *pak-1* and *pix-1* in the dorsal/ventral epidermis to regulate embryonic elongation.

DISCUSSION AND FUTURE DIRECTIONS

DISCUSSION

Formins other than fhod-1, have a little or no role in embryonic elongation

Although essential regulators of the *C. elegans* embryonic elongation (e.g., *let-502* and *mel-11*) are well characterized, little is known about their non-myosin downstream targets that modulate the actin cytoskeleton. *C. elegans fhod-1*, which encodes a protein homologous to the human FHOD1 and FHOD3, is a member of an actin nucleator family of proteins, the formins. *fhod-1* acts in early embryonic elongation downstream of the *let-502/mel-11* pathway (VANNESTE *et al.* 2013). However, the *fhod-1* null mutation is not fully penetrant, suggesting redundancy with other genes that probably act in the same pathway. Testing potential players such as the other six formin genes (*daam-1, inft-1, inft-2, frl-1, fozi-1,* and *cyk-1)* encoded by the *C. elegans* genome had no dramatic effect on the *fhod-1* phenotype (Figures 22 to 25). Only two of these genes, *inft-1* and *cyk-1,* had at best weak additive effects on *fhod-1* elongation arrest. In combination with *fhod-1, inft-1* and *cyk-1* decreased hatching of *let-502* (tested by RNAi); however, early arrest of these animals may be a result of defects before elongation onset. Tests for potential redundancy were negative when carried out on the most sensitive formin double mutant, *fhod-1; inft-1,* suggesting the involvement of a quadruple redundancy. Additionally, the main components of another family of actin nucleators, the actin related protein Arp2/3 complex, showed that they have no detectable role in embryonic elongation. A caveat to these experiments may be that formin RNAi was not efficient; however, strains with null formin mutations had little or effect on elongation (Figure 22).

My data reveal that *fhod-1* may be the major (perhaps the only) actin nucleator involved in actin regulation during elongation. An alternative possibility is that *fhod-1* function is enhanced by myosin II and myosin represents the redundant pathway. Interestingly, myosin II was proposed to interact and may bind directly, or via an adaptor protein, to mammalian FHOD1, as it colocalizes with FHOD1 within stress fibres. FHOD1 colocalization with myosin II is likely mediated by the GBD and FH3 domains of FHOD1 (SCHULZE *et al.* 2014). Moreover, myosin 1E was found to affect actin dynamics by being localized to actin polymerization sites in lamellipodia, suggesting colocalization with actin nucleating factors (GUPTA *et al.* 2013). In mammalian cells, the serine/threonine ROCK kinase can activate both FHOD1 and myosin II by phosphorylation (AMANO *et al.* 1996; KIMURA *et al.* 1996;HANNEMANN *et al.* 2008a). In *C. elegans*, LET-502/ROCK kinase can activate non-muscle myosin (NMY-1 and NMY-2) (PIEKNY *et al.* 2003). Thus, *fhod-1* function in embryonic elongation might be facilitated by myosin.

Muscle genes are likely not involved in early elongation

Embryonic elongation occurs in two phases. The first is controlled mainly by the *let-502/mel-11* pathway, which drives epidermal actomyosin contraction whereas the second phase is controlled by muscle genes, which drive muscle cell contraction (WILLIAMS and WATERSTON 1994; WISSMANN *et al.* 1999). The redundant pathway during early elongation involves *fem-2* and *pak-1* (PIEKNY *et al.* 2000; GALLY *et al.* 2009; VANNESTE *et al.* 2013). However, the tissue in which latter genes act is unknown. I examined the possibility that muscle genes, which are known to function in late elongation might also have a role in early elongation that was previously obscured by the

role of epidermis. For this purpose, I tested two muscle genes that are known to be necessary for late elongation that encode biochemically different proteins, PAT-4 (an integrin-linked kinase; ILK) and MYO-3 (myosin heavy chain A) (MILLER *et al.* 1983; HONDA and EPSTEIN 1990; GETTNER *et al.* 1995; MACKINNON *et al.* 2002; LIN *et al.* 2003;CHISHOLM and HARDIN 2005). However, depletion of *pat-4* and *myo-3* alone or combined with *mel-11*; *let-502* showed no effect on early elongation, suggesting that muscle genes function is restricted to muscle cells in late elongation (Figure 27). It has recently been proposed that *pak-1* functioning in the epidermis and is redundant with *let-502/mel-11* during early elongation (MARTIN *et al.* 2014).

fhod-1::gfp is expressed homogenously during morphogenesis

Previous observations using an antibody to FHOD-1 supported the genetic analysis that revealed that FHOD-1 acts in seam cells to control early embryonic elongation (between 1.2-fold and 2-fold stages) (VANNESTE *et al.* 2013); however, the antibody failed to detect FHOD-1 expression before the 2.5 fold stage. As a perhaps more sensitive approach, I used a FHOD-1::GFP. This FHOD-1::GFP construct, which was previously shown to rescue muscle defects in adults (MI-MI *et al.* 2012), was able to rescue the *fhod-1* elongation defects as well. This indicates that *gfp*-tagged *fhod-1* is expressed and functions in a manner similar to that of the endogenous gene. Using anti-GFP antibody staining, I was able to show that FHOD-1 is expressed cytoplasmically in all cells before the gastrula stage and through the whole process of embryonic elongation (Figures 28-30). The expression was homogenous in epidermal cells. FHOD-1 appeared to be expressed in higher levels in seam cells, but only in late elongation. Ubiquitous epidermal expression was reported for some elongation related genes, but with gene

function being required only in a specific cell subset, including *rga-2*, *pix-1*, *rhgf-2* (B. Chan, M.Sc. thesis),(MARTIN *et al.* 2014), *fem-2* (this work). A tissue-specific promoter approach to drive *fhod-1*expression in a cell-specific manner may be helpful in this context.

C46H11.11 (fhod-1) encodes a novel short isoform

Defining the *fhod-1* (*C46H11.11*) full length cDNA using an RT-PCR approach reveals that *C46H11.11* encodes two *fhod-1* isoforms (Figure 33). These two isoforms were given the names *fhod-1a*, long isoform (*C46H11.11a*), and *fhod-1b*, short isoform (*C46H11.11b*). The short isoform *fhod-1b* omits exon 8 of the long isoform. Protein sequence alignment analysis indicated that the alternatively spliced exon 8, which encodes 157 amino acids, is a nematode specific structure that lies in the CC (Coiled-Coil) domain (Figure 39).

The alternative FHOD-1a exon 8 is predicted to encode a coiled-coil domain of 83 residues. Protein alignment analysis of the predicted coiled-coil domain defined a conserved region of about 25 amino acids that appears to be nematode specific. Indeed, a stretch of eight residues among the 25 amino acids consensus are highly conserved between *C. elegans, C. remanei* and *C. briggsae* (Figure 35). Additionally, the predicted domain shows a relatively high similarity (51%) to the human and mouse FHOD3 coiled-coil domain, albeit with the introduction of several gaps.

Coiled-coil domain is a secondary structure composed of two or more alpha helices that twist to form a helical cable structure. The cable structures can play a mechanical role in forming stiff bundles of fibres and thus eliminating or shortening of the FHOD-1 coiled-coil regions may result in a change in protein structure or

conformation. I did not find temporal differences in the *fhod-1* mRNA expression by RT-PCR between embryos and adults (Figure 33, although the experiments were not done quantitatively). Although, importance of the alternative splicing event is not clear, it is possible that the two isoforms act in a tissue-specific manner. Two functions were described for FHOD-1 in *C. elegans*, in muscle development and embryonic elongation (MI-MI *et al.* 2012; VANNESTE *et al.* 2013). *fhod-1* isoforms may act independently to control muscle growth and embryonic elongation. Antibody staining specific to epitopes within the alternative exon 8 will be necessary to examine this hypothesis. Previously identified splicing events in the mouse and human FHOD3 at the protein's N-terminus and the C-terminus resulted in heart-specific and muscle-specific isoforms, respectively (KANAYA *et al.* 2005; ISKRATSCH *et al.* 2010).

Figure 39. *fhod-1* isoforms

(A) Schematic drawing of the cDNA of the *C. elegans C46H11.11a* (*fhod-1* long isoform) and the *C46H11.11b* (*fhod-1* short isoform), with protein-coding exons colour-coded to match predicted product structural domains (B). Introns are shown as the black lines between exons. The new intron resulted from the alternative splicing of exon 8 is shown in red. Colour-coding represent FHOD-1 domains as following: specific GTP-binding domain (GBD; gray), diaphanous inhibitory domain (DID; green), helical or coiled-coil (CC) regions (blue), formin homology domain 1 (FH1; light blue), the formin homology domain 2 (FH2; red) and the diaphanous autoregulatory domain (DAD; purple). (B) Schematic drawing of the *C. elegans* FHOD-1 predicted proteins; FHOD-1a (long isoform) and FHOD-1b(short isoform). The short isoform of the protein appear to lack the entire region of the large central coiled-coil domain (CC; dotted lines). Protein domains are not drawn to scale.

Figure 39. *fhod-1* isoforms

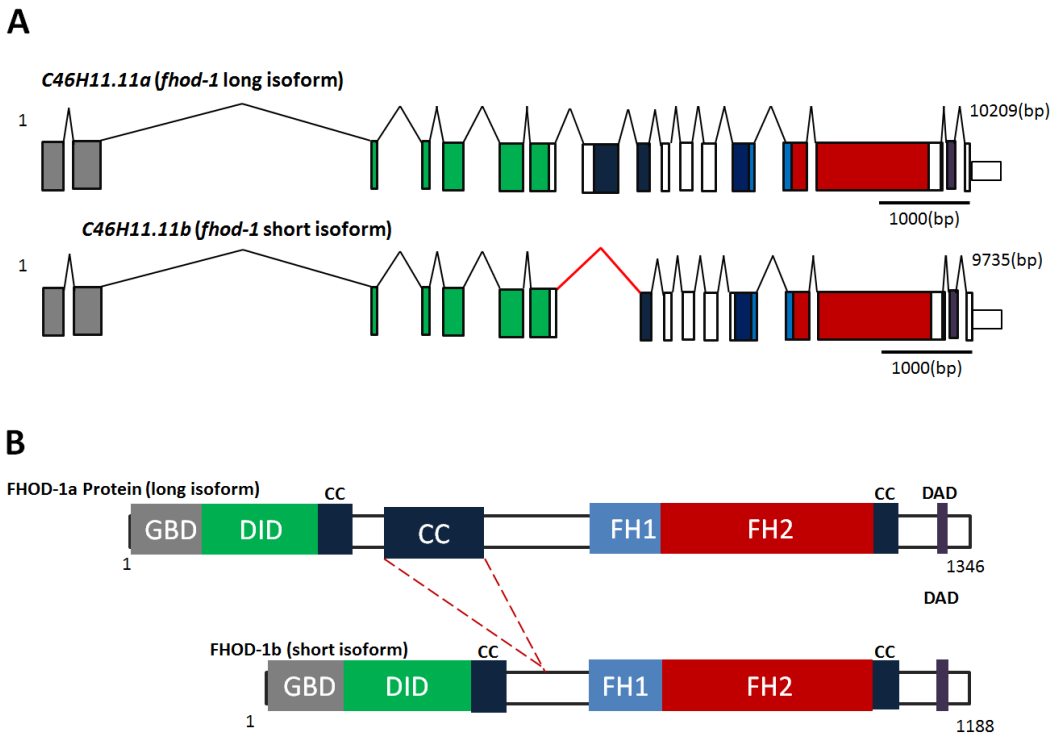

fem-2::gfp expression and function in embryonic elongation

Genetic analysis revealed that *C. elegans fem-2*, which encodes a PP2c phosphatase, is required for proper embryonic elongation, in addition to its well established role in sexual differentiation (KIMBLE *et al.* 1984; HODGKIN 1986; PILGRIM *et al.* 1995; CHIN-SANG and SPENCE 1996; HANSEN and PILGRIM 1998; PIEKNY *et al.* 2000; VANNESTE *et al.* 2013). *pak-1* and its activator *pix-1* (CDC42/RAC-specific GEF) are suggested to act in the dorsal/ventral epidermis (ZHANG *et al.* 2011; MARTIN *et al.* 2014), whereas, it is not known where *fem-2* is expressed or functions. To tackle this issue, I examined the *fem-2* expression using a *fem-2::gfp* genomic fusion and the *fem-2* cDNA constructs was driven by tissue-specific promoters to examine where it functions in embryonic elongation.

I first showed that the *fem-2::gfp* could rescue *fem-2* elongation defects, demonstrating that it was expressed in the relevant tissues involved in elongation. The expression profile of *fem-2::gfp* showed that it is expressed early in embryonic development, before the gastrula stage (Figure 37). The expression continue to the adulthood, albeit with changes in expression levels and distribution. Indeed, the *fem-2* mRNA was previously reported to be expressed in all developmental stages, with higher expression levels in adults (Pilgrim et al., 1995). *fem-2* expression was detected ubiquitously and in high levels at the onset of embryonic development at 1.2 fold stage, suggesting that it is expressed early enough in the epidermis. The expression appeared to be more specific or may be restricted to pharynx and intestine at larval stages. In adults, *fem-2* appeared to be expressed in specific tissues such as pharynx, vulva muscle cells and intestine.

Epidermal cell markers such as *ajm-1* antibody or a GFP reporter, which are specific for seam cells borders, may be needed to track epidermal expression during early elongation (using specific cell promoters approach may cover this caveat, see below). Additionally, raising a FEM-2 specific antibody would be helpful in visualizing maternal expression of *fem-2,* along with the likely zygotic expression presented here. The function of *fem-2* in elongation is thought to depend on maternal expression (Piekny et al., 2000). However, the *fem-2::gfp* construct is apparently expressed before the start of embryonic elongation (at 1.2 fold stage), indicating that it may resemble enogenous *fem-2* expression. Notably, the *fem-2::gfp* genomic fusion was not able to rescue *fem-2(b245)* fertility, suggesting that the construct is silenced in the germline (See below for a more detailed discussion).

fem-2 functions mainly in dorsal/ventral epidermal cells

Using tissue-specific promoters, I was able to show that *fem-2* acts in dorsal/ventral epidermal cells to regulate embryonic elongation. *Pelt-3::fem-2* construct, which drives *fem-2(+)* expression in dorsal/ventral epidermis, was able to rescue, partially at least, the *fem-2* elongation defects and worked as well as *fem-2* driven by its native promoter in the sensitized *fem-2; fhod-1* background (Figure 38). However, expression of *fem-2* cDNA under the seam cell specific promoter *ceh-16* or muscle cell specific promoter *myo-3* had at best weak rescuing effects on *fem-2; fhod-1* elongation arrest. These findings suggest that *fem-2* is required in the dorsal/ventral epidermal cells during early elongation. A caveat to this approach might be that I was not able to confirm the expression of the promoters in the specific tissues. However, *fem-2, elt-3, ceh-16* and *myo-3* promoters that were used here are well characterized (OKKEMA *et al.*

1993;GILLEARD *et al.* 1999;CASSATA *et al.* 2005; GALLY *et al.* 2009). Additionally, *elt-3, ceh-16* and *myo-3* promoters were previously used to rescue elongation defects (GILLEARD *et al.*1999; DIOGON *et al.* 2007; GALLY *et al.* 2009)(B. Chan, M.Sc. thesis).

Analysis of the other two components of the *fem-2* elongation pathway, *pak-1* and *pix-1*, suggest that they may be required mainly in the dorsal/ventral epidermal cells as well (ZHANG *et al.* 2011; MARTIN *et al.* 2014). My observations, along with the data presented here, suggest that the *fem-2/pak-1* elongation pathway may act in dorsal/ventral epidermal cells in parallel to the *let-502/mel-11* pathway, which act mainly in seam cells (WISSMANN *et al.* 1999). Function of *fem-2* in the dorsal/ventral cells does not contradict the essential role of seam cells in initiating the actomyosin contraction of the epidermal cells (PRIESS and HIRSH 1986). *let-502* plays a prominent role in controlling the essential contractile forces in seam cells, is inhibited in dorsal lateral cells by *mel-11* and *rga-2*, which function mainly in dorsal/ventral cells (GALLY *et al.* 2009). Thus, the contraction of the dorsal/lateral cells may not be completely passive as previously proposed (PRIESS and HIRSH 1986), but controlled, at least partially, by the *fem-2/pak-1/pix*-1 pathway. Redundancy between genes and pathways that control morphogenesis is acknowledged widely in various systems as an evidence of the robustness of biological processes (COOKE *et al.* 1997; NOWAK *et al.* 1997; COSTANZO *et al.* 2010; RAMANI *et al.* 2012).

The homogenous expression of *fem-2::gfp* may imply that *fem-2* expression is needed for other functions during embryonic development. In fact, *fem-2* is required for the development of both somatic and germline cell and its role in sex determination is well characterized (KIMBLE *et al.* 1984; HODGKIN 1986; PILGRIM *et al.* 1995; CHIN-SANG and SPENCE 1996; HANSEN and PILGRIM 1998; PIEKNY *et al.* 2000). The failure of the

Pfem-2::fem-2 construct to rescue *fem-2(b245)* sterility remains the main caveat of my experiments. It may be a result of the inability of multi-copy transgenes to be expressed in germline (FIRE *et al.* 1990; HOPE 1991; MELLO *et al.* 1991;KELLY *et al.* 1997). The previous reports of rescue of *fem-2(b245)* sterility (PILGRIM *et al.* 1995) may be due to many reasons including the specific constructs, which were usually fosmid and lambda clones that were larger than my constructs and involved more of the upstream and downstream sequences (PILGRIM *et al.* 1995). In fact, one of my *Pfem-2::fem-2* lines showed some swelling in the hermaphrodite tail, likely indicating weak masculinization due to excess *fem-2(+)*. *fem-2* rescuing constructs that failed to completely rescue *fem-2* sex defects were previously reported to induce apparent masculinization of the somatic gonad and the tail structures (CHIN-SANG and SPENCE 1996). These observations imply that rescuing constructs used here likely were successfully expressed in epidermis to rescue the elongation defect of *fem-2(b245)*, but were not efficiently expressed in the gonads and therefore it could not rescue the fertility of these animals.

FUTURE DIRECTIONS

C. elegans embryonic elongation is controlled by a network of genes that is not completely characterized. Specifically, little is known about the genes which act downstream of the elongation pathway to regulate actin dynamics. The only actin nucleator identified was the formin encoding gene *fhod-1* (Vanneste et al., 2013). Here, I identified two other formin genes that may have a minor role in elongation, *inft-1* and *cyk-1*; however, identifying other actin regulating genes that might be redundant with *fhod-1* may require a forward genetic screen. Such approach can use, in addition to *fhod-1* single mutant, the *fhod-1; inft-1* or *let-502 fhod-1* double mutant as a sensitive back

ground for elongation defects. Additionally, I was able to confirm that the temporal function of muscle genes (e.g., *pat-4* and *myo-3*) is restricted to the late phase of embryonic elongation.

The current study was successful in identifying a novel isoform for *fhod-1*. The new short isoform (named *fhod-1b*) occurs as a result of an alternative splicing event that eliminates the eighth exon of the previously predicted long isoform *fhod-1a*. Future work will examine whether the new isoform has a specific temporal or spatial expression. Immunostaining analysis for FHOD-1b expression may use an antibody that is specific to the region encoded by the boundary of the two adjacent exons for the alternatively spliced exon 8. Epidermal cell specific markers such as MH27 antibody (anti-AJM-1) can be used to determine whether FHOD-1b is expressed in lateral epidermal cells, as it was seen for the long isoform. Time course analysis of the gene expression is necessary to determine whether it acts in embryonic elongation and at which stage. To determine where *fhod-1b* is required during embryonic elongation, I can use the tissue specific promoters approach. Lateral epidermal cells specific promoter *ceh-16*, dorsal/ventral specific promoter *elt-3* and muscle specific promoter *myo-3* can be used to drive *fhod-1b* cDNA expression in these specific tissues. The *fhod-1* endogenous promoter has to be cloned to be used as a control for the rescuing experiments.

The current study successfully showed that *fem-2* functions mainly in dorsal/ventral epidermal cells to control embryonic elongation. *fem-2* functions in an independent elongation pathway, *fem-2/pak-1*, which acts in parallel to the central elongation pathway *let-502/mel-11*. Little is known about the *fem-2/pak-1* elongation pathway. For instance it is not known whether there are other components that act

upstream or downstream of *fem-2/pak-1* other than *pix-1*. Potential targets for *fem-2/pak-1* pathway may include MLC-4, which can be phosphorylated by LET-502 as well. Whether the *fem-2/pak-1* pathway works on the same cytoskeletal filaments as the *let-502/mel-11* pathway need to be further investigated. *let-502/mel-11* was found to mainly regulate myosin dynamics and thus, inducing actomyosin contraction in seam cells. However careful analysis is required to investigate whether *fem-2/pak-1* is able to regulate myosin contraction in the epidermis during embryonic elongation or if the relationship is indirect.

REFERENCES

Aamodt, E. J., and J. G. Culotti, 1986 Microtubules and microtubule-associated proteins from the nematode *Caenorhabditis elegans*: periodic cross-links connect microtubules in vitro. J Cell Biol 103**:** 23-31.

Alberts, A. S., 2001 Identification of a carboxyl-terminal diaphanous-related formin homology protein autoregulatory domain. J Biol Chem 276**:** 2824-2830.

Alberts, A. S., N. Bouquin, L. H. Johnston and R. Treisman, 1998 Analysis of RhoA-binding proteins reveals an interaction domain conserved in heterotrimeric G protein beta subunits and the yeast response regulator protein Skn7. J Biol Chem 273**:** 8616-8622.

Albertson, D. G., and J. N. Thomson, 1976 The pharynx of Caenorhabditis elegans. Philos Trans R Soc Lond B Biol Sci 275**:** 299-325.

Altun-Gultekin, Z., Y. Andachi, E. L. Tsalik, D. Pilgrim, Y. Kohara *et al.*, 2001 A regulatory cascade of three homeobox genes, ceh-10, ttx-3 and ceh-23, controls cell fate specification of a defined interneuron class in C. elegans. Development 128**:** 1951-1969.

Amano, M., M. Ito, K. Kimura, Y. Fukata, K. Chihara *et al.*, 1996 Phosphorylation and activation of myosin by Rho-associated kinase (Rho-kinase). J Biol Chem 271**:** 20246-20249.

Andachi, Y., 2004 Caenorhabditis elegans T-box genes tbx-9 and tbx-8 are required for formation of hypodermis and body-wall muscle in embryogenesis. Genes Cells 9**:** 331-344.

Araujo, S. J., and G. Tear, 2003 Axon guidance mechanisms and molecules: lessons from invertebrates. Nat Rev Neurosci 4**:** 910-922.

Aronoff, R., J. E. Mellem, A. V. Maricq, R. Sprengel and P. H. Seeburg, 2004 Neuronal toxicity in *Caenorhabditis elegans* from an editing site mutant in glutamate receptor channels. J Neurosci 24**:** 8135-8140.

Arvanitis, D., and A. Davy, 2008 Eph/ephrin signaling: networks. Genes Dev 22**:** 416-429.

Asakura, T., N. Waga, K. Ogura and Y. Goshima, 2010 Genes required for cellular UNC-6/netrin localization in *Caenorhabditis elegans*. Genetics 185**:** 573-585.

Aspenstrom, P., N. Richnau and A. S. Johansson, 2006 The diaphanous-related formin DAAM1 collaborates with the Rho GTPases RhoA and Cdc42, CIP4 and Src in regulating cell morphogenesis and actin dynamics. Exp Cell Res 312**:** 2180-2194.

Aspock, G., G. Ruvkun and T. R. Burglin, 2003 The Caenorhabditis elegans ems class homeobox gene ceh-2 is required for M3 pharynx motoneuron function. Development 130**:** 3369-3378.

Auld, V., 1999 Glia as mediators of growth cone guidance: studies from insect nervous systems. Cell Mol Life Sci 55**:** 1377-1385.

Avery, L., 1993 Motor neuron M3 controls pharyngeal muscle relaxation timing in *Caenorhabditis elegans*. J Exp Biol 175**:** 283-297.

Avery, L., and H. R. Horvitz, 1989 Pharyngeal pumping continues after laser killing of the pharyngeal nervous system of *C. elegans*. Neuron 3**:** 473-485.

Avery, L., and J. H. Thomas, 1997 Feeding and Defecation.

Axang, C., M. Rauthan, D. H. Hall and M. Pilon, 2008 Developmental genetics of the *C. elegans* pharyngeal neurons NSML and NSMR. BMC Dev Biol 8**:** 38.

Baarlink, C., and R. Grosse, 2008 A GBD uncovered: the FHOD1 N terminus is formin'. Structure 16**:** 1287-1288.

Bacaj, T., M. Tevlin, Y. Lu and S. Shaham, 2008 Glia are essential for sensory organ function in *C. elegans*. Science 322**:** 744-747.

Batchelder, E. L., C. L. Thomas-Virnig, J. D. Hardin and J. G. White, 2007 Cytokinesis is not controlled by calmodulin or myosin light chain kinase in the *Caenorhabditis elegans* early embryo. FEBS Lett 581**:** 4337-4341.

Bate, C. M., 1976 Pioneer neurones in an insect embryo. Nature 260**:** 54-56.

Bentley, D., and M. Caudy, 1983 Pioneer axons lose directed growth after selective killing of guidepost cells. Nature 304**:** 62-65.

Bishop, A. L., and A. Hall, 2000 Rho GTPases and their effector proteins. Biochem J 348 Pt 2**:** 241-255.

Bray, D., 1984 Axonal growth in response to experimentally applied mechanical tension. Dev Biol 102**:** 379-389.

Bremer, A., and U. Aebi, 1992 The structure of the F-actin filament and the actin molecule. Curr Opin Cell Biol 4**:** 20-26.

Brenner, S., 1974 The genetics of *Caenorhabditis elegans*. Genetics 77**:** 71-94.

Brockie, P. J., J. E. Mellem, T. Hills, D. M. Madsen and A. V. Maricq, 2001 The *C. elegans* glutamate receptor subunit NMR-1 is required for slow NMDA-activated currents that regulate reversal frequency during locomotion. Neuron 31**:** 617-630.

Brose, K., K. S. Bland, K. H. Wang, D. Arnott, W. Henzel *et al.*, 1999 Slit proteins bind Robo receptors and have an evolutionarily conserved role in repulsive axon guidance. Cell 96**:** 795-806.

Broverman, S., M. MacMorris and T. Blumenthal, 1993 Alteration of Caenorhabditis elegans gene expression by targeted transformation. Proc Natl Acad Sci U S A 90**:** 4359-4363.

Brunet, P., L. Dou, C. Cerini and Y. Berland, 2003 Protein-bound uremic retention solutes. Adv Ren Replace Ther 10**:** 310-320.

Buchman, A. R., and P. Berg, 1988 Comparison of intron-dependent and intron-independent gene expression. Mol Cell Biol 8**:** 4395-4405.

Bulow, H. E., T. Boulin and O. Hobert, 2004 Differential functions of the C. elegans FGF receptor in axon outgrowth and maintenance of axon position. Neuron 42**:** 367-374.

Burridge, K., and K. Wennerberg, 2004 Rho and Rac take center stage. Cell 116**:** 167-179.

Cassata, G., G. Shemer, P. Morandi, R. Donhauser, B. Podbilewicz *et al.*, 2005 *ceh-16/engrailed* patterns the embryonic epidermis of *Caenorhabditis elegans*. Development 132**:** 739-749.

Castellani, V., and G. Rougon, 2002 Control of semaphorin signaling. Curr Opin Neurobiol 12**:** 532-541.

Chada, S., P. Lamoureux, R. E. Buxbaum and S. R. Heidemann, 1997 Cytomechanics of neurite outgrowth from chick brain neurons. J Cell Sci 110 (Pt 10)**:** 1179-1186.

Chalkia, D., N. Nikolaidis, W. Makalowski, J. Klein and M. Nei, 2008 Origins and evolution of the formin multigene family that is involved in the formation of actin filaments. Mol Biol Evol 25**:** 2717-2733.

Chan, P. M., L. Lim and E. Manser, 2008 PAK is regulated by PI3K, PIX, CDC42, and PP2Calpha and mediates focal adhesion turnover in the hyperosmotic stress-induced p38 pathway. J Biol Chem 283**:** 24949-24961.

Chan, S. S., H. Zheng, M. W. Su, R. Wilk, M. T. Killeen *et al.*, 1996 UNC-40, a *C. elegans* homolog of DCC (Deleted in Colorectal Cancer), is required in motile cells responding to UNC-6 netrin cues. Cell 87**:** 187-195.

Chauvet, S., S. Cohen, Y. Yoshida, L. Fekrane, J. Livet *et al.*, 2007 Gating of Sema3E/PlexinD1 signaling by neuropilin-1 switches axonal repulsion to attraction during brain development. Neuron 56**:** 807-822.

Chesarone, M. A., A. G. DuPage and B. L. Goode, 2010 Unleashing formins to remodel the actin and microtubule cytoskeletons. Nat Rev Mol Cell Biol 11**:** 62-74.

Chesarone, M. A., and B. L. Goode, 2009 Actin nucleation and elongation factors: mechanisms and interplay. Curr Opin Cell Biol 21**:** 28-37.

Chilton, J. K., 2006 Molecular mechanisms of axon guidance. Dev Biol 292**:** 13-24.

Chin-Sang, I. D., S. E. George, M. Ding, S. L. Moseley, A. S. Lynch *et al.*, 1999 The ephrin VAB-2/EFN-1 functions in neuronal signaling to regulate epidermal morphogenesis in *C. elegans*. Cell 99**:** 781-790.

Chin-Sang, I. D., and A. M. Spence, 1996 *Caenorhabditis elegans* sex-determining protein FEM-2 is a protein phosphatase that promotes male development and interacts directly with FEM-3. Genes & Development 10**:** 2314-2325.

Chisholm, A., and M. Tessier-Lavigne, 1999 Conservation and divergence of axon guidance mechanisms. Curr Opin Neurobiol 9**:** 603-615.

Chisholm, A. D., and J. Hardin, 2005 Epidermal morphogenesis, pp. 1-22 in *WormBook*, edited by The_*C._elegans*_Research_Community. www.wormbook.org).

Choi, T., M. Huang, C. Gorman and R. Jaenisch, 1991 A generic intron increases gene expression in transgenic mice. Mol Cell Biol 11**:** 3070-3074.

Colamarino, S. A., and M. Tessier-Lavigne, 1995 The role of the floor plate in axon guidance. Annu Rev Neurosci 18**:** 497-529.

Colon-Ramos, D. A., and K. Shen, 2008 Cellular conductors: glial cells as guideposts during neural circuit development. PLoS Biol 6**:** e112.

Conrad, R., R. F. Liou and T. Blumenthal, 1993 Conversion of a trans-spliced *C. elegans* gene into a conventional gene by introduction of a splice donor site. EMBO J 12**:** 1249-1255.

Conradt, B., and H. R. Horvitz, 1998 The *C. elegans* protein EGL-1 is required for programmed cell death and interacts with the Bcl-2-like protein CED-9. Cell 93**:** 519-529.

Consortium, *C. e.* G., 1999 How the worm was won. The C. elegans genome sequencing project. Trends Genet 15**:** 51-58.

Cooke, J., M. A. Nowak, M. Boerlijst and J. Maynard-Smith, 1997 Evolutionary origins and maintenance of redundant gene expression during metazoan development. Trends Genet 13**:** 360-364.

Costa, M., B. W. Draper and J. R. Priess, 1997 The role of actin filaments in patterning the *Caenorhabditis elegans* cuticle. Developmental Biology 184**:** 373-384.

Costa, M., W. Raich, C. Agbunag, B. Leung, J. Hardin *et al.*, 1998 A putative catenin-cadherin system mediates morphogenesis of the *Caenorhabditis elegans* embryo. Journal of Cell Biology 141**:** 297-308.

Costanzo, M., A. Baryshnikova, J. Bellay, Y. Kim, E. D. Spear *et al.*, 2010 The genetic landscape of a cell. Science 327**:** 425-431.

Craig, R., R. Smith and J. Kendrick-Jones, 1983 Light-chain phosphorylation controls the conformation of vertebrate non-muscle and smooth muscle myosin molecules. Nature 302**:** 436-439.

Culotti, J. G., and D. C. Merz, 1998 DCC and netrins. Curr Opin Cell Biol 10**:** 609-613.

D'Souza, J., M. Hendricks, S. Le Guyader, S. Subburaju, B. Grunewald *et al.*, 2005 Formation of the retinotectal projection requires Esrom, an ortholog of PAM (protein associated with Myc). Development 132**:** 247-256.

Davis, M. W., M. Hammarlund, T. Harrach, P. Hullett, S. Olsen *et al.*, 2005 Rapid single nucleotide polymorphism mapping in *C. elegans*. BMC Genomics 6**:** 118.

Demarco, R. S., and E. A. Lundquist, 2010 RACK-1 acts with Rac GTPase signaling and UNC-115/abLIM in *Caenorhabditis elegans* axon pathfinding and cell migration. PLoS Genet 6**:** e1001215.

DeWard, A. D., K. M. Eisenmann, S. F. Matheson and A. S. Alberts, 2010 The role of formins in human disease. Biochim Biophys Acta 1803**:** 226-233.

Di Vizio, D., J. Kim, M. H. Hager, M. Morello, W. Yang *et al.*, 2009 Oncosome formation in prostate cancer: association with a region of frequent chromosomal deletion in metastatic disease. Cancer Res 69**:** 5601-5609.

Dickson, B. J., 2002 Molecular mechanisms of axon guidance. Science 298**:** 1959-1964.

Ding, M., W. M. Woo and A. D. Chisholm, 2004 The cytoskeleton and epidermal morphogenesis in *C. elegans*. Exp Cell Res 301**:** 84-90.

Diogon, M., F. Wissler, S. Quintin, Y. Nagamatsu, S. Sookhareea *et al.*, 2007 The RhoGAP RGA-2 and LET-502/ROCK achieve a balance of actomyosin-dependent forces in *C. elegans* epidermis to control morphogenesis. Development 134**:** 2469-2479.

Dominguez, R., and K. C. Holmes, 2011 Actin structure and function. Annu Rev Biophys 40**:** 169-186.

Dwyer, J., M. Pluess, T. Iskratsch, C. G. Dos Remedios and E. Ehler, 2014 The formin FHOD1 in cardiomyocytes. Anat Rec (Hoboken) 297**:** 1560-1570.

Elul, T., and R. Keller, 2000 Monopolar protrusive activity: a new morphogenic cell behavior in the neural plate dependent on vertical interactions with the mesoderm in Xenopus. Dev Biol 224**:** 3-19.

Etienne-Manneville, S., and A. Hall, 2002 Rho GTPases in cell biology. Nature 420**:** 629-635.

Faix, J., and R. Grosse, 2006 Staying in shape with formins. Dev Cell 10**:** 693-706.

Favaro, P. M., S. de Souza Medina, F. Traina, D. S. Basseres, F. F. Costa *et al.*, 2003 Human leukocyte formin: a novel protein expressed in lymphoid malignancies and associated with Akt. Biochem Biophys Res Commun 311**:** 365-371.

Fire, A., K. Kondo and R. Waterston, 1990 Vectors for low copy transformation of C. elegans. Nucleic Acids Res 18**:** 4269-4270.

Fire, A., S. Xu, M. K. Montgomery, S. A. Kostas, S. E. Driver *et al.*, 1998 Potent and specific genetic interference by double-stranded RNA in *Caenorhabditis elegans*. Nature 391**:** 806-811.

Fleming, T., S. C. Chien, P. J. Vanderzalm, M. Dell, M. K. Gavin *et al.*, 2010 The role of *C. elegans* Ena/VASP homolog UNC-34 in neuronal polarity and motility. Dev Biol 344**:** 94-106.

Fradkin, L. G., G. Garriga, P. C. Salinas, J. B. Thomas, X. Yu *et al.*, 2005 Wnt signaling in neural circuit development. J Neurosci 25**:** 10376-10378.

Francis, R., and R. H. Waterston, 1991 Muscle cell attachment in Caenorhabditis elegans. J Cell Biol 114**:** 465-479.

Fraser, A. G., R. S. Kamath, P. Zipperlen, M. Martinez-Campos, M. Sohrmann *et al.*, 2000 Functional genomic analysis of C. elegans chromosome I by systematic RNA interference. Nature 408**:** 325-330.

Fujii, T., F. Nakao, Y. Shibata, G. Shioi, E. Kodama *et al.*, 2002 Caenorhabditis elegans PlexinA, PLX-1, interacts with transmembrane semaphorins and regulates epidermal morphogenesis. Development 129**:** 2053-2063.

Fujisawa, K., J. L. Wrana and J. G. Culotti, 2007 The slit receptor EVA-1 coactivates a SAX-3/Robo mediated guidance signal in *C. elegans*. Science 317**:** 1934-1938.

Fukuhara, S., H. Chikumi and J. S. Gutkind, 2000 Leukemia-associated Rho guanine nucleotide exchange factor (LARG) links heterotrimeric G proteins of the G(12) family to Rho. FEBS Lett 485**:** 183-188.

Fukushige, T., M. G. Hawkins and J. D. McGhee, 1998 The GATA-factor *elt-2* is essential for formation of the *Caenorhabditis elegans* intestine. Developmental Biology 198**:** 286-302.

Gallo, G., and P. C. Letourneau, 1998 Axon guidance: GTPases help axons reach their targets. Curr Biol 8**:** R80-82.

Gally, C., F. Wissler, H. Zahreddine, S. Quintin, F. Landmann *et al.*, 2009 Myosin II regulation during *C. elegans* embryonic elongation: LET-502/ROCK, MRCK-1 and PAK-1, three kinases with different roles. Development 136**:** 3109-3119.

Gasteier, J. E., R. Madrid, E. Krautkramer, S. Schroder, W. Muranyi *et al.*, 2003 Activation of the Rac-binding partner FHOD1 induces actin stress fibers via a ROCK-dependent mechanism. J Biol Chem 278**:** 38902-38912.

Gaudet, J., and S. E. Mango, 2002 Regulation of organogenesis by the Caenorhabditis elegans FoxA protein PHA-4. Science 295**:** 821-825.

George, S. E., K. Simokat, J. Hardin and A. D. Chisholm, 1998 The VAB-1 Eph receptor tyrosine kinase functions in neural and epithelial morphogenesis in *C. elegans*. Cell 92**:** 633-643.

Gettner, S. N., C. Kenyon and L. F. Reichardt, 1995 Characterization of beta *pat-3* heterodimers, a family of essential integrin receptors in *C. elegans*. Journal of Cell Biology 129**:** 1127-1141.

Ghenea, S., J. R. Boudreau, N. P. Lague and I. D. Chin-Sang, 2005 The VAB-1 Eph receptor tyrosine kinase and SAX-3/Robo neuronal receptors function together during C. elegans embryonic morphogenesis. Development 132**:** 3679-3690.

Gilleard, J. S., Y. Shafi, J. D. Barry and J. D. McGhee, 1999 ELT-3: A Caenorhabditis elegans GATA factor expressed in the embryonic epidermis during morphogenesis. Dev Biol 208**:** 265-280.

Ginzburg, V. E., P. J. Roy and J. G. Culotti, 2002 Semaphorin 1a and semaphorin 1b are required for correct epidermal cell positioning and adhesion during morphogenesis in C. elegans. Development 129**:** 2065-2078.

Gitai, Z., T. W. Yu, E. A. Lundquist, M. Tessier-Lavigne and C. I. Bargmann, 2003 The netrin receptor UNC-40/DCC stimulates axon attraction and outgrowth through enabled and, in parallel, Rac and UNC-115/AbLIM. Neuron 37**:** 53-65.

Goode, B. L., and M. J. Eck, 2007 Mechanism and function of formins in the control of actin assembly. Annu Rev Biochem 76**:** 593-627.

Gorska, M. M., S. J. Stafford, O. Cen, S. Sur and R. Alam, 2004 Unc119, a novel activator of Lck/Fyn, is essential for T cell activation. J Exp Med 199**:** 369-379.

Graham, P. L., J. J. Johnson, S. Wang, M. H. Sibley, M. C. Gupta *et al.*, 1997 Type IV collagen is detectable in most, but not all, basement membranes of *Caenorhabditis elegans* and assembles on tissues that do not express it. J Cell Biol 137**:** 1171-1183.

Griffith, L. M., S. M. Downs and J. A. Spudich, 1987 Myosin light chain kinase and myosin light chain phosphatase from Dictyostelium: effects of reversible phosphorylation on myosin structure and function. J Cell Biol 104**:** 1309-1323.

Grill, B., W. V. Bienvenut, H. M. Brown, B. D. Ackley, M. Quadroni *et al.*, 2007 *C. elegans* RPM-1 regulates axon termination and synaptogenesis through the Rab GEF GLO-4 and the Rab GTPase GLO-1. Neuron 55**:** 587-601.

Gupta, P., N. C. Gauthier, Y. Cheng-Han, Y. Zuanning, B. Pontes *et al.*, 2013 Myosin 1E localizes to actin polymerization sites in lamellipodia, affecting actin dynamics and adhesion formation. Biol Open 2**:** 1288-1299.

Hall, A., and G. Lalli, 2010 Rho and Ras GTPases in axon growth, guidance, and branching. Cold Spring Harb Perspect Biol 2**:** a001818.

Hannemann, S., R. Madrid, J. Stastna, T. Kitzing, J. Gasteier *et al.*, 2008a The Diaphanous-related Formin FHOD1 associates with ROCK1 and promotes Src-dependent plasma membrane blebbing. J Biol Chem 283**:** 27891-27903.

Hannemann, S., R. Madrid, J. Stastna, T. Kitzing, J. Gasteier *et al.*, 2008b The diaphanous related formin FHOD1 associates with ROCK1 and promotes Src-dependent plasma membrane blebbing. J Biol Chem 283**:** 27891-27903.

Hansen, D., and D. Pilgrim, 1998 Molecular evolution of a sex determination protein. FEM-2 (pp2c) in Caenorhabditis. Genetics 149**:** 1353-1362.

Hao, J. C., T. W. Yu, K. Fujisawa, J. G. Culotti, K. Gengyo-Ando *et al.*, 2001 *C. elegans* slit acts in midline, dorsal-ventral, and anterior-posterior guidance via the SAX-3/Robo receptor. Neuron 32**:** 25-38.

Harris, E. S., T. J. Gauvin, E. G. Heimsath and H. N. Higgs, 2010 Assembly of filopodia by the formin FRL2 (FMNL3). Cytoskeleton (Hoboken) 67**:** 755-772.

Harris, J. E., J. A. Govindan, I. Yamamoto, J. Schwartz, I. Kaverina *et al.*, 2006 Major sperm protein signaling promotes oocyte microtubule reorganization prior to fertilization in *Caenorhabditis elegans*. Dev Biol 299**:** 105-121.

Hartshorne, D. J., 1998 Myosin phosphatase: subunits and interactions. Acta Physiol Scand 164**:** 483-493.

Hedgecock, E. M., J. G. Culotti and D. H. Hall, 1990 The unc-5, unc-6, and unc-40 genes guide circumferential migrations of pioneer axons and mesodermal cells on the epidermis in *C. elegans*. Neuron 4**:** 61-85.

Heid, P. J., W. B. Raich, R. Smith, W. A. Mohler, K. Simokat *et al.*, 2001 The zinc finger protein DIE-1 is required for late events during epithelial cell rearrangement in *C. elegans*. Developmental Biology 236**:** 165-180.

Heidemann, S. R., P. Lamoureux and R. E. Buxbaum, 1995 Cytomechanics of axonal development. Cell Biochem Biophys 27**:** 135-155.

Heiman, M. G., and S. Shaham, 2009 DEX-1 and DYF-7 establish sensory dendrite length by anchoring dendritic tips during cell migration. Cell 137**:** 344-355.

Hidalgo, A., 2003 Neuron-glia interactions during axon guidance in *Drosophila*. Biochem Soc Trans 31**:** 50-55.

Hidalgo, A., and G. E. Booth, 2000 Glia dictate pioneer axon trajectories in the *Drosophila* embryonic CNS. Development 127**:** 393-402.

Higgs, H. N., 2005 Formin proteins: a domain-based approach. Trends Biochem Sci 30**:** 342-353.

Higgs, H. N., and K. J. Peterson, 2005 Phylogenetic analysis of the formin homology 2 domain. Mol Biol Cell 16**:** 1-13.

Hilliard, M. A., and C. I. Bargmann, 2006 Wnt signals and frizzled activity orient anterior-posterior axon outgrowth in *C. elegans*. Dev Cell 10**:** 379-390.

Hodgkin, J., 1986 Sex determination in the nematode *C. elegans*: analysis of *tra-3* suppressors and characterization of fem genes. Genetics 114**:** 15-52.

Honda, S., and H. F. Epstein, 1990 Modulation of muscle gene expression in Caenorhabditis elegans: differential levels of transcripts, mRNAs, and

polypeptides for thick filament proteins during nematode development. Proc Natl Acad Sci U S A 87**:** 876-880.

Hope, I. A., 1991 'Promoter trapping' in Caenorhabditis elegans. Development 113**:** 399-408.

Hoppe, P. E., R. C. Andrews and P. D. Parikh, 2003 Differential requirement for the nonhelical tailpiece and the C terminus of the myosin rod in Caenorhabditis elegans muscle. Mol Biol Cell 14**:** 1677-1690.

Huber, A. B., A. L. Kolodkin, D. D. Ginty and J. F. Cloutier, 2003 Signaling at the growth cone: ligand-receptor complexes and the control of axon growth and guidance. Annu Rev Neurosci 26**:** 509-563.

Hutter, H., 2003 Extracellular cues and pioneers act together to guide axons in the ventral cord of *C. elegans*. Development 130**:** 5307-5318.

Hutter, H., 2004 Five-colour in vivo imaging of neurons in *Caenorhabditis elegans*. J Microsc 215**:** 213-218.

Hutter, H., I. Wacker, C. Schmid and E. M. Hedgecock, 2005 Novel genes controlling ventral cord asymmetry and navigation of pioneer axons in C. elegans. Dev Biol 284**:** 260-272.

Ikegami, R., H. Zheng, S. H. Ong and J. Culotti, 2004 Integration of semaphorin-2A/MAB-20, ephrin-4, and UNC-129 TGF-beta signaling pathways regulates sorting of distinct sensory rays in C. elegans. Dev Cell 6**:** 383-395.

Ikonen, E., J. B. de Almeid, K. R. Fath, D. R. Burgess, K. Ashman *et al.*, 1997 Myosin II is associated with Golgi membranes: identification of p200 as nonmuscle myosin II on Golgi-derived vesicles. J Cell Sci 110 (Pt 18)**:** 2155-2164.

Ishii, N., W. G. Wadsworth, B. D. Stern, J. G. Culotti and E. M. Hedgecock, 1992 UNC-6, a laminin-related protein, guides cell and pioneer axon migrations in *C. elegans*. Neuron 9**:** 873-881.

Iskratsch, T., S. Lange, J. Dwyer, A. L. Kho, C. dos Remedios *et al.*, 2010 Formin follows function: a muscle-specific isoform of FHOD3 is regulated by CK2 phosphorylation and promotes myofibril maintenance. J Cell Biol 191**:** 1159-1172.

Iskratsch, T., S. Reijntjes, J. Dwyer, P. Toselli, I. R. Degano *et al.*, 2012 Two distinct phosphorylation events govern the function of muscle FHOD3. Cell Mol Life Sci.

Iskratsch, T., C. H. Yu, A. Mathur, S. Liu, V. Stevenin *et al.*, 2013 FHOD1 is needed for directed forces and adhesion maturation during cell spreading and migration. Dev Cell 27**:** 545-559.

Jan, Y. N., A. Ghysen, I. Christoph, S. Barbel and L. Y. Jan, 1985 Formation of neuronal pathways in the imaginal discs of *Drosophila melanogaster*. J Neurosci 5**:** 2453-2464.

Johnston, R. J., Jr., J. W. Copeland, M. Fasnacht, J. F. Etchberger, J. Liu *et al.*, 2006 An unusual Zn-finger/FH2 domain protein controls a left/right asymmetric neuronal fate decision in C. elegans. Development 133**:** 3317-3328.

Kamath, R. S., A. G. Fraser, Y. Dong, G. Poulin, R. Durbin *et al.*, 2003 Systematic functional analysis of the *Caenorhabditis elegans* genome using RNAi. Nature 421**:** 231-237.

Kamath, R. S., M. Martinez-Campos, P. Zipperlen, A. G. Fraser and J. Ahringer, 2001 Effectiveness of specific RNA-mediated interference through ingested double-stranded RNA in *Caenorhabditis elegans*. Genome Biol 2**:** RESEARCH0002.

Kanaya, H., R. Takeya, K. Takeuchi, N. Watanabe, N. Jing *et al.*, 2005 Fhos2, a novel formin-related actin-organizing protein, probably associates with the nestin intermediate filament. Genes Cells 10**:** 665-678.

Katoh, K., Y. Kano, M. Amano, H. Onishi, K. Kaibuchi *et al.*, 2001 Rho-kinase--mediated contraction of isolated stress fibers. Journal of Cell Biology 153**:** 569-584.

Keller, R., J. Shih and A. Sater, 1992 The cellular basis of the convergence and extension of the Xenopus neural plate. Dev Dyn 193**:** 199-217.

Kelly, W. G., S. Xu, M. K. Montgomery and A. Fire, 1997 Distinct requirements for somatic and germline expression of a generally expressed *Caenorhabditis elegans* gene. Genetics 146**:** 227-238.

Khaitlina, S. Y., 2001 Functional specificity of actin isoforms. Int Rev Cytol 202**:** 35-98.

Kimble, J., L. Edgar and D. Hirsh, 1984 Specification of male development in Caenorhabditis elegans: the fem genes. Dev Biol 105**:** 234-239.

Kimura, K., M. Ito, M. Amano, K. Chihara, Y. Fukata *et al.*, 1996 Regulation of myosin phosphatase by Rho and Rho-associated kinase (Rho-kinase). [see comments.]. Science 273**:** 245-248.

Knobel, K. M., W. S. Davis, E. M. Jorgensen and M. J. Bastiani, 2001 UNC-119 suppresses axon branching in *C. elegans*. Development 128**:** 4079-4092.

Koka, S., C. L. Neudauer, X. Li, R. E. Lewis, J. B. McCarthy *et al.*, 2003 The formin-homology-domain-containing protein FHOD1 enhances cell migration. J Cell Sci 116**:** 1745-1755.

Komuro, H., and E. Yacubova, 2003 Recent advances in cerebellar granule cell migration. Cell Mol Life Sci 60**:** 1084-1098.

Koppen, M., J. S. Simske, P. A. Sims, B. L. Firestein, D. H. Hall *et al.*, 2001 Cooperative regulation of AJM-1 controls junctional integrity in Caenorhabditis elegans epithelia. Nat Cell Biol 3**:** 983-991.

Korswagen, H. C., D. Y. Coudreuse, M. C. Betist, S. van de Water, D. Zivkovic *et al.*, 2002 The Axin-like protein PRY-1 is a negative regulator of a canonical Wnt pathway in *C. elegans*. Genes Dev 16**:** 1291-1302.

Lai, T., and G. Garriga, 2004 The conserved kinase UNC-51 acts with VAB-8 and UNC-14 to regulate axon outgrowth in *C. elegans*. Development 131**:** 5991-6000.

Lee, S. H., and R. Dominguez, 2010 Regulation of actin cytoskeleton dynamics in cells. Mol Cells 29**:** 311-325.

Lettre, G., and M. O. Hengartner, 2006 Developmental apoptosis in *C. elegans*: a complex CEDnario. Nat Rev Mol Cell Biol 7**:** 97-108.

Li, F., and H. N. Higgs, 2003 The mouse Formin mDia1 is a potent actin nucleation factor regulated by autoinhibition. Curr Biol 13**:** 1335-1340.

Li, H., G. Kulkarni and W. G. Wadsworth, 2008 RPM-1, a *Caenorhabditis elegans* protein that functions in presynaptic differentiation, negatively regulates axon outgrowth by controlling SAX-3/robo and UNC-5/UNC5 activity. J Neurosci 28**:** 3595-3603.

Lin, R., 2003 A gain-of-function mutation in *oma-1*, a *C. elegans* gene required for oocyte maturation, results in delayed degradation of maternal proteins and embryonic lethality. Developmental Biology 258**:** 226-239.

Lin, X., H. Qadota, D. G. Moerman and B. D. Williams, 2003 C. elegans PAT-6/actopaxin plays a critical role in the assembly of integrin adhesion complexes in vivo. Curr Biol 13**:** 922-932.

Liu, Z., A. Nukazuka and S. Takagi, 2007 Improved method for visualizing cells revealed dynamic morphological changes of ventral neuroblasts during ventral cleft closure of Caenorhabditis elegans. Dev Growth Differ 49**:** 49-59.

Livesey, F. J., 1999 Netrins and netrin receptors. Cell Mol Life Sci 56**:** 62-68.

Lodish, H., A. Berk, L. Zipursky, P. Matsudaira, D. Baltimore *et al.*, 1999 *Molecular Cell Biology*. W. H. Freeman & Co., New York.

Loverde, J. R., R. E. Tolentino and B. J. Pfister, 2011 Axon stretch growth: the mechanotransduction of neuronal growth. J Vis Exp.

Lundquist, E. A., 2006 Small GTPases. WormBook**:** 1-18.

Lundquist, E. A., R. K. Herman, J. E. Shaw and C. I. Bargmann, 1998 UNC-115, a conserved protein with predicted LIM and actin-binding domains, mediates axon guidance in *C. elegans*. Neuron 21**:** 385-392.

Lupas, A., M. Van Dyke and J. Stock, 1991 Predicting coiled coils from protein sequences. Science 252**:** 1162-1164.

Mackinnon, A. C., H. Qadota, K. R. Norman, D. G. Moerman and B. D. Williams, 2002 *C. elegans* PAT-4/ILK Functions as an Adaptor Protein within Integrin Adhesion Complexes. Curr Biol 12**:** 787-797.

MacMorris, M., S. Broverman, S. Greenspoon, K. Lea, C. Madej *et al.*, 1992 Regulation of vitellogenin gene expression in transgenic Caenorhabditis elegans: short sequences required for activation of the vit-2 promoter. Mol Cell Biol 12**:** 1652-1662.

MacMorris, M., J. Spieth, C. Madej, K. Lea and T. Blumenthal, 1994 Analysis of the VPE sequences in the Caenorhabditis elegans vit-2 promoter with

extrachromosomal tandem array-containing transgenic strains. Mol Cell Biol 14**:** 484-491.

MacNeil, L. T., W. R. Hardy, T. Pawson, J. L. Wrana and J. G. Culotti, 2009 UNC-129 regulates the balance between UNC-40 dependent and independent UNC-5 signaling pathways. Nat Neurosci 12**:** 150-155.

Maduro, M., and D. Pilgrim, 1995 Identification and cloning of unc-119, a gene expressed in the Caenorhabditis elegans nervous system. Genetics 141**:** 977-988.

Maduro, M. F., M. Gordon, R. Jacobs and D. B. Pilgrim, 2000 The UNC-119 family of neural proteins is functionally conserved between humans, Drosophila and C. elegans. J Neurogenet 13**:** 191-212.

Mains, P. E., K. J. Kemphues, S. A. Sprunger, I. A. Sulston and W. B. Wood, 1990 Mutations affecting the meiotic and mitotic divisions of the early *Caenorhabditis elegans* embryo. Genetics 126**:** 593-605.

Maloof, J. N., J. Whangbo, J. M. Harris, G. D. Jongeward and C. Kenyon, 1999 A Wnt signaling pathway controls hox gene expression and neuroblast migration in *C. elegans*. Development 126**:** 37-49.

Maro, G. S., M. P. Klassen and K. Shen, 2009 A beta-catenin-dependent Wnt pathway mediates anteroposterior axon guidance in *C. elegans* motor neurons. PLoS One 4**:** e4690.

Martin, E., S. Harel, B. Nkengfac, K. Hamiche, M. Neault *et al.*, 2014 pix-1 controls early elongation in parallel with mel-11 and let-502 in Caenorhabditis elegans. PLoS One 9**:** e94684.

Materi, W., and D. Pilgrim, 2005 Novel *Caenorhabditis elegans unc-119* axon outgrowth defects correlate with behavioral phenotypes that are partially rescued by nonneural *unc-119*. Genesis 42**:** 104-116.

McDermott, K. W., D. S. Barry and S. S. McMahon, 2005 Role of radial glia in cytogenesis, patterning and boundary formation in the developing spinal cord. J Anat 207**:** 241-250.

McMullan, R., S. Lax, V. H. Robertson, D. J. Radford, S. Broad *et al.*, 2003 Keratinocyte Differentiation Is Regulated by the Rho and ROCK Signaling Pathway. Curr Biol 13**:** 2185-2189.

Mello, C., and A. Fire, 1995 DNA transformation. Methods Cell Biol 48**:** 451-482.

Mello, C. C., J. M. Kramer, D. Stinchcomb and V. Ambros, 1991 Efficient gene transfer in *C.elegans*: extrachromosomal maintenance and integration of transforming sequences. EMBO J 10**:** 3959-3970.

Merz, D. C., and J. G. Culotti, 2000 Genetic analysis of growth cone migrations in Caenorhabditis elegans. J Neurobiol 44**:** 281-288.

Mi-Mi, L., S. Votra, K. Kemphues, A. Bretscher and D. Pruyne, 2012 Z-line formins promote contractile lattice growth and maintenance in striated muscles of *C. elegans*. J Cell Biol 198**:** 87-102.

Miller, D. M., 3rd, I. Ortiz, G. C. Berliner and H. F. Epstein, 1983 Differential localization of two myosins within nematode thick filaments. Cell 34**:** 477-490.

Miller, D. M., F. E. Stockdale and J. Karn, 1986 Immunological identification of the genes encoding the four myosin heavy chain isoforms of Caenorhabditis elegans. Proc Natl Acad Sci U S A 83**:** 2305-2309.

Min, K., J. Kang and J. Lee, 2010 A modified feeding RNAi method for simultaneous knock-down of more than one gene in Caenorhabditis elegans. Biotechniques 48**:** 229-232.

Morck, C., C. Axang, M. Goksor and M. Pilon, 2006 Misexpression of acetylcholinesterases in the *C. elegans pha-2* mutant accompanies ultrastructural defects in pharyngeal muscle cells. Dev Biol 297**:** 446-460.

Morck, C., C. Axang and M. Pilon, 2003 A genetic analysis of axon guidance in the *C. elegans* pharynx. Dev Biol 260**:** 158-175.

Morck, C., M. Rauthan, F. Wagberg and M. Pilon, 2004 *pha-2* encodes the *C. elegans* ortholog of the homeodomain protein HEX and is required for the formation of the pharyngeal isthmus. Dev Biol 272**:** 403-418.

Najarro, E. H., L. Wong, M. Zhen, E. P. Carpio, A. Goncharov *et al.*, 2012 *Caenorhabditis elegans* flamingo cadherin *fmi-1* regulates GABAergic neuronal development. J Neurosci 32**:** 4196-4211.

Nakao, F., M. L. Hudson, M. Suzuki, Z. Peckler, R. Kurokawa *et al.*, 2007 The PLEXIN PLX-2 and the ephrin EFN-4 have distinct roles in MAB-20/Semaphorin 2A signaling in Caenorhabditis elegans morphogenesis. Genetics 176**:** 1591-1607.

Neidt, E. M., C. T. Skau and D. R. Kovar, 2008 The cytokinesis formins from the nematode worm and fission yeast differentially mediate actin filament assembly. J Biol Chem 283**:** 23872-23883.

Norris, A. D., J. O. Dyer and E. A. Lundquist, 2009 The Arp2/3 complex, UNC-115/abLIM, and UNC-34/Enabled regulate axon guidance and growth cone filopodia formation in *Caenorhabditis elegans*. Neural Dev 4**:** 38.

Norris, A. D., and E. A. Lundquist, 2011 UNC-6/netrin and its receptors UNC-5 and UNC-40/DCC modulate growth cone protrusion in vivo in *C. elegans*. Development 138**:** 4433-4442.

Nowak, M. A., M. C. Boerlijst, J. Cooke and J. M. Smith, 1997 Evolution of genetic redundancy. Nature 388**:** 167-171.

O'Donnell, M., R. K. Chance and G. J. Bashaw, 2009 Axon growth and guidance: receptor regulation and signal transduction. Annu Rev Neurosci 32**:** 383-412.

Ogura, K., T. Okada, S. Mitani, K. Gengyo-Ando, D. L. Baillie *et al.*, 2010 Protein phosphatase 2A cooperates with the autophagy-related kinase UNC-51 to regulate axon guidance in *Caenorhabditis elegans*. Development 137**:** 1657-1667.

Ogura, K., C. Wicky, L. Magnenat, H. Tobler, I. Mori *et al.*, 1994 Caenorhabditis elegans unc-51 gene required for axonal elongation encodes a novel serine/threonine kinase. Genes Dev 8**:** 2389-2400.

Oikonomou, G., and S. Shaham, 2011 The glia of *Caenorhabditis elegans*. Glia 59**:** 1253-1263.

Okkema, P. G., S. W. Harrison, V. Plunger, A. Aryana and A. Fire, 1993 Sequence requirements for myosin gene expression and regulation in Caenorhabditis elegans. Genetics 135**:** 385-404.

Patel, F. B., Y. Y. Bernadskaya, E. Chen, A. Jobanputra, Z. Pooladi *et al.*, 2008 The WAVE/SCAR complex promotes polarized cell movements and actin enrichment in epithelia during C. elegans embryogenesis. Dev Biol 324**:** 297-309.

Petersen, J., O. Nielsen, R. Egel and I. M. Hagan, 1998 FH3, a domain found in formins, targets the fission yeast formin Fus1 to the projection tip during conjugation. J Cell Biol 141**:** 1217-1228.

Pettitt, J., E. A. Cox, I. D. Broadbent, A. Flett and J. Hardin, 2003 The Caenorhabditis elegans p120 catenin homologue, JAC-1, modulates cadherin-catenin function during epidermal morphogenesis. J Cell Biol 162**:** 15-22.

Pfister, B. J., A. Iwata, A. G. Taylor, J. A. Wolf, D. F. Meaney *et al.*, 2006 Development of transplantable nervous tissue constructs comprised of stretch-grown axons. J Neurosci Methods 153**:** 95-103.

Piekny, A. J., J. L. Johnson, G. D. Cham and P. E. Mains, 2003 The *Caenorhabditis elegans* nonmuscle myosin genes *nmy-1* and *nmy-2* function as redundant components of the *let-502*/Rho-binding kinase and *mel-11*/myosin phosphatase pathway during embryonic morphogenesis. Development 130**:** 5695-5704.

Piekny, A. J., and P. E. Mains, 2002 Rho-binding kinase (LET-502) and myosin phosphatase (MEL-11) regulate cytokinesis in the early *Caenorhabditis elegans* embryo. Journal of Cell Science 115**:** 2271-2282.

Piekny, A. J., and P. E. Mains, 2003 Squeezing an Egg into a Worm: *C. elegans* Embryonic Morphogenesis. ScientificWorldJournal 3**:** 1370-1381.

Piekny, A. J., A. Wissmann and P. E. Mains, 2000 Embryonic morphogenesis in *Caenorhabditis elegans* integrates the activity of LET-502 Rho-binding kinase, MEL-11 myosin phosphatase, DAF-2 insulin receptor and FEM-2 PP2c phosphatase. Genetics 156**:** 1671-1689.

Pilgrim, D., A. McGregor, P. Jackle, T. Johnson and D. Hansen, 1995 The *C. elegans* sex-determining gene *fem-2* encodes a putative protein phosphatase. Molecular Biology of the Cell 6**:** 1159-1171.

Pilon, M., 2008 Fishing lines, time-delayed guideposts, and other tricks used by developing pharyngeal neurons in *Caenorhabditis elegans*. Dev Dyn 237**:** 2073-2080.

Pilon, M., and C. Morck, 2005 Development of *Caenorhabditis elegans* pharynx, with emphasis on its nervous system. Acta Pharmacol Sin 26**:** 396-404.

Pocock, R., J. Ahringer, M. Mitsch, S. Maxwell and A. Woollard, 2004 A regulatory network of T-box genes and the even-skipped homologue vab-7 controls patterning and morphogenesis in C. elegans. Development 131**:** 2373-2385.

Pollard, T. D., 2007 Regulation of actin filament assembly by Arp2/3 complex and formins. Annu Rev Biophys Biomol Struct 36**:** 451-477.

Portereiko, M. F., and S. E. Mango, 2001 Early morphogenesis of the Caenorhabditis elegans pharynx. Dev Biol 233**:** 482-494.

Poznanski, A., S. Minsuk, D. Stathopoulos and R. Keller, 1997 Epithelial cell wedging and neural trough formation are induced planarly in Xenopus, without persistent vertical interactions with mesoderm. Dev Biol 189**:** 256-269.

Praitis, V., E. Ciccone and J. Austin, 2005 SMA-1 spectrin has essential roles in epithelial cell sheet morphogenesis in *C. elegans*. Dev Biol 283**:** 157-170.

Priess, J. R., and D. I. Hirsh, 1986 Caenorhabditis elegans morphogenesis: the role of the cytoskeleton in elongation of the embryo. Dev Biol 117**:** 156-173.

Puche, A. C., and M. T. Shipley, 2001 Radial glia development in the mouse olfactory bulb. J Comp Neurol 434**:** 1-12.

Ramani, A. K., T. Chuluunbaatar, A. J. Verster, H. Na, V. Vu *et al.*, 2012 The majority of animal genes are required for wild-type fitness. Cell 148**:** 792-802.

Raper, J., and C. Mason, 2010 Cellular strategies of axonal pathfinding. Cold Spring Harb Perspect Biol 2**:** a001933.

Rauthan, M., C. Morck and M. Pilon, 2007 The *C. elegans* M3 neuron guides the growth cone of its sister cell M2 via the Kruppel-like zinc finger protein MNM-2. Dev Biol 311**:** 185-199.

Refai, O., P. Rohs, P. E. Mains and J. Gaudet, 2013 Extension of the Caenorhabditis elegans Pharyngeal M1 neuron axon is regulated by multiple mechanisms. G3 (Bethesda) 3**:** 2015-2029.

Rodger, J., L. Salvatore and P. Migani, 2012 Should I stay or should I go? Ephs and ephrins in neuronal migration. Neurosignals 20**:** 190-201.

Roh-Johnson, M., and B. Goldstein, 2009 In vivo roles for Arp2/3 in cortical actin organization during C. elegans gastrulation. J Cell Sci 122**:** 3983-3993.

Round, J., and E. Stein, 2007 Netrin signaling leading to directed growth cone steering. Curr Opin Neurobiol 17**:** 15-21.

Roy, P. J., H. Zheng, C. E. Warren and J. G. Culotti, 2000 *mab-20* encodes Semaphorin-2a and is required to prevent ectopic cell contacts during epidermal morphogenesis in *Caenorhabditis elegans*. Development 127**:** 755-767.

Sarov, M., S. Schneider, A. Pozniakovski, A. Roguev, S. Ernst *et al.*, 2006 A recombineering pipeline for functional genomics applied to Caenorhabditis elegans. Nat Methods 3**:** 839-844.

Sawa, M., S. Suetsugu, A. Sugimoto, H. Miki, M. Yamamoto *et al.*, 2003 Essential role of the *C. elegans* Arp2/3 complex in cell migration during ventral enclosure. J Cell Sci 116**:** 1505-1518.

Schaefer, A. M., G. D. Hadwiger and M. L. Nonet, 2000 *rpm-1*, a conserved neuronal gene that regulates targeting and synaptogenesis in *C. elegans*. Neuron 26**:** 345-356.

Schmitz, C., P. Kinge and H. Hutter, 2007 Axon guidance genes identified in a large-scale RNAi screen using the RNAi-hypersensitive *Caenorhabditis elegans* strain *nre-1*(*hd20*) *lin-15b*(*hd126*). Proc Natl Acad Sci U S A 104**:** 834-839.

Schmitz, C., I. Wacker and H. Hutter, 2008 The Fat-like cadherin CDH-4 controls axon fasciculation, cell migration and hypodermis and pharynx development in *Caenorhabditis elegans*. Dev Biol 316**:** 249-259.

Schonichen, A., M. Alexander, J. E. Gasteier, F. E. Cuesta, O. T. Fackler *et al.*, 2006 Biochemical characterization of the diaphanous autoregulatory interaction in the formin homology protein FHOD1. J Biol Chem 281**:** 5084-5093.

Schonichen, A., and M. Geyer, 2010 Fifteen formins for an actin filament: a molecular view on the regulation of human formins. Biochim Biophys Acta 1803**:** 152-163.

Schonichen, A., H. G. Mannherz, E. Behrmann, A. J. Mazur, S. Kuhn *et al.*, 2013 FHOD1 is a combined actin filament capping and bundling factor that selectively associates with actin arcs and stress fibers. J Cell Sci 126**:** 1891-1901.

Schulte, A., B. Stolp, A. Schonichen, O. Pylypenko, A. Rak *et al.*, 2008 The human formin FHOD1 contains a bipartite structure of FH3 and GTPase-binding domains required for activation. Structure 16**:** 1313-1323.

Schulze, N., M. Graessl, A. Blancke Soares, M. Geyer, L. Dehmelt *et al.*, 2014 FHOD1 regulates stress fiber organization by controlling the dynamics of transverse arcs and dorsal fibers. J Cell Sci 127**:** 1379-1393.

Schwarz, V., J. Pan, S. Voltmer-Irsch and H. Hutter, 2009 IgCAMs redundantly control axon navigation in *Caenorhabditis elegans*. Neural Dev 4**:** 13.

Severson, A. F., D. L. Baillie and B. Bowerman, 2002 A Formin Homology Protein and a Profilin Are Required for Cytokinesis and Arp2/3-Independent Assembly of Cortical Microfilaments in *C. elegans*. Curr Biol 12**:** 2066-2075.

Shai, S., 2006 WormBook: Methods in Cell Biology. The C. elegans Research Community, WormBook WormBook, ed. .

Shakir, M. A., J. S. Gill and E. A. Lundquist, 2006 Interactions of UNC-34 Enabled with Rac GTPases and the NIK kinase MIG-15 in *Caenorhabditis elegans* axon pathfinding and neuronal migration. Genetics 172**:** 893-913.

Sheffield, M., T. Loveless, J. Hardin and J. Pettitt, 2007 *C. elegans* Enabled exhibits novel interactions with N-WASP, Abl, and cell-cell junctions. Curr Biol 17**:** 1791-1796.

Shekarabi, M., and T. E. Kennedy, 2002 The *netrin-1* receptor DCC promotes filopodia formation and cell spreading by activating *Cdc42* and *Rac1*. Mol Cell Neurosci 19**:** 1-17.

Shelton, C. A., J. C. Carter, G. C. Ellis and B. Bowerman, 1999a The nonmuscle myosin regulatory light chain gene *mlc-4* is required for cytokinesis, anterior-posterior

polarity, and body morphology during *Caenorhabditis elegans* embryogenesis. Journal of Cell Biology 146**:** 439-451.

Shelton, C. A., J. C. Carter, G. C. Ellis and B. Bowerman, 1999b The nonmuscle myosin regulatory light chain gene mlc-4 is required for cytokinesis, anterior-posterior polarity, and body morphology during Caenorhabditis elegans embryogenesis. J Cell Biol 146**:** 439-451.

Silver, J., S. E. Lorenz, D. Wahlsten and J. Coughlin, 1982 Axonal guidance during development of the great cerebral commissures: descriptive and experimental studies, in vivo, on the role of preformed glial pathways. J Comp Neurol 210**:** 10-29.

Simske, J. S., and J. Hardin, 2001 Getting into shape: epidermal morphogenesis in *Caenorhabditis elegans* embryos. Bioessays 23**:** 12-23.

Simske, J. S., M. Koppen, P. Sims, J. Hodgkin, A. Yonkof *et al.*, 2003 The cell junction protein VAB-9 regulates adhesion and epidermal morphology in C. elegans. Nat Cell Biol 5**:** 619-625.

Sit, S. T., and E. Manser, 2011 Rho GTPases and their role in organizing the actin cytoskeleton. J Cell Sci 124**:** 679-683.

Smit, R. B., R. Schnabel and J. Gaudet, 2008 The HLH-6 transcription factor regulates *C. elegans* pharyngeal gland development and function. PLoS Genet 4**:** e1000222.

Smith, C. W., K. Pritchard and S. B. Marston, 1987 The mechanism of Ca2+ regulation of vascular smooth muscle thin filaments by caldesmon and calmodulin. J Biol Chem 262**:** 116-122.

Smith, D. H., 2009 Stretch growth of integrated axon tracts: extremes and exploitations. Prog Neurobiol 89**:** 231-239.

Smith, R. C., W. Z. Cande, R. Craig, P. J. Tooth, J. M. Scholey *et al.*, 1983 Regulation of myosin filament assembly by light-chain phosphorylation. Philos Trans R Soc Lond B Biol Sci 302**:** 73-82.

Somlyo, A. P., and A. V. Somlyo, 2000 Signal transduction by G-proteins, rho-kinase and protein phosphatase to smooth muscle and non-muscle myosin II. Journal of Physiology 522 Pt 2**:** 177-185.

Soto, M. C., H. Qadota, K. Kasuya, M. Inoue, D. Tsuboi *et al.*, 2002 The GEX-2 and GEX-3 proteins are required for tissue morphogenesis and cell migrations in *C. elegans*. Genes Dev 16**:** 620-632.

Spieth, J., M. MacMorris, S. Broverman, S. Greenspoon and T. Blumenthal, 1988 Regulated expression of a vitellogenin fusion gene in transgenic nematodes. Dev Biol 130**:** 285-293.

Spindler, S. R., I. Ortiz, S. Fung, S. Takashima and V. Hartenstein, 2009 *Drosophila* cortex and neuropile glia influence secondary axon tract growth, pathfinding, and fasciculation in the developing larval brain. Dev Biol 334**:** 355-368.

Steimel, A., L. Wong, E. H. Najarro, B. D. Ackley, G. Garriga *et al.*, 2010 The Flamingo ortholog FMI-1 controls pioneer-dependent navigation of follower axons in *C. elegans*. Development 137**:** 3663-3673.

Struckhoff, E. C., and E. A. Lundquist, 2003 The actin-binding protein UNC-115 is an effector of Rac signaling during axon pathfinding in *C. elegans*. Development 130**:** 693-704.

Sulston, J. E., and J. A. Hodgkin, 1988 The Nematode *Caernorhabditis elegans*. Cold Spring Harbor Laboratory Press, Cold Spring Harbor, NY, **:** 587–606.

Sulston, J. E., and H. R. Horvitz, 1977 Post-embryonic cell lineages of the nematode, *Caenorhabditis elegans*. Dev Biol 56**:** 110-156.

Sulston, J. E., E. Schierenberg, J. G. White and J. N. Thomson, 1983 The embryonic cell lineage of the nematode *Caenorhabditis elegans*. Dev Biol 100**:** 64-119.

Swan, K. A., A. F. Severson, J. C. Carter, P. R. Martin, H. Schnabel *et al.*, 1998 *cyk-1*: a *C. elegans* FH gene required for a late step in embryonic cytokinesis. Journal of Cell Science 111**:** 2017-2027.

Sweeney, H. L., and A. Houdusse, 2010a Myosin VI rewrites the rules for myosin motors. Cell 141**:** 573-582.

Sweeney, H. L., and A. Houdusse, 2010b Structural and functional insights into the Myosin motor mechanism. Annu Rev Biophys 39**:** 539-557.

Takeya, R., and H. Sumimoto, 2003 Fhos, a mammalian formin, directly binds to F-actin via a region N-terminal to the FH1 domain and forms a homotypic complex via the FH2 domain to promote actin fiber formation. J Cell Sci 116**:** 4567-4575.

Takeya, R., K. Taniguchi, S. Narumiya and H. Sumimoto, 2008 The mammalian formin FHOD1 is activated through phosphorylation by ROCK and mediates thrombin-induced stress fibre formation in endothelial cells. Embo J 27**:** 618-628.

Tessier-Lavigne, M., and C. S. Goodman, 1996 The molecular biology of axon guidance. Science 274**:** 1123-1133.

Tojo, H., I. Kaieda, H. Hattori, N. Katayama, K. Yoshimura *et al.*, 2003 The Formin family protein, formin homolog overexpressed in spleen, interacts with the insulin-responsive aminopeptidase and profilin IIa. Mol Endocrinol 17**:** 1216-1229.

Totsukawa, G., Y. Yamakita, S. Yamashiro, D. J. Hartshorne, Y. Sasaki *et al.*, 2000 Distinct roles of ROCK (Rho-kinase) and MLCK in spatial regulation of MLC phosphorylation for assembly of stress fibers and focal adhesions in 3T3 fibroblasts. J Cell Biol 150**:** 797-806.

Trujillo, G., K. Nakata, D. Yan, I. N. Maruyama and Y. Jin, 2010 A ubiquitin E2 variant protein acts in axon termination and synaptogenesis in *Caenorhabditis elegans*. Genetics 186**:** 135-145.

Tulgren, E. D., S. T. Baker, L. Rapp, A. M. Gurney and B. Grill, 2011 PPM-1, a PP2Calpha/beta phosphatase, regulates axon termination and synapse formation in *Caenorhabditis elegans*. Genetics 189**:** 1297-1307.

Uribe, R., and D. Jay, 2009 A review of actin binding proteins: new perspectives. Mol Biol Rep 36**:** 121-125.

Uyeda, T. Q., P. D. Abramson and J. A. Spudich, 1996 The neck region of the myosin motor domain acts as a lever arm to generate movement. Proc Natl Acad Sci U S A 93**:** 4459-4464.

Van Aelst, L., and M. Symons, 2002 Role of Rho family GTPases in epithelial morphogenesis. Genes & Development 16**:** 1032-1054.

Van Eyk, J. E., D. K. Arrell, D. B. Foster, J. D. Strauss, T. Y. Heinonen *et al.*, 1998 Different molecular mechanisms for Rho family GTPase-dependent, Ca2+-independent contraction of smooth muscle. J Biol Chem 273**:** 23433-23439.

van Gelder, M. M., I. A. van Rooij, R. K. Miller, G. A. Zielhuis, L. T. de Jong-van den Berg *et al.*, 2010 Teratogenic mechanisms of medical drugs. Hum Reprod Update 16**:** 378-394.

Vanneste, C. A., D. Pruyne and P. E. Mains, 2013 The role of the formin gene *fhod-1* in *C. elegans* embryonic morphogenesis. Worm 2**:** e25040.

Vavylonis, D., Q. Yang and B. O'Shaughnessy, 2005 Actin polymerization kinetics, cap structure, and fluctuations. Proc Natl Acad Sci U S A 102**:** 8543-8548.

Wadsworth, W. G., H. Bhatt and E. M. Hedgecock, 1996 Neuroglia and pioneer neurons express UNC-6 to provide global and local netrin cues for guiding migrations in C. elegans. Neuron 16**:** 35-46.

Wan, H. I., A. DiAntonio, R. D. Fetter, K. Bergstrom, R. Strauss *et al.*, 2000 Highwire regulates synaptic growth in *Drosophila*. Neuron 26**:** 313-329.

Watanabe, N., and C. Higashida, 2004 Formins: processive cappers of growing actin filaments. Exp Cell Res 301**:** 16-22.

Welch, M. D., A. Iwamatsu and T. J. Mitchison, 1997 Actin polymerization is induced by Arp2/3 protein complex at the surface of Listeria monocytogenes. Nature 385**:** 265-269.

Westendorf, J. J., R. Mernaugh and S. W. Hiebert, 1999 Identification and characterization of a protein containing formin homology (FH1/FH2) domains. Gene 232**:** 173-182.

Wicks, S. R., R. T. Yeh, W. R. Gish, R. H. Waterston and R. H. Plasterk, 2001 Rapid gene mapping in *Caenorhabditis elegans* using a high density polymorphism map. Nat Genet 28**:** 160-164.

Williams-Masson, E. M., P. J. Heid, C. A. Lavin and J. Hardin, 1998 The cellular mechanism of epithelial rearrangement during morphogenesis of the Caenorhabditis elegans dorsal hypodermis. Dev Biol 204**:** 263-276.

Williams-Masson, E. M., A. N. Malik and J. Hardin, 1997 An actin-mediated two-step mechanism is required for ventral enclosure of the *C. elegans* hypodermis. Development 124**:** 2889-2901.

Williams, B. D., and R. H. Waterston, 1994 Genes critical for muscle development and function in *Caenorhabditis elegans* identified through lethal mutations. J Cell Biol 124**:** 475-490.

Wissmann, A., J. Ingles and P. E. Mains, 1999 The Caenorhabditis elegans mel-11 myosin phosphatase regulatory subunit affects tissue contraction in the somatic gonad and the embryonic epidermis and genetically interacts with the Rac signaling pathway. Dev Biol 209**:** 111-127.

Wissmann, A., J. Ingles, J. D. McGhee and P. E. Mains, 1997a *Caenorhabditis elegans* LET-502 is related to Rho-binding kinases and human myotonic dystrophy kinase and interacts genetically with a homolog of the regulatory subunit of smooth muscle myosin phosphatase to affect cell shape. Genes & Development 11**:** 409-422.

Wissmann, A., J. Ingles, J. D. McGhee and P. E. Mains, 1997b Caenorhabditis elegans LET-502 is related to Rho-binding kinases and human myotonic dystrophy kinase and interacts genetically with a homolog of the regulatory subunit of smooth muscle myosin phosphatase to affect cell shape. Genes Dev 11**:** 409-422.

Withee, J., B. Galligan, N. Hawkins and G. Garriga, 2004 *Caenorhabditis elegans* WASP and Ena/VASP proteins play compensatory roles in morphogenesis and neuronal cell migration. Genetics 167**:** 1165-1176.

Wu, M., and M. A. Herman, 2006 A novel noncanonical Wnt pathway is involved in the regulation of the asymmetric B cell division in C. elegans. Dev Biol 293**:** 316-329.

Yacubova, E., and H. Komuro, 2003 Cellular and molecular mechanisms of cerebellar granule cell migration. Cell Biochem Biophys 37**:** 213-234.

Yang, Y., and E. A. Lundquist, 2005 The actin-binding protein UNC-115/abLIM controls formation of lamellipodia and filopodia and neuronal morphogenesis in *Caenorhabditis elegans*. Mol Cell Biol 25**:** 5158-5170.

Yoshimura, S., J. I. Murray, Y. Lu, R. H. Waterston and S. Shaham, 2008 *mls-2* and *vab-3* Control glia development, *hlh-17/Olig* expression and glia-dependent neurite extension in *C. elegans*. Development 135**:** 2263-2275.

Young, P. E., A. M. Richman, A. S. Ketchum and D. P. Kiehart, 1993 Morphogenesis in *Drosophila* requires nonmuscle myosin heavy chain function. Genes & Development 7**:** 29-41.

Yu, T. W., and C. I. Bargmann, 2001 Dynamic regulation of axon guidance. Nat Neurosci 4 Suppl**:** 1169-1176.

Yu, T. W., J. C. Hao, W. Lim, M. Tessier-Lavigne and C. I. Bargmann, 2002 Shared receptors in axon guidance: SAX-3/Robo signals via UNC-34/Enabled and a Netrin-independent UNC-40/DCC function. Nat Neurosci 5**:** 1147-1154.

Zhang, H., R. Constantine, S. Vorobiev, Y. Chen, J. Seetharaman *et al.*, 2011a UNC119 is required for G protein trafficking in sensory neurons. Nat Neurosci 14**:** 874-880.

Zhang, H., F. Landmann, H. Zahreddine, D. Rodriguez, M. Koch *et al.*, 2011b A tension-induced mechanotransduction pathway promotes epithelial morphogenesis. Nature 471**:** 99-103.

Zhen, M., X. Huang, B. Bamber and Y. Jin, 2000 Regulation of presynaptic terminal organization by *C. elegans* RPM-1, a putative guanine nucleotide exchanger with a RING-H2 finger domain. Neuron 26**:** 331-343.

Zheng, J., P. Lamoureux, V. Santiago, T. Dennerll, R. E. Buxbaum *et al.*, 1991 Tensile regulation of axonal elongation and initiation. J Neurosci 11**:** 1117-1125.

APPENDIX

Figure 40. The effect of growth cone mutations on the g1P gland cell projection

g1P is labelled by *phat-1::wCherry* (red) and the M1 neuron is labelled by *glr-2::gfp* (green). The g1P projection often shows abnormalities in the mutants (arrows), but unlike the M1 axon in these mutants, always extends the length of the pharynx. The respective cell bodies are indicated by arrowheads and abnormalities by arrows. (A,B) *unc-51*. (C,D) *unc-34.* (E,F) *unc-115.* Scale bar in (A) = 10 µm. This figure was included as supplemental material in Refai et al.

Figure 40. The effect of growth cone mutations on the g1P gland cell projection

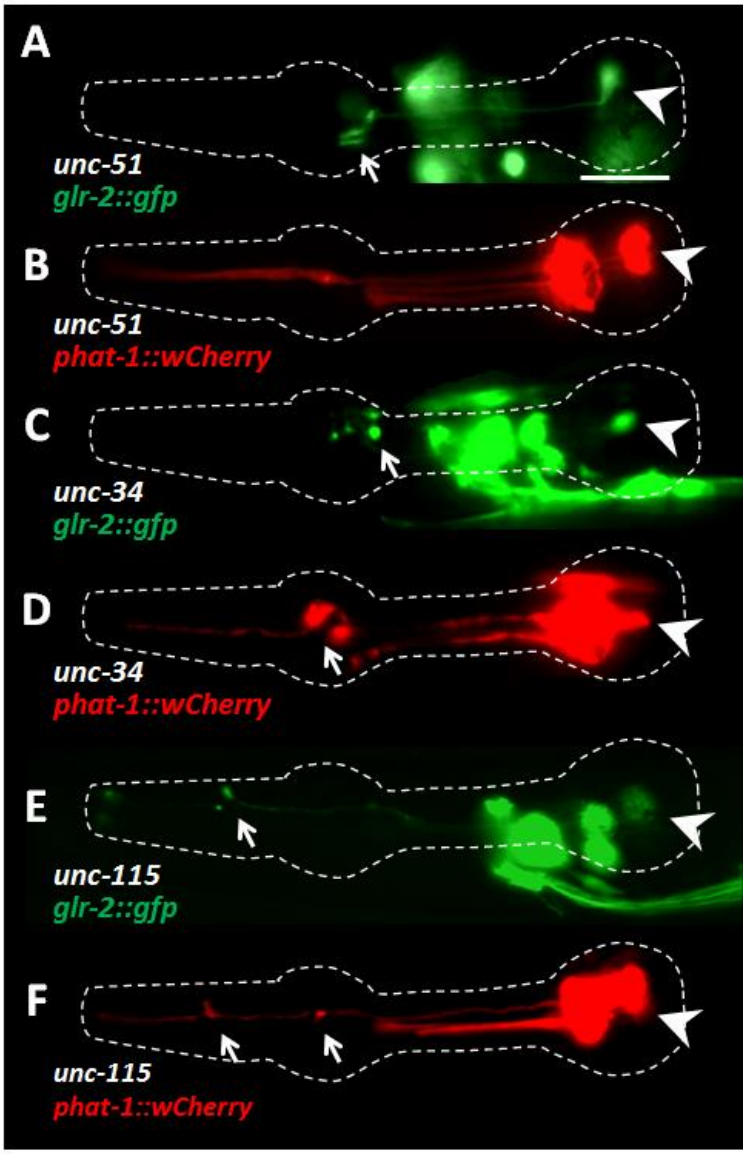

Figure 41. Sequence alignments for FHOD1 proteins showed that *fhod-1*_exon 8 (157 amino acids; highlighted) is not conserved

Eight orthologs**,** including the nematodes *C. elegans [Ce], C. remanei [Cre], C. briggsae [Cbr] , fruit fly (D. melanogaster [Dm]), mouse (M. Musculus [Mm])* and *human (H. Sapiens [Hs])* were examined. Alignment sequence analysis were carried out using the Multiple Sequence Alignment tool, Clustal Omega (www.ebi.ac.uk/Tools/msa/clustalo/). Residues are coloured in *Clustal X* according to their physicochemical properties, as following: red [basic residues (HRK)], blue [hydrophobic residues (AVFPMILW)], green [hydroxyl, sulfhydryl, amine residues (STNQY)], magenta [acidic residues (DE)], orange [the smallest amino acid, G], other colours denote unusual amino/imino acids, etc.

Figure 41. Sequence alignments for FHOD1 proteins showed that *fhod-1*_exon 8 (157 amino acids; highlighted) is not conserved

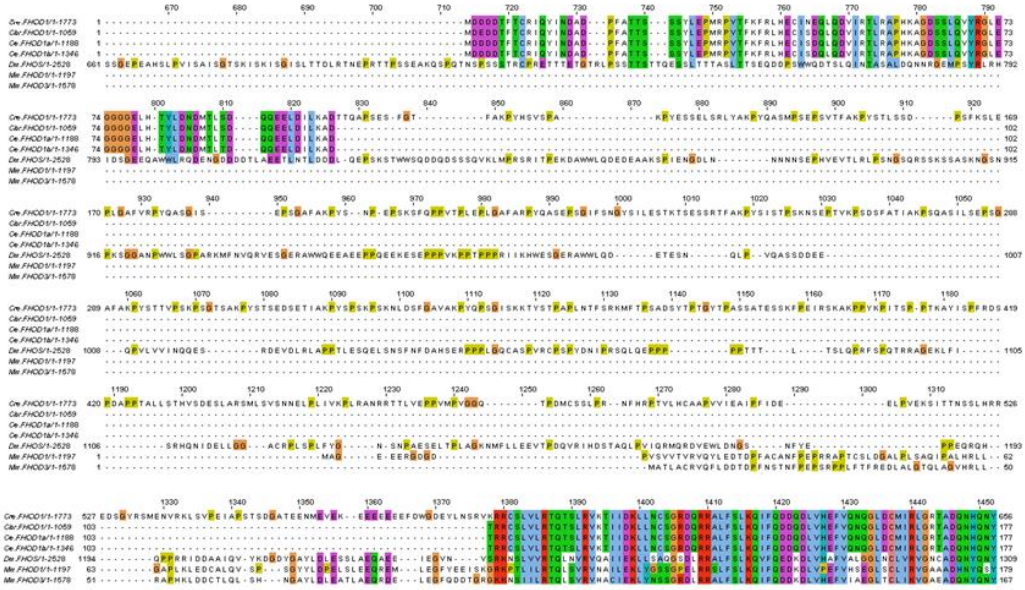

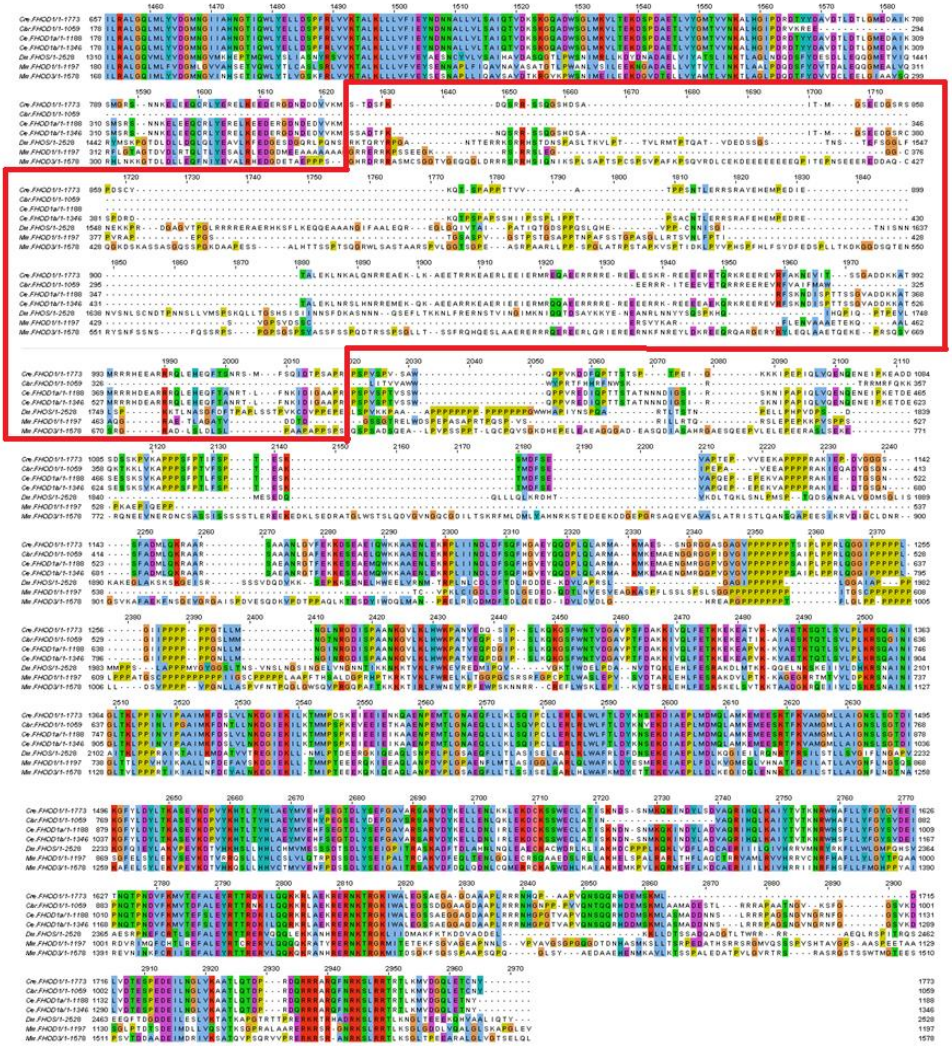

Figure 42: Predicted coiled-coil domains of *fhod-1* isoforms

fhod-1 short isoform (left panel; arrow) lack a predicted large coiled coil domain (right panel; arrow). Analysis were carried out using available tools in (http://www.ebi.ac.uk/interpro/) and (http://embnet.vital-it.ch/software/COILS_form.html)

Figure 42. Predicted coiled-coil domains of *fhod-1* isoforms